UNIVERSITÀ DEGLI STUDI DI TRIESTE

XXIX CICLO DEL DOTTORATO DI RICERCA IN
Ambiente e Vita

Funding agency: OGS, National Institute of Oceanography and Experimental Geophysics

MODELLING THE MERCURY BIOGEOCHEMICAL CYCLE IN COASTAL AND MARINE ENVIRONMENTS

Settore scientifico-disciplinare: **BIO/07**

Ph.D. candidate
GINEVRA ROSATI

Ph.D. program Coordinator
GIORGIO ALBERTI

Supervisor
DONATA MELAKU CANU

Co-Supervisor
COSIMO SOLIDORO

ANNO ACCADEMICO 2015/2016

Abstract

The alteration of mercury (Hg) biogeochemical cycle induced by anthropic activities has caused widespread concern, owing to methylmercury (MeHg) toxicity that poses a human health hazard. Due to its speciation among oxidized (Hg^{II}), reduced (Hg^{0}) and organic compounds (MeHg, Me_2Hg) mercury has a complex cycle that causes its global distribution in the biosphere and its biomagnification along marine food webs, eventually resulting in human exposure through fish consumption. Significant advances have been made over the past decades that have improved our knowledge of biogeochemical mechanisms controlling environmental levels of Hg species. However, synergistic and antagonistic effects among processes and environmental variability often act as confounding factors in the understanding of such mechanisms. Mathematical models provide a thorough framework for the investigation of biogeochemical cycles from a holistic perspective, taking into account the most relevant processes while allowing discerning among the contributions of individual factors affecting modelled concentrations.

The goal of this dissertation is to gain insight into the processes that affect Hg cycle, by analyzing case studies of coastal and marine environments. Available observational data were used to simulate Hg dynamics at the study sites by means of a dynamic box model that simulates Hg fate and transport (WASP7). Here is presented the model implementation for 4 case studies, which overall highlights how different processes dominate the Hg cycle across ecosystems, depending on hydrodynamic features, local pollution sources and other biogeochemical forcing.

Chapter 1 provides an overview of the Hg cycle and of the most recent findings, with a comparative perspective on coastal and ocean dynamics. Chapter 2 presents a model implementation in a 2D domain, aimed at representing a shallow coastal lagoon of the Northern Mediterranean Sea affected by historical Hg pollution (Marano – Grado Lagoon). The model is used to estimate present-day concentrations and fluxes of Hg and MeHg, evaluating the contribution of the lagoon to the wider cycle of Hg in the Mediterranean area. In Chapter 3, the implementation of the lagoon developed in Chapter 2 is extended to perform long-term scenario analysis (100 years), with the aim of evaluating possible outcomes of both climate change and a management action such as removal of riverine Hg input. Chapter 4 investigates the dynamics of Hg and MeHg under changeable redox conditions, in the permanently stratified water of the Black Sea, focusing on the open question of the occurrence of Hg methylation in sulfidic environments. In Chapter 5 the model is applied to a heavily polluted harbor of the Southern Mediterranean Sea (Augusta Bay) subjected to fishing ban. The model is used to estimate

MeHg concentrations and, together with measurements of Hg_T in the trophic web, it is employed to derive bioaccumulation factors (BAF) and investigate biomagnification.

Thesis content

Introduction to the work

The alteration of global biogeochemical cycles driven by human exploitation of natural resources (e.g. carbon, nitrogen, mercury) has led to a number of unintended adverse effects on the environment, with negative implications for human health and safety, spanning from higher uncertainty in food provision, to pollutants exposure and increased probability of natural hazards. Consequently, the scientific community has increased its awareness of the role of humans as essential components of ecosystems, whose well-being relies on natural services provided by ecosystems that in turn are affected by anthropogenic activities. In the year 2000, the idea of 'Anthropocene' was proposed, as a geological era in which human activities have induced remarkable changes in the biosphere, observable on a planetary scale (Crutzen and Stoermer, 2000). While the benefits of the technological advancements that drive those changes still concern a small fraction of global population, the more sensitive communities are generally those which contributed less to consumption of goods and services (Biermann et al., 2016). Nonetheless, it is becoming increasingly clear how the long-term detrimental effects of environmental alterations involve everyone and that our current choices will determine the legacy to the future generations. Such considerations emphasize the need for enhanced interdisciplinary efforts toward the understanding of the complex interactions among drivers of change, to support sustainable development strategies at local and international levels, aimed at promoting human wellbeing within healthy ecosystems.

This work focuses on Hg dynamics in marine environments, analyzing case studies of coastal and marine environments through model simulations supported by observational constraints. The biogeochemical cycle of mercury (Hg) has been substantially modified by anthropogenic drivers, and its levels in the environment have increased by a factor 5 – 10 compared to natural levels (Amos et al., 2013; Horowitz et al., 2014). Concerns about the presence of mercury in the environment first arose after the first large outbreak in the 50s in Japan, when the population of the coastal city of Minamata started to suffer from symptoms of neurological pathologies. The environmental disaster was caused by massive dumping of organic Hg compounds (such as methylmercury, MeHg) into the Minamata bay, which caused their bioaccumulation in fish and shellfish, leading to intoxication of thousands people with many fatalities (Harada, 1995). Exposure scenarios as dramatic as those experienced in Minamata are very unlikely to occur again because Hg is generally released in its inorganic form. Moreover the increased awareness of the exposure risks that has led to the ban of Hg from industrial processes (Minamata Convention). However, Hg is persistent in the environment and is distributed all over the biosphere including remote ecosystems and oceanic fishes, especially top

predators (Mason et al., 2012). Although emissions from natural and anthropogenic sources are mostly in inorganic forms (oxidized, Hg^{II} and elemental, Hg^{0}), Hg is converted to MeHg in waters and sediments by anoxic bacteria.

Therefore, it is important to identify sources and sinks of Hg and MeHg on global and local scales and to understand the major biogeochemical controls on Hg methylation, demethylation and bioaccumulation. At the same time, it is important to protect communities exposed to locally high Hg levels (Dellinger et al., 2012) and to further investigate effects of low-dose chronic exposure on infants (including foetus), adults and wildlife (Karagas et al., 2012; Scheuhammer et al., 2012). The development of effective remediation strategies is required to manage critical sites, as emphasized by the theme of next conference on Hg as a global pollutant (ICGMP2017) that is *'understanding the multiple factors that accelerate and attenuate recovery of mercury contamination in response to environmental inputs on local to global scales'* (http://mercury2017.com/home/overview/, visited 2/7/2017). Although intensively studied, the triggers of MeHg production and bioaccumulation across different ecosystems are still somewhat poorly understood owing to both the number and complexity of processes involved (e.g. Cossa et al., 2012; Hsu-Kim et al., 2013; Mason et al., 2012; Sonke et al., 2013) and to the analytical difficulties in measuring compounds that often occur at picomolar or femtomolar levels (Heimbürger et al., 2015; Lamborg et al., 2012).

Mathematical models offer a useful support to harmonize the observed levels of Hg species in environmental compartments with our current understanding of the processes that have determined them. Moreover, models can improve our ability to assess Hg fluxes within and among systems by reproducing the temporal and spatial variability of processes induced by environmental forcing. The structure of a deterministic model provides also a rigorous framework, constrained by the model assumptions, to test hypotheses about a given process and to explore possible environmental outcomes of different management scenarios.

This contribution has investigated Hg dynamics across coastal and marine ecosystems by integrating observations and modeling with the aim of analyzing the impacts of Hg transport and transformation processes on environmental compartments. The model used to carry out the research is a deterministic box model designed for flexible implementation in 1, 2 or 3 dimensions (WASP7, Wool et al., 2001). Here it has been applied to a 2D representation of a shallow coastal lagoon (1 m depth) of the Northern Adriatic affected by historical Hg pollution, to a 1D representation of a deeper bay of the Southern Mediterranean Sea (15 m depth) and to a 1D modeling of the redox gradient of the Black Sea basin (2200 m depth). Chapter 1 of the dissertation gives an overview of the Hg biogeochemical cycle with a comparative perspective on coastal and ocean dynamics, looking at the more recent experimental

findings and modeling efforts. Chapter 2 analyzes Hg dynamics in the Marano-Grado Lagoon, which has stored high amount of Hg in its sediment owing to historical Hg mining in the area and more recent industrial activity. The model was used to estimate Hg species fluxes and concentrations, assessing the contribution of the lagoon to the budget of Hg in the Mediterranean Sea (Melaku Canu et al., 2015). Chapter 3 built on the work developed for the Marano-Grado lagoon (Chapter 2) extending the runs over the long-term (100 years), with the aim of evaluating possible outcomes of climate change and of management scenarios, such as removal of riverine Hg input. The natural recovery time of the lagoon sediment is also estimated through a longer simulation recursively run under current conditions (Canu and Rosati, 2017). Chapter 4 focuses on the open scientific controversies on Hg methylation under different redox conditions. We conduct an analysis of Hg cycle down through the water column of the Black Sea, the redox structure of which is similar the ones of sedimentary environments and stratified water bodies worldwide thus representing a 'natural laboratory' (Rosati et al., *in prep.*). Chapter 5 investigates MeHg dynamics in the heavily polluted harbor of Augusta Bay, currently subjected to fishing ban. The model, supported by measurements of Hg in the trophic web, is used to estimate water MeHg levels and to derive specie-specific bioaccumulation factors (BAF) that summarize the Hg enrichment of each species and can be useful to estimate responses of the ecosystem to future changes.

References

Amos, H.M., Jacob, D.J., Streets, D.G., Sunderland, E.M., 2013. Legacy impacts of all-time anthropogenic emissions on the global mercury cycle. Global Biogeochem. Cycles 27, 410–421. doi:10.1002/gbc.20040

Biermann, F., Bai, X., Bondre, N., Broadgate, W., Arthur Chen, C.-T., Dube, O.P., Erisman, J.W., Glaser, M., van der Hel, S., Lemos, M.C., Seitzinger, S., Seto, K.C., 2016. Down to Earth: Contextualizing the Anthropocene. Glob. Environ. Chang. 39, 341–350. doi:10.1016/j.gloenvcha.2015.11.004

Canu, D., Rosati, G., 2017. Long-term scenarios of mercury budgeting and exports for a Mediterranean hot spot (Marano-Grado Lagoon, Adriatic Sea). Estuar. Coast. Shelf Sci. 1–11. doi:10.1016/j.ecss.2016.12.005

Cossa, D., Harmelin-Vivien, M., Mellon-Duval, C., Loizeau, V., Averty, B., Crochet, S., Chou, L., Cadiou, J.-F., 2012. Influences of bioavailability, trophic position, and growth on methylmercury in hakes (Merluccius merluccius) from Northwestern Mediterranean and Northeastern Atlantic. Environ. Sci. Technol. 46, 4885–93. doi:10.1021/es204269

Crutzen, P.J., Stoermer, E.F., 2000. The "Anthropocene." IGBP Newsl. 41, 17–18.

Dellinger, J., Dellinger, M., Yauck, J.S., 2012. Mercury Exposure in Vulnerable Populations:, in: Mercury in the Environment, Pattern and Process. University of California Press, pp. 289–300.

Harada, M., 1995. Minamata Disease: Methylmercury Poisoning in Japan Caused by Environmental Pollution. Crit. Rev. Toxicol. 25, 1–24. doi:10.3109/10408449509089885

Horowitz, H.M., Jacob, D.J., Amos, H.M., Streets, D.G., Sunderland, E.M., 2014. Historical Mercury Releases from Commercial Products : Global Environmental Implications. Environ. Sci. Technol. 48, 10242–10250. doi:dx.doi.org/10.1021/es501337j

Hsu-Kim, H., Kucharzyk, K.H., Zhang, T., Deshusses, M.A., 2013. Mechanisms regulating mercury bioavailability for methylating microorganisms in the aquatic environment: A critical review. Environ. Sci. Technol. 47, 2441–2456. doi:10.1021/es304370g

Karagas, M.R., Choi, A.L., Oken, E., Horvat, M., Schoeny, R., Kamai, E., Cowell, W., Grandjean, P., Korrick, S., 2012. Evidence on the Human Health Effects of Low-Level Methylmercury Exposure. Environ. Health Perspect. 120, 799–806. doi:10.1289/ehp.1104494

Lamborg, C.H., Hammerschmidt, C.R., Gill, G.A., Mason, R.P., Gichuki, S., 2012. An intercomparison of procedures for the determination of total mercury in seawater and recommendations regarding mercury speciation during GEOTRACES cruises. Limnol. Oceanogr. Methods 10, 90–100. doi:10.4319/lom.2012.10.90

Heimbürger, L-E., Lagane, C., Laffont, L., Cossa, D, Sonke J.E., 2015. Mercury measurements in the oceans - results of the 2013 and 2014 GEOTRACES intercalibration exercises, in: 12th International Conference on Mercury as a Global Pollutant. Jeju, Korea, p. 153.

Mason, R.P., Choi, A.L., Fitzgerald, W.F., Hammerschmidt, C.R., Lamborg, C.H., Soerensen, A.L., Sunderland, E.M., 2012. Mercury biogeochemical cycling in the ocean and policy implications. Environ. Res. 119, 101–117. doi:10.1016/j.envres.2012.03.013

Melaku Canu, D., Rosati, G., Solidoro, C., Heimbürger, L.-E., Acquavita, A., 2015. A comprehensive assessment of the mercury budget in the Marano–Grado Lagoon (Adriatic Sea) using a combined observational modeling approach. Mar. Chem. 177, 742–752. doi:10.1016/j.marchem.2015.10.013

Scheuhammer, A.M., Basu, N., Evers, D.C., Heinz, G.H., Sandheinrich, M.B., Bank, M.S., Bank (Edited By), M.S., 2012. Ecotoxicology of mercury in fish and wildlife: Recent advances, in: Bank, M.S. (Ed.), Mercury in the Environment: Pattern and Process. University of California Press, Berkley, CA, pp. 223–238. doi:10.1525/california/9780520271630.003.0011

Sonke, J.E., Heimbürger, L.E., Dommergue, A., 2013. Mercury biogeochemistry: Paradigm shifts, outstanding issues and research needs. Comptes Rendus - Geosci. 345, 213–224. doi:10.1016/j.crte.2013.05.002

Wool, T.A., Ambrose, R.B., Martin, J.L., Comer, E.A., 2001. Water Quality Analysis Simulation Program (WASP) Version 6.0: User's Manual.

Chapter 1 – Mercury cycle: from sources to receptors

1.1 Global sources and sinks of Hg

Mercury (Hg) is an element naturally occurring in the Earth's mineral reservoir, however its levels in the biosphere have been dramatically increased by anthropic activities (Amos et al., 2015, 2014, 2013; Driscoll et al., 2013; Horowitz et al., 2014; Mason et al., 2012). The more relevant species, the abundances of which vary across environmental compartments, are inorganic Hg species (dissolved and particulate oxidized mercury compounds, Hg^{II} and elemental mercury, $Hg^{0}_{(g)}$), and organic Hg species (dissolved and particulate methylmercury compounds, MeHg and dimethylmercury, $Me_2Hg_{(g)}$). Most Hg is emitted in its inorganic forms (Hg^{II}, Hg^{0}) and cycles for decades among surface environmental compartments (atmosphere, surface water, soils, biomasses) being transported on a long range. Eventually, Hg is removed from water through particles scavenging and sequestration into ocean sediments, on a time scale of centuries (Amos et al., 2014). Biogeochemical models constrained by global observations suggest that global Hg reservoirs have been altered since pre-industrial times due to emissions from gold mining. Emissions increased further during the industrial age and peaked in the mid-late 20th century (Amos et al., 2015). As a result, in the last 100 years the atmospheric and surface water Hg reservoirs are increased of about 200% (Mason et al., 2012).

Natural and anthropic Hg sources are distinguished between primary and secondary: primary sources cause emission of the Hg sequestered within stable lithospheric reservoir, while secondary sources are due to the cycling of Hg that is re-emitted after its deposition on environmental compartment (Amos et al., 2013; Driscoll et al., 2013; Kocman et al., 2013). Natural primary sources include volcanoes, geothermal activity, hydrothermal vents and degassing from soils enriched in cinnabar (HgS) and account for about 1% of total current emissions to the atmosphere and less than 10% of emissions to the ocean (Amos et al., 2013; Mason et al., 2012). Primary anthropic sources are related to the usage of lithogenic Hg in industrial processes and account for 20 – 30% of global emission to atmosphere. Secondary emission are estimated to be about 80% of total emissions (Amos et al., 2013; Mason et al., 2012). Most of Hg emissions from primary and secondary sources is toward the atmosphere (20 – 45 Mmol/y), while 20 – 33 Mmol/y are deposited or transported to the ocean and 15 – 16 Mmol/y deposit to the land (Amos et al., 2014, 2013; Mason et al., 2012).

The very first anthropic application of Hg was as amalgam in silver and gold mining. Novel applications were developed during the industrial age, spanning from the use of Hg as catalyst in the production of chemicals (e.g. in chlor-alkali plants and in plants of acetaldehyde, vinyl chloride and vinyl acetate) to its use as component of commercial products (e.g. paints, batteries, lamps,

pharmaceuticals, dental amalgams, pesticides, wiring devices and explosives). Moreover, Hg is used to process non-ferrous metals and it is emitted as by-product of fossil fuels processing and burning (Horowitz et al., 2014; Kocman et al., 2013). According to the emission inventory for the year 2010, primary causes of Hg emissions to the atmosphere are: artisanal small-scale gold mining (37%), coal burning (24%), and production of nonferrous metals (10%) (AMAP/UNEP, 2013).

1.2 Global budget for Hg and MeHg in the ocean

Wet and dry deposition of atmospheric Hg is the foremost source of Hg to the ocean (80 – 90%), resulting from atmospheric oxidation of Hg^0 to Hg^{II} mediated by Br and/or O_3 – OH (Amos et al., 2014, 2013; Gencarelli et al., 2015; Mason et al., 2012). Rivers account only for 10 – 20% of Hg sources to the ocean, but can be highly relevant on regional scales, as their load is mostly retained in transitional and coastal environments or in the shelves (Amos et al., 2014; Conaway et al., 2003; Covelli et al., 2007; Mason et al., 2012; Zhang et al., 2015). Inputs from hydrothermal vents are estimated to be lower than 3 Mmol/y (~10%). Groundwater inputs and benthic sediment fluxes together account for 0.5 to 4 Mmol/y (2 – 20%); however they can be enhanced in some locations due to point-source emissions and/or secondary emissions from sediment that have acted as repository of Hg pollution (Emili et al., 2012; Mason et al., 2012; Melaku Canu et al., 2015; Salvagio Manta et al., 2016).

MeHg dynamics are far different from those of inorganic Hg, as the occurrence of MeHg in marine water is attributed mostly to *in-situ* sources. According to the budget estimated by Mason et al., (2012), the two main sources of MeHg to the upper ocean (<1000 m depth) are degradation of Me_2Hg (41% of total input) and in situ methylation (39%, 0.76 Mmol/y). Much smaller contributions come from pore-water MeHg fluxes (11%), rivers (5%) and atmospheric deposition (2.6%). About 60% of MeHg input is converted to Hg^{II} or Hg^0 upon biological and photochemical demethylation. Bioaccumulation account for 10% of removal from water, whilst sinking and advective fluxes to deeper water account for 25%. Less than 1% is lost through evasion of Me_2Hg to the atmosphere.

1.3 Transport and transformations of Hg species in the marine environment

1.3.1 Speciation and transport

The residence time and the bioavailability of Hg in the marine environment depends on its speciation among a number of particulates, dissolved and gaseous compounds of oxidized Hg (Hg^{II}), methylmercury (MeHg), elemental mercury (Hg^0) and dimethylmercury (Me_2Hg), which undergoes different biogeochemical transport and transformation processes (Figure 1) and are characterized by different bioavailability and bioaccumulation efficiency. The term total Hg (Hg_T) is generally used to refer to the Hg species as a whole. Marine bioaccumulation processes begin with accumulation by phytoplankton of available compounds of MeHg and Hg, which are transferred to higher trophic levels through predator-prey interactions. Due to the continuous exposition and the slow elimination rates of MeHg from the body, organisms experience increasing body burden with age. Moreover, as feeding activity is the main pathway of MeHg transfer, biomagnification occurs and MeHg content increases along with the trophic level (Cossa et al., 2012; Hammerschmidt and Fitzgerald, 2006). By contrast, dissolved gaseous mercury species (DGM, Hg^0 + Me_2Hg) tend to leave the system by volatilization to the atmosphere, thus lowering surface water concentrations. Production of Hg^0 occurs both in euphotic water, aphotic water and sediment upon photochemical and biological transformations of Hg^{II} and MeHg (Black et al., 2012a; Monperrus et al., 2007a; Rolfhus and Fitzgerald, 2001). Me_2Hg is produced by microbes in intermediate and deep water, where it can constitute up to 80% of methylated Hg pool, and can be a source of MeHg (Jonsson et al., 2016; Lehnherr et al., 2011).

In the ocean, Hg^{II} and MeHg are mostly in the dissolved phase (Hg_D and $MeHg_D$, operationally defined by filtration at 0.2 or 0.45 μm), while particulate compounds (Hg_P, $MeHg_P$) account for less than 10% (Bowman et al., 2015). Hg and MeHg bind strongly to ligands of marine and terrestrial DOM (dissolved organic matter), but can be also complexed to chloride ions ($HgCl_3^-$, $HgCl_4^{2-}$ and MeHgCl, Morel et al., 1998). In rivers, estuaries and shallow bays, Hg_P and $MeHg_P$ compounds are far more important (Bloom et al., 2004; Choe et al., 2003; Conaway et al., 2003; Melaku Canu et al., 2015), and a significant fraction of Hg_D and $MeHg_D$ can be in the colloidal phase within macroaggregates of phytoplanktonic macrogels, bacteria, organic and inorganic particles (Choe et al., 2003; Koron et al., 2011). The particulate fraction of Hg^{II} and MeHg result from: 1) their uptake by phytoplankton; 2) their affinity to organosulfur compounds of organic particulate (POM); 3) their affinity to calcium carbonate ($CaCO_3$) and oxides of Mn and Fe (Lamborg et al., 2016; Muresan et al., 2007; Schartup et al., 2014). The adsorption of Hg_P and $MeHg_P$ on sinking solids can eventually result in their deposition to the sediment. Accumulation of Hg species into the sediment occurs when a system is depositional (net sedimentation), however diagenetic remineralization of natural organic matter (NOM) causes release of dissolved Hg species that

can be methylated/demethylated and re-emitted to the water through pore-water diffusion. Diffusion of Hg_D and $MeHg_D$ from pore-water can be enhanced by bioturbation and by variations of redox conditions at the sediment-water interface (Benoit et al., 2009; Emili et al., 2014). Particulate species are either sequestered in deep sediment upon burial, or move to the water column when the wave/current induced bottom shear stress promotes sediment resuspension.

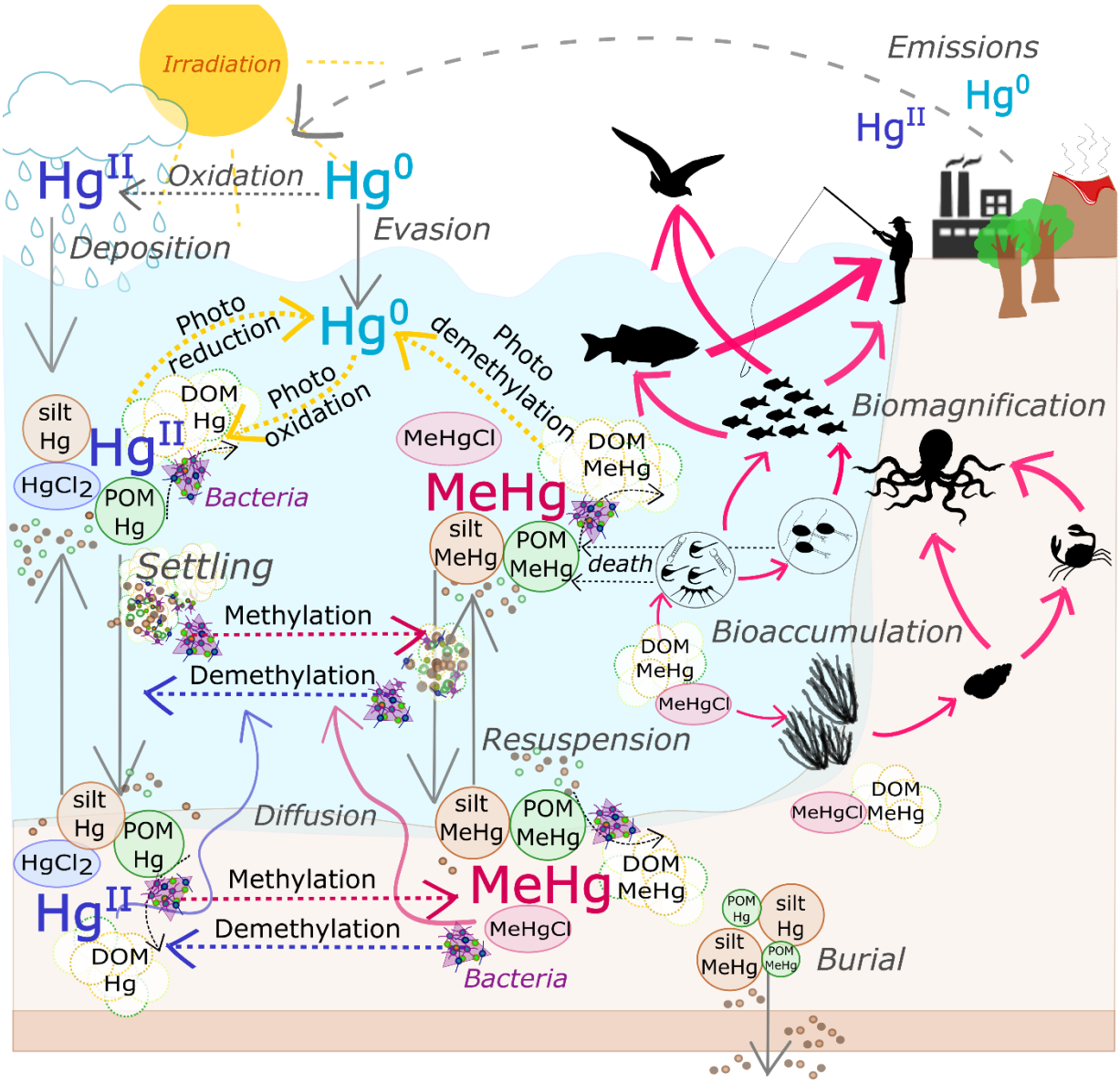

Figure 1. The cycling of Hg in the marine environment. Three main Hg species are represented (Hg^{II}, oxidized mercury; Hg^0, elemental mercury; MeHg, methylmercury) with their partitioning to solids (POM and silt) and dissolved phases (DOM, Cl^-). Transport processes among abiotic compartments are indicated by the grey arrows and text. Transformation processes are indicated by the dashed colored arrows and black text; processes mediated by bacteria (i.e. methylation, demethylation, POM and DOM remineralization) are marked with a violet triangle. Bioaccumulation at the base of the trophic web and biomagnification at higher trophic levels are illustrated by the purple arrows, whose size increase along with organisms MeHg content.

1.3.2 Transformations

The cycling of Hg species in the marine environment is sustained by photochemical and biological transformations, namely photo-reduction, photo-oxidation, photo-demethylation (or photo-degradation), microbial methylation and demethylation, and microbial reduction. All these processes concur to determine Hg levels and bioavailability in different niches of the ecosystem, affecting bioaccumulation.

Photochemical transformations

In euphotic waters, photochemical transformations induce an intensive cycling between Hg_D^{II}, Hg^0 and $MeHg_D$, prompted by UV radiations. On the one hand, photo-reduction and photo-demethylation lead to production of Hg^0 that volatilizes to the atmosphere mitigating surface concentrations. On the other hand, photo-oxidation of Hg^0 gives rise to Hg^{II} that is retained in the system. Rates of all the photochemical reactions increase with irradiance, however observations suggest that in addition to light availability there are other kinetic limitations, due either to direct interactions of Hg with chromophoric DOM ligands, or to indirect effects of chromophoric DOM that produces highly reactive radical species (Black et al., 2012a; Lalonde et al., 2004; Rolfhus and Fitzgerald, 2004).

Photo-reduction ($Hg^{II} \rightarrow Hg^0$) is thought to be mediated by chromophoric DOM ligands that adsorb solar radiation and transfer electrons from DOM to Hg^{II}, or alternatively it might involve the DOM mediated photolytic formation of an intermediate reductants such as $HO_2\cdot$ (Fantozzi et al., 2013; Qureshi et al., 2010; Rolfhus and Fitzgerald, 2004; Whalin et al., 2007).

MeHg photo-demethylation (or photo-degradation, $MeHg \rightarrow Hg^0$) rates are affected by DOM composition and decrease with salinity; the reaction seems to be mediated by radicals ($\cdot OH$, $\cdot O_2$) generated by humic acids (Black et al., 2012b; Kim et al., 2014; Whalin et al., 2007).

Likewise, photo-oxidation ($Hg^0 \rightarrow Hg^{II}$) is likely mediated by free radicals ($\cdot OH$, $\cdot O_2$) and might involve an intermediate Hg species (Lalonde et al., 2004; Qureshi et al., 2010). Contrasting to photo-demethylation, net photo-oxidation rates have been reported to increase with salinity, possibly because the reverse reaction of photo-reduction is inhibited by halides (Cl^- and Br^-) that stabilize Hg^{II} (Lalonde et al., 2004, 2001; Qureshi et al., 2010). Another study along a salinity gradient, did not detect such a relation, however it was carried out under more variable natural light conditions (Whalin et al., 2007). It is also possible that the variation of DOM composition across sites acted as a confounding factor in those studies. For instance, Soerensen et al., (2013) observed higher DGM ($Hg^0 + Me_2Hg$) concentrations in offshore stations (salinity ≥ 35) than in the nearshore stations (salinity <35) of the Northwest Atlantic, probably because the ageing of terrestrial DOM moving offshore (increasing C/N ratio) reduces the stability of Hg-DOM complexes and favour photo-reduction (Schartup et al., 2015b).

	Salinity	Light	DOM	Rates
Photo-reduction	↙ ^ § possible inhibition due to Cl^- # no effect ? ɜ possible confounding effect due to DOM quality	↗ § UV-B ʔ $k_{ph.red}$ [% d^{-1}] $=6.95 \cdot 10^{-3}$ [I] – 0.05 ; (I, Wm^{-2})	↗ ж ʔ chromophoric DOM ligands transfer electrons to Hg^{II} or create intermediate reductants ($HO_2 \cdot$) ↙ ɜ terrestrial DOM may limit reducible Hg pool	$k_{ph.red}$ [h^{-1}] § 0.15 – 0.93 in ocean water # 0.1 – 9 in coastal, estuarine, shelf waters
Photo-oxidation	$k_{ph.ox}$ [h^{-1}] ↗ ^ 0.26 at sal~0 0.64 at sal~15 ↙ # 1.5 – 3.6 at sal~7 1.16 –1.8 at sal~28	↗ ^ UV-A, visible	↗ ^ chromophoric DOM, through photochemical production of radicals ($\cdot OH$, $\cdot O_2$)	$k_{ph.ox}$ [h^{-1}] § 0.4 – 1.9 in ocean water # 1.16 –1.8 in coastal, estuarine, shelf waters
Photo-demethylation	$k_{ph.dem}$ [$E^{-1}m^{-2}$] ↙ * 0.006 – 0.015 at sal from 25 to 5	↗ * UV-B, UV-A, visible $k_{ph.dem}$ [$E^{-1}m^{-2}$] 0.008 – 0.01 at salinity 25	↗ * chromophoric DOM through photochemical production of radicals ($\cdot OH$, $\cdot O_2$)	$k_{ph.dem}$ [$E^{-1}m^{-2}$] * 0.008 - 0.01 at salinity 25 # $k_{ph.dem}$ [h^{-1}] ~ 0.018 in ocean water

* Black et al., (2012); ж Fantozzi et al., (2013); ^ Lalonde et al., (2004); § Qureshi et al., (2010); ʔ Rolfhus and Fitzgerald, (2004); ɜ Schartup et al., (2015b); # Whalin et al., (2007).

Table 1. Environmental controls on photochemical transformations of Hg species

Methylation

Methylation of Hg^{II} to MeHg is driven by anaerobic bacteria in marine sediment (Bouchet et al., 2013; Hammerschmidt et al., 2004; Hollweg et al., 2010; Hollweg et al., 2009; Monperrus et al., 2007b; Schartup et al., 2013) and water (Heimbürger et al., 2015, 2010, Monperrus et al., 2007a, 2007b; Schartup et al., 2015a; Sharif et al., 2014; Sunderland et al., 2009), including hypoxic and anoxic micro-environments within marine snow and sinking particles (Ortiz et al., 2015).

Methylation is related to bacterial remineralization of NOM (DOM + POM) that cause release of Hg_D^{II} from POM and/or from oxides of Fe and Mn (Cossa et al., 2009; Heimbürger et al., 2010; Muresan et al., 2007; Sunderland et al., 2009). Therefore, methylation is controlled by environmental factors that affect both the bioavailability of Hg_D^{II} and the functioning of the microbial community (Cossa et al., 2014; Merritt and Amirbahman, 2009). Recent research has found that methylation rates are higher in coastal sediment with higher POM content (Schartup et al., 2013) and that some DOM components like cysteine can enhance methylation whilst others inhibit it (Schaefer et al., 2011; Schaefer and Morel, 2009).

Sulfides have been long considered responsible for hindering Hg_D^{II} bioavailability at levels about 10 μM (Benoit et al., 2001, 1999a, 1999b; Lamborg et al., 2008; Muresan et al., 2007), however this hypothesis has been questioned (Hsu-Kim et al., 2013; Merritt and Amirbahman, 2009 and reference therein). Previously unknown interactions among Hg, DOM and sulfides have been reported to decrease the stability of Hg precipitates with sulfides ($HgS_{(s)}$) and alter their nucleation, thus affecting Hg^{II} bioavailability and methylation (Deonarine and Hsu-Kim, 2009; Gerbig et al., 2011; Hsu-Kim et al., 2013; Jonsson et al., 2012; Kucharzyk et al., 2015; Ravichandran et al., 1999, 1998; Skyllberg, 2008; Slowey, 2010; Waples et al., 2005; Zhang et al., 2012; T. Zhang et al., 2014).

Dimethylmercury (Me_2Hg) production from methylation of Hg^{II} (slower) or MeHg (faster) has been observed in the Canadian Arctic, however previous studies suggested that Me_2Hg may be the primary product of Hg^{II} methylation in other locations, and indicated a link with primary productivity levels. Me_2Hg can be a source of MeHg through demethylation, but owing to analytical issues there is high uncertainty on its decomposition rates (see Lehnherr et al., 2011 and reference therein). Methylation to Me_2Hg has been detected also on sulfide mineral surfaces (Fe_1S^{1-}, $HgS_{(s)}$, $CdS_{(s)}$), through a mechanism that seems to involve two MeHg molecules adsorbed on the minerals surface (Jonsson et al., 2016 and reference therein).

Demethylation and biotic Hg reduction

Two pathways of microbial demethylation have been identified, an oxidative pathway that yields Hg^{II} and CO_2, and a reductive pathway that yields Hg^0 and CH_4. It has been proposed that reductive demethylation dominates at high Hg concentrations, whereas oxidative pathway is more important in uncontaminated sites (Marvin-DiPasquale et al., 2000). This is supported by the fact that reductive demethylation is induced by the presence of a groups of genes that confers resistance to Hg toxicity upon bacteria, because Hg^0 produced can diffuse out of the cell. These groups of genes ('*mer operon'*) exist in various configurations and can be transferred from one bacteria to another one (transposon). Thus, in a highly contaminated environment the bacterial population can adapt to Hg levels, becoming enriched in Hg resistant organisms (Barkay et al., 2003). In the polluted Lagoon of Marano-Grado, the relative importance of oxidative and reductive demethylation was observed to vary spatially and seasonally, with increasing reductive demethylation in winter (Hines et al., 2012).

Depending on the configuration of the *mer operon*, bacterial detoxification can be effective on both MeHg and Hg^{II} (broad spectrum resistance) or limited to biotic Hg^{II} reduction (narrow spectrum resistance) (Barkay et al., 2003). Observed rates of biotic reduction are lower than those of photo-reduction but still significant, and this process is relevant in the aphotic zone of the water column (Rolfhus and Fitzgerald, 2004). Dark abiotic and biotic oxidation of Hg^0 have been reported as well, but considered negligible because of very low rates (Barkay et al., 2003; Lalonde et al., 2004).

	Temperature	NOM	Bacteria	HS
Methylation	↗ ♦ⱥ many reports of increase with temperature	↗ ИФ thiols and cysteine increase Hg uptake and methylation ↙ ◘ NO_3 inhibits methylation	↗ Ƨo MeHg levels correlates to AOU ↗ Ƨo MeHg levels correlates to PO_4^{2-} ↗ *correlates to sulfate reduction in sediment	↙ ɻ inhibition at S^{2}>10 ↗ # HS with DOM increase Hg solubility ↗↙ ν positive correlation in water, negative in sediment
Methylation to Me_2Hg	?	↗? ¤ increases with high primary production	¤π produced from microbial methylation of Hg^{II} or MeHg	?
Demethylation	↗ ♦ ⱥ increases (possibly less than methylation rate)	↗ ɜ DOM quality influence stability and bioavailability of MeHg complexes. ↗ ◘ NO_3 enhances methylation	↗□ At least two pathways: *Oxidative*, yields Hg^{II} + CO_2 *Reductive*, yields Hg^0 + CH_4	↗ ¤ increases with S^{2-}
Biotic reduction	↗ ʔ $k_{bio.red}$ [d^{-1}] 0.4 % at 9°C 0.8 % at 23°C	?	↗ ʔ $k_{bio.red}$ [% d^{-1}] =0.26 [$B_{abundance}$] + 0.18	?

ɻ(Benoit et al., 1999b); Ƨ(Cossa et al., 2009); #(Gerbig et al., 2011); ƀ (Graham et al., 2012); *(Han et al., 2007); o(Heimbürger et al., 2010); ◘(Hines et al., 2012); ¤(Hollweg et al., 2010); π(Jonsson et al., 2016) ¤(Lehnherr et al., 2011) ♦(Liu et al., 2015); □(Marvin-DiPasquale et al., 2000); ν(Muresan et al., 2007); ʔ(Rolfhus and Fitzgerald, 2004); И(Schaefer et al., 2011; Schaefer and Morel, 2009); ɜ(Schartup et al., 2015b); ⱥ(Ullrich et al., 2001)

Table 2. Environmental controls on biological transformations of Hg species

1.3.2 Distribution patterns of Hg species in water and sediment: a comparative perspective

Concentrations of Hg species are highest in coastal and estuarine ecosystems and decrease toward the open sea due to dilution effect (Tables 3 and 4). In marine water and sediment, Hg^{II} compounds are the most abundant and their spatial distribution depends on atmospheric deposition patterns and on local sources of contamination. The distribution of MeHg and Hg^0 is more affected by biological and physical forcing, but depends also on the amount and sources of Hg_T (natural *vs* anthropogenic).

The fraction of Hg_T as DGM is higher in oceanic water (~15%) than in coastal water (~7%) (Soerensen et al., 2013) and depends on photochemical and biological reduction/demethylation of Hg^{II} and MeHg to Hg^0, as well as on Me_2Hg production at depth. In the sediment, DGM can originate from these biological transformations (see 1.3.2), but also from tectonic activity (Kotnik et al., 2007).

The fraction of Hg as MeHg (%MeHg) is usually higher in intermediate or deep water and is highly variable both in coastal water (3 – 70% of Hg_T) and in the ocean (5 – 15%, up to 80% in Southern Ocean) as summarized in Table 3. The %MeHg in the solid phase within the sediment is much lower, often less than 1% (Table 4).

Water

Mason et al., (2012) reviewed oceanic concentrations of Hg species measured in the last 30 years. Reported Hg_T levels ranges from 0.3 to ~3 pM, while methylated species concentrations (MeHg + Me_2Hg), vary from 20 to 860 fM accounting in most cases for 5 – 15 % of Hg_T; except for high values reported for the Southern Ocean (at depth>1000 m MeHg built up 80% of Hg_T; Cossa et al., 2011).

The vertical variability of Hg^{II} is usually characterized by low Hg_D concentrations in surface water and highest concentrations within or above the thermocline, where particle remineralization is maximum. Different vertical profiles have been observed, due to the uneven temporal distribution of anthropic inputs to surface water and to the effects of local physical drivers (Mason et al., 2012).

MeHg vertical profiles are somewhat more consistent, displaying minimum $MeHg_D$ concentrations in surface water (due to photo-demethylation and uptake by phytoplankton) and maximum concentrations in intermediate low-oxygen water. Concentrations of MeHg in the ocean and in the Mediterranean Sea correlate well to apparent oxygen utilization (AOU) and phosphates concentrations. This *nutrient-like* distribution reflects the release of inorganic Hg^{II} associated with the NOM and its methylation driven by heterotrophic bacterioplankton (Cossa et al., 2011, 2009; Hammerschmidt and Bowman, 2012; Heimbürger et al., 2010; Mason et al., 2012). Because of the biological origin of MeHg, its concentrations are highly variable and their spatial distribution can differ from that of Hg_T (Hammerschmidt and Bowman, 2012; Kotnik et al., 2015). The presence of nano- and picoplankton appear to be conducive to methylation, as the slow sinking velocity of these

small phytoplanktonic cells favor their microbial degradation in the water column (Heimbürger et al., 2010; Monperrus et al., 2007a). Although methylation rates increase with temperature, observations on seasonal variability of MeHg levels in water are somewhat inconsistent (Conaway et al., 2003; Kotnik et al., 2015, 2007; Monperrus et al., 2007a), probably because plankton phenology and post-bloom heterotrophic activity, are much stronger driver than the temperature itself. In coastal sites, MeHg concentrations can be affected by the amount of riverine input, which typically increases with high river flow (Conaway et al., 2003).

By contrast, Hg^0 in surface water exhibits diel and seasonal variability due to the effect of solar radiation. However, the diel course of Hg^0 concentrations is affected by the wind-induced turbulence on surface water, which enhances the gas exchange between the water and the atmosphere (Andersson et al., 2007; Costa and Liss, 2000; Fantozzi et al., 2007; Monperrus et al., 2007a). Water mixing, downwelling and upwelling also contribute to the redistribution of Hg species in the water column and to their oceanic transport (Bowman et al., 2015; Fantozzi et al., 2007).

It has been observed that in polluted systems the speciation of Hg seems to be shifted toward higher %DGM and lower %MeHg (Kotnik et al., 2015).

	Hg_T pM	Hg_D pM	MeHg pM	Hg^0 pM	Me_2Hg pM	MeHg%
Ocean	♦ 0.3 – 3	? >90% of Hg_T	♦ 0.02 – 0.5	∋ 0.05 – 0.4 ◘ 0.02 – 0.25	♦ 0.02 – 0.8	♦ 5 – 15% 80% deep Sothern Ocean
Mediterranean						
Alboran Sea	§1.1 (0.6 – 1.5) *highest at surface*	n.a.	§ 0.18 (0.09 – 0.25) *highest at bottom*	§ 0.3 0.14 – 0.5 *highest at bottom*	§ <0.001	§ 18% (6 – 32%)
SW Basin	§ 1.7 (0.5 – 2.5) ф 0.75 – 1.4 *Algerian Sea*	ф 0.2 – 0.36	§ 0.13 (0.07 – 0.21) *spring > than summer* ф 0.2 - 0.36	§ 0.27 (0.24 – 0.29) ф DGM 0.1 -0.27	§ 0.004 (0.001 – 0.008) ф 0.02	§ 7% (3 – 11%) ф 26%
NW Basin	§ 0.6 (0.4 – 1.1) ў 1 – 1.7 *Gulf of Lion*	n.a.	§ 0.08 (0.05 – 0.12) И 0.3 (0.04 – 0.82) *Ligurian Sea*	§ 0.26 (0.1 - 0.4) v DGM 0.06 – 0.09 *Sardinian Sea*	n.a.	§ 5% – 23%
Tirrenian	§ 1.2 (0.9 – 1.8)	n.a.	§ 0.3 (0.1 – 0.46)	§ 0.19 (0.08 – 0.33)	§ 0.005 (0.002 – 0.012)	§ 26% (6 – 50%)

Ionian Sea	ẞ 1.5 (1 – 1.9) ƀ 0.9 *March* –1.7 *Aug* o 4.5 (1.5 –17) *Sep*	o 3.3 (1– 10)	ẞ 0.35 (0.18 – 0.66) ƀ 0.6 - 0.7	ẞ 0.26 (0.13 – 0.38) ƀ DGM 0.2 *March* – 0.46 *Aug* o DGM 0.08 – 0.2 *Sep*	ƀ 0.06 *March* – 0.1 *Aug*	ẞ 24% (14 – 43%) ƀ 40% *Aug* – 70% *March*
Adriatic Sea	ƨ 3.3 (0.8 – 6.9)		ƨ 0.6 (0.12 – 2.5) *summer – autumn no sign. diff.*	ƨ DGM 0.28 (0.1 – 1.1) *summer – autumn no sign. diff.*	ƨ 0.005 – 0.029	ƨ 3 – 72%
Polluted sites						
Gulf of Trieste	ƨ 4.5 – 6.9 ṁ <0.2 – 70	ṁ 0.9 – 24	ƨ 0.46–0.68 ṁ <0.001 – 0.3	ƨ DGM 0.5 – 0.98	*n.a.*	ƨ 6 – 12% ṁ 0.001 – 0.6%
Venice Lagoon	ɣ 15 – 145	ɣ 5 –16	ɣ 0.13 – 1	*n.a.*	*n.a.*	ɣ 0.22 – 1%
Marano-Grado Lagoon	□ 39 *model*	□20–80	□ 0.25 *model*	0.29 *model*	*n.a.*	□ 0.64%
Thau Lagoon	ẞ 3.4 (1.9 – 4.4)	ẞ 2.4 (1.4 – 3.3)	ẞ 0.36 (0.18 – 0.53)	ẞ DGM 0.3 (0.08 – 0.58)		ẞ 8 – 13%
Augusta bay	*< 9 – 130	*n.a.*	*n.a.*	*n.a.*	*n.a.*	*n.a.*
S. Francisco estuary	ʒ 0.73 – 440	ʒ 0.4 – 170	ʒ 0.1 – 1.3	ʒ DGM 0.9 (0.1– 2.7)	*n.a.*	ʒ <0.001 – 5%

ɣBloom et al., (2004); ʔBowman et al., (2015); ʒConaway et al., (2003); ɣ̃Cossa et al., (2012); ṁFaganeli et al., (2003); oFantozzi et al., (2013); vGårdfeldt et al., (2003); ИHeimbürger et al., (2010); ƨKotnik et al., (2015); ẞKotnik et al., (2007); ♦Mason et al., (2012); □Melaku Canu et al., (2015); ƀMonperrus et al., (2007a);

*Salvagio Manta et al., (2016); ◘Soerensen et al., (2013); ɜSoerensen et al., (2010)

Table 3. Observed concentrations of Hg species in water across ecosystems

Sediment

The spatial correlation between Hg_T and MeHg in the sediment is often poor, and many studies have been devoted to identifying major biogeochemical controls of methylation and MeHg distribution in sediment (e.g. Acquavita et al., 2012; Hammerschmidt et al., 2004; Han et al., 2008; Schartup et al., 2013; Sunderland et al., 2006). In small-scale studies, the spatial distribution of Hg_P often relates to that of POM, and an inverse relationship between methylation and POM was observed at some sites. Therefore, it was hypothesized that POM, by increasing the amount of Hg in the solid phase (hereon partition coefficient, $K_D=\frac{[Hg_P]}{[Hg_D]}$, in L/kg), would have hindered methylation (e.g. Hammerschmidt et al., 2004). However, such a relation was not observed in larger scale studies (Ogrinc et al., 2007; Schartup et al., 2013). Schartup et al., (2013) reanalyzed data from previous studies and expanded the dataset to a broader geographic area and contamination range, finding no correlation between K_D, POM content and methylation. Rather, methylation rates tended to increase at higher POM levels and lower Hg_P/POM ratios. The authors proposed that the quality of POM and DOM are more important factors than POM abundance in controlling Hg partitioning, and Schartup et al., (2014) identified total sulfur content of NOM as best proxy for K_D, owing to the high affinity of Hg to organosulfur compounds. By integrating data from freshwater and marine sediment in contaminated and pristine sites, Cossa et al., (2014) concluded that the relation between Hg_T and MeHg follows a Michaelis–Menten type curve, limited by availability of labile organic substrates. The authors also highlight that %MeHg in sediment is lower with higher Hg_T levels.

$MeHg_P$ vertical profiles in sediment are generally enriched at surface or subsurface, where also methylation rates are maximum. This vertical distribution have been attributed to the build-up of sulfides at depth that causes precipitation of HgS/FeS and modifies the speciation of Hg_D^{II} compounds reducing their bioavailability to bacteria (Benoit et al., 2001, 1999a, 1999b). However there is some evidence of methylation or high MeHg concentrations at high sulfide levels, and it has been pointed out that the depth of maximum sediment methylation is also coincident with the zone of greatest activity of sulfate reducing bacteria (which are well known methylating organisms), where a rapid cycling of labile OM occurs. Thus, the reason behind the decrease of methylation rates with depth would be the lack of electron donor for the microbial metabolism rather than the limited bioavailability of Hg_D^{II} compounds (see Merritt and Amirbahman, 2009 and chapter 4 of this work).

	Hg_T nmol g	$MeHg_T$ pmol/g	%MeHg Sed	Hg_D nM	$MeHg_D$ pM	Pore-water %MeHg	log K_D Hg	log K_D MeHg
Ocean	♦ *0.03 – 0.34*	♦ 0.4 – 5	♦ 0.7 – 1.7%	♦ 0.008 - 0.043	♦ 0.2 - 6.6	♦ 0.9 - 34%	♦3.2 - *4.5*	♦1.79 – 4.16
Mediterranean								
Adriatic Sea	*o 0.02 – 3.5*	*n.a.*	*n.a.*	*o 0.003 – 0.3*	*o0.2 – 17*	*o1.2 – 62%*	*n.a.*	*n.a.*
Other basins	ν *0.06 - 2.23*	ν *0.37 – 14.8*	*ν* 2%	ν *0.08 – 3*	ν *10 – 300*	ν 5 – 25%	*ν 1.85 – 3.64*	*ν 0.98 – 2.37*
Polluted sites								
Gulf of Trieste	ϕ1 – 157	ϕ 0.5 - 23	ϕ 0.01 – 0.02%	ϕ 0.015 – 0.2	ϕ 0.9 – 9	ϕ 1 – 6%	ϕ 6 – 7.7	ϕ 2 – 4.1
Venice	∂ 1 – 30 ጠ 1 – 6	∂ 2 – 11 ጠ 0.5 – 7.9	∂ 0.45% ጠ 0.04 - 0.1%	∂ 25 – 200 ጠ 0.02 – 0.15	∂ 0.2 – 7.5 ጠ 0.2 – 15	ጠ 4.3%	ጠ 4.56 – 5.01	∂ 6.3 – 6.89 ጠ 1.96 – 3.3
Marano-Grado Lagoon	* 3 – 50	* 2.3 – 40	* 0.01 – 0.3%	^ 39 – 2000	^ 0.8 - 11	^ 0.1 – 20%	^ 3.34 – 5.6	^2.84 – 4.11
Augusta Bay	0.5 – 2000	*n.a.*	*n.a.*	*n.a.*	*n.a.*	*n.a.*	*n.a.*	*n.a.*
Thau lagoon	ϗ 1.7 – 2.3	ϗ 0.35 – 13	ϗ 0.02 – 0.8%	ϗ 15 – 85	ϗ 0.5 – 2.5	ϗ 3 –15%	ϗ 4.92	ϗ 2.96 - 4.63
S. Francisco estuary	϶ 1 (0.1– 2.8)	϶ 2 (0.5 – 5)	϶ <0.1 – 1.8%	-	-	-	-	-

* Acquavita et al., (2012); ϶ Conaway et al., (2003); ^ Emili et al., (2012); ϕ Faganeli et al., (2014); ∂ Guédron et al., 2012); ጠ (Han et al., 2008, 2007); ♦ Hollweg et al., (2010); o Kotnik et al., (2015); ϗMuresan et al., (2007); ν (Ogrinc et al., 2007)

Table 4. Observed concentrations of Hg species in sediment across ecosystems.

Biota

Marine phytoplankton take-up Hg^{II} and MeHg from water and this process results in a bioaccumulation factor of $10^{3.5-4.2}$ ($BAF_{Hg} = \frac{[Hg_{biota\ w.w.}]}{[Hg_{water}]}$ or $BAF_{MeHg} = \frac{[MeHg_{biota\ w.w.}]}{[MeHg_{water}]}$, L/kg).

At higher trophic levels, MeHg is assimilated from food sources and slowly removed from the body, whereas Hg^{II} is poorly assimilated. Therefore, along trophic webs there is a progressive increase of BAF (up to 10^7 in top predators) and of %MeHg in biological tissues, which is called biomagnification (Faganeli et al., 2014; Hammerschmidt and Fitzgerald, 2006; Horvat et al., 2014; Mason et al., 2012). Concentrations of MeHg in individuals increase with age (i.e. weight, length), and the species-specific biomagnification power depends on the habitat, feeding preference and metabolic features such as the growth rate (Bonsignore et al., 2013; Cossa et al., 2012; Giani et al., 2012; Horvat et al., 2014).

Pelagic fish of the Mediterranean Sea have higher Hg levels than that of Atlantic Ocean (Cossa and Coquery, 2005); a comparative study on hakes attributed the differences to the shallower thermohalocline (that is a site of high methylation) in the Mediterranean Sea and to the slower growth rate of the Mediterranean hake compared to the Atlantic hake. The study also pointed out that biomagnification power increases in adult specimens because of a shift of their feeding habits from crustaceans and benthos to pelagic prey fish (Cossa et al., 2012). Moreover, despite lower Hg_T water concentrations offshore, bioaccumulation was higher in specimens captured offshore than in those captured inshore, suggesting lower MeHg levels (not assessed) or bioavailability near-shore. MeHg bioavailability can be a critical factor, as shown in a study performed at Long Island Sound where, despite highest MeHg concentrations in coastal water, bioaccumulation was highest in plankton sampled in offshore water. The increased MeHg bioavailability offshore was attributed to the decreasing content and ageing of terrestrial OM (Schartup et al., 2015b).

1.4 Biogeochemical Models of Hg cycling

Different research groups have implemented a number of biogeochemical models for simulating Hg cycling in marine systems at global, regional and ecosystem scale (Amos et al., 2014; Canu and Rosati, 2017; Driscoll et al., 2012; Melaku Canu et al., 2015; Schartup et al., 2015a; Soerensen et al., 2016a, 2016b, 2010; Y. Zhang et al., 2014; Zhang et al., 2015). These efforts have been devoted to: 1) reconcile the observed environmental Hg concentrations or transfer rates with the processes that have determined them; 2) use observational data limited in space and time to extrapolate a broader picture; 3) estimate Hg exposure for humans and wildlife; 4) explore the effects of remediation actions; 5) provide forecasts of long term evolution of a given system; 6) test assumptions about processes; 7) highlight research gaps and needs.

Although the modeling of marine Hg has been carried out with different levels of complexity and spatial resolutions, the fundamental structure of the models is similar. It relies on the use of reaction coefficients to parametrize transformations assuming first order kinetics; on the use of partition coefficients (K_D, L/kg) to describe the distribution of Hg species among dissolved and particulate compounds; and on the use of advective water fluxes, coefficients and empirical relations to parametrize transport processes. Transport processes involving particulate and dissolved Hg species in water and sediment (i.e. advective transport, settling, resuspension, burial, evasion) are expounded in section 1.3.1, whilst transformations processes (i.e. photo-reduction, photo-oxidation, photo-demethylation and microbial methylation and demethylation) are introduced in section 1.3.2. A comprehensive representation of the cycle is given in Figure 1.

One of the key uncertainties in the modeling of Hg cycle is the estimate of Hg^0 evasion from water, due to a lack of mechanistic understanding of photoreactions that produce DGM, and to uncertainties in the parametrization of the gas exchange transfer processes induced by wind (AMAP/UNEP, 2013; Melaku Canu et al., 2015; Sharif et al., 2013; Soerensen et al., 2013; Zhang et al., 2014). Photochemical transformations are parameterized as first order reactions limited by light availability (which is in turn a function of solar irradiation at surface, depth and attenuation coefficient). It is generally assumed that photo-reduction involve only a fraction of Hg^{II} (reducible pool) because some Hg^{II} complexes appear to be refractory to reduction due to stabilization by Cl^- or by allochthonous DOM ligands, however the effects of DOM composition on Hg reducible pool are still not clear (Soerensen et al., 2013, 2010). The use of different parametrization for gas exchange lead to a 30% difference in evasion rates, and the variability induced by the use of different Hg^0 concentrations and wind speed is about 300% (Soerensen et al., 2013).

Another issue is the use of partition coefficients (K_D) to parametrize the distribution of Hg species among dissolved and particulate compounds, which is related to the composition of sediments (or suspended solids) and shows huge spatial and seasonal variability (see Table 4 and reference therein). In oceanic models only organic solids are relevant, and the K_D values of Hg and MeHg to POM are assumed to be constant in space and time (Soerensen et al., 2010; Y. Zhang et al., 2014).

In the box model used within this manuscript (WASP model, Wool et al., 2001), the K_D coefficients for Hg and MeHg are computed as the weighted mean of independent K_D coefficients specified for each modelled solid component (silts-clays, sands, POM). Therefore, by changing the sediment composition in space (which can be done through initial conditions) and in time (which can be done through the parametrization of POM production and degradation) it is possible to induce slight variations of the overall K_D. However, the values of K_D coefficients for the single solid components (silts-clays, sands, POM) cannot differ among boxes.

Diffusion from pore-water has been identified as another process that needs to be better addressed, due to its relevance in shallow environments. Research has found that in bioturbated sediment, the estimate of fluxes assuming passive diffusion driven by Fick's law can lead to substantial underestimation of the diffusive fluxes observed in the field (Benoit et al., 2009; Emili et al., 2012).

The synthesis presented in this chapter has highlighted the importance of biological processes in the cycling of Hg. The most recent evidence suggests that there is a need to take a further step in the modeling of Hg cycling, toward an integration with biogeochemical models that simulate the cycle of NOM and its remineralization in water column and sediment. A first modeling study toward this direction has been recently performed in the Baltic Sea (Soerensen et al., 2016b). The quality of NOM must be taken into account, discerning at least between a labile and a refractory pool, because it affects many aspects of the Hg cycle by:

1) influencing the partition of Hg and MeHg (especially organosulfur compounds) and thus their transport and bioavailability (e.g. Schartup et al., 2013);
2) enhancing bacterial Hg uptake and methylation rates due to induction of cellular active transport mechanisms (some kind of thiols, whilst other inhibit the processes, Schaefer et al., 2011);
3) mediating photochemical mechanisms in surface water, due to the action of chromophoric DOM that produces extremely reactive free radicals (e.g. Lalonde et al., 2004; Rolfhus and Fitzgerald, 2004);
4) fuelling or limiting the activity of bacterial community (Cossa et al., 2014);
5) conditioning MeHg bioavailability to phytoplankton (Schartup et al., 2015b)

1.5 References

Acquavita, A., Covelli, S., Emili, A., Berto, D., Faganeli, J., Giani, M., Horvat, M., Koron, N., Rampazzo, F., 2012. Mercury in the sediments of the Marano and Grado Lagoon (northern Adriatic Sea): Sources, distribution and speciation. Estuar. Coast. Shelf Sci. 113, 20–31. doi:10.1016/j.ecss.2012.02.012

AMAP/UNEP, 2013. Technical Background Report for the Global Mercury Assessment 2013. Oslo, Norway / UNEP ChemicalsBranch, Geneva, Switzerland.

Amos, H.M., Jacob, D.J., Kocman, D., Horowitz, H.M., Zhang, Y., Dutkiewicz, S., Horvat, M., Corbitt, E.S., Krabbenhoft, D.P., Sunderland, E.M., 2014. Global biogeochemical implications of mercury discharges from rivers and sediment burial. Environ. Sci. Technol. 48, 9514–9522. doi:10.1021/es502134t

Amos, H.M., Jacob, D.J., Streets, D.G., Sunderland, E.M., 2013. Legacy impacts of all-time anthropogenic emissions on the global mercury cycle. Global Biogeochem. Cycles 27, 410–421. doi:10.1002/gbc.20040

Amos, H.M., Sonke, J.E., Obrist, D., Robins, N., Hagan, N., Horowitz, H.M., Mason, R.P., Witt, M., Hedgecock, I.M., Corbitt, E.S., Sunderland, E.M., 2015. Observational and modeling constraints on global anthropogenic enrichment of mercury. Environ. Sci. Technol. 49, 4036–4047. doi:10.1021/es5058665

Andersson, M.E., Gårdfeldt, K., Wängberg, I., Sprovieri, F., Pirrone, N., Lindqvist, O., 2007. Reprint of "Seasonal and daily variation of mercury evasion at coastal and off shore sites from the Mediterranean Sea." Mar. Chem. 107, 104–116. doi:10.1016/j.marchem.2007.06.020

Barkay, T., Miller, S.M., Summers, A.O., 2003. Bacterial mercury resistance from atoms to ecosystems. FEMS Microbiol. Rev. 27, 355–384. doi:10.1016/S0168-6445(03)00046-9

Benoit, J.M., Gilmour, C.C., Mason, R.P., 2001. Aspects of bioavailability of mercury for methylation in pure cultures of Desulfobulbus propionicus (1pr3). Appl. Environ. Microbiol. 67, 51–58. doi:10.1128/AEM.67.1.51-58.2001

Benoit, J.M., Gilmour, C.C., Mason, R.P., Heyes, A., 1999a. Sufide Controls on Bioavailability to Methylating Bacteria in Sediment Pore Waters. Environ. Sci. Technol. 33, 951–957.

Benoit, J.M., Mason, R.P., Gilmour, C.C., 1999b. Estimation of mercury-sulfide speciation in sediment pore waters using octanol-water partitioning and implications for availability to methylating bacteria. Environ. Toxicol. Chem. 18, 2138–2141. doi:10.1002/etc.5620181004

Benoit, J.M., Shull, D.H., Harvey, R.M., Beal, S.A., 2009. Effect of bioirrigation on sediment - water exchange of methylmercury in Boston Harbour, Massachusetts. Environ. Sci. Technol. 3669–3674.

Black, F.J., Poulin, B.A., Flegal, A.R., 2012a. Factors controlling the abiotic photo-degradation of monomethylmercury in surface waters. Geochim. Cosmochim. Acta 84, 492–507. doi:10.1016/j.gca.2012.01.019

Black, F.J., Poulin, B.A., Flegal, A.R., 2012b. Factors controlling the abiotic photo-degradation of monomethylmercury in surface waters. Geochim. Cosmochim. Acta 84, 492–507. doi:10.1016/j.gca.2012.01.019

Bloom, N.S., Moretto, L.M., Scopece, P., Ugo, P., 2004. Seasonal cycling of mercury and monomethyl mercury in the Venice Lagoon (Italy). Mar. Chem. 91, 85–99. doi:10.1016/j.marchem.2004.06.002

Bonsignore, M., Salvagio Manta, D., Oliveri, E., Sprovieri, M., Basilone, G., Bonanno, A., Falco,

F., Traina, A., Mazzola, S., 2013. Mercury in fishes from Augusta Bay (southern Italy): Risk assessment and health implication. Food Chem. Toxicol. 56, 184–194. doi:10.1016/j.fct.2013.02.025

Bouchet, S., Amouroux, D., Rodriguez-Gonzalez, P., Tessier, E., Monperrus, M., Thouzeau, G., Clavier, J., Amice, E., Deborde, J., Bujan, S., Grall, J., Anschutz, P., 2013. MMHg production and export from intertidal sediments to the water column of a tidal lagoon (Arcachon Bay, France). Biogeochemistry 114, 341–358. doi:10.1007/s10533-012-9815-z

Bowman, K.L., Hammerschmidt, C.R., Lamborg, C.H., Swarr, G., 2015. Mercury in the North Atlantic Ocean: The U.S. GEOTRACES zonal and meridional sections. Deep. Res. Part II Top. Stud. Oceanogr. 116, 251–261. doi:10.1016/j.dsr2.2014.07.004

Canu, D., Rosati, G., 2017. Long-term scenarios of mercury budgeting and exports for a Mediterranean hot spot (Marano-Grado Lagoon, Adriatic Sea). Estuar. Coast. Shelf Sci. 1–11. doi:10.1016/j.ecss.2016.12.005

Choe, K.-Y., Gill, G.A., Lehman, R., 2003. Distribution of particulate, colloidal, and dissolved mercury in San Francisco Bay estuary. 1. Total mercury. Limnol. Oceanogr. 48, 1535–1546. doi:10.4319/lo.2003.48.4.1547

Conaway, C.H., Squire, S., Mason, R.P., Flegal, A.R., 2003. Mercury speciation in the San Francisco Bay estuary. Mar. Chem. 80, 199–225. doi:http://dx.doi.org/10.1016/S0304-4203(02)00135-4

Cossa, D., Averty, B., Pirrone, N., 2009. The origin of methylmercury in open Mediterranean waters. Limnol. Oceanogr. 54, 837–844. doi:10.4319/lo.2009.54.3.0837

Cossa, D., Coquery, M., 2005. The Mediterranean Mercury Anomaly, a Geochemical or a Biologocal Issue, in: Saliot, A. (Ed.), The Mediterranean Sea. Springer Berlin Heidelberg, Berlin, Heidelberg, pp. 177–208. doi:10.1007/b107147

Cossa, D., Garnier, C., Buscail, R., Elbaz-Poulichet, Francoise Mikac, N., Patel-Sorrentino, Nathalie Tessier, E., Rigaud, S., Lenoble, V., Gobeil, C., 2014. A Michaelis–Menten type equation for describing methylmercury dependence on inorganic mercury in aquatic sediments. Biogeochemistry 119, 35–43.

Cossa, D., Harmelin-Vivien, M., Mellon-Duval, C., Loizeau, V., Averty, B., Crochet, S., Chou, L., Cadiou, J.-F., 2012. Influences of bioavailability, trophic position, and growth on methylmercury in hakes (Merluccius merluccius) from Northwestern Mediterranean and Northeastern Atlantic. Environ. Sci. Technol. 46, 4885–93. doi:10.1021/es204269w

Cossa, D., Heimbürger, L.E., Lannuzel, D., Rintoul, S.R., Butler, E.C. V, Bowie, A.R., Averty, B., Watson, R.J., Remenyi, T., 2011. Mercury in the Southern Ocean. Geochim. Cosmochim. Acta 75, 4037–4052. doi:10.1016/j.gca.2011.05.001

Costa, M., Liss, P., 2000. Photoreduction and evolution of mercury from seawater. Sci. Total Environ. 261, 125–135. doi:10.1016/S0048-9697(00)00631-8

Covelli, S., Piani, R., Acquavita, A., Predonzani, S., Faganeli, J., 2007. Transport and dispersion of particulate Hg associated with a river plume in coastal Northern Adriatic environments. Mar. Pollut. Bull. 55, 436–450. doi:10.1016/j.marpolbul.2007.09.006

Deonarine, A., Hsu-Kim, H., 2009. Precipitation of Mercuric Sulfide Nanoparticles in NOM-Containing Water: Implications for the Natural Environment. Environ. Sci. Technol. 43, 2368–2373. doi:10.1021/es803130h

Driscoll, C.T., Hammerschmidt, C.R., Gilmour, C.C., Greenfield, B.K., Buckman, K.L., Lamborg, C.H., 2012. Nutrient supply and mercury dynamics in marine ecosystems: A conceptual

model. Environ. Res. 119, 118–131. doi:10.1016/j.envres.2012.05.002

Driscoll, C.T., Mason, R.P., Chan, H.M., Jacob, D.J., Pirrone, N., 2013. Mercury as a Global Pollutant: Sources, Pathways, and Effects. Environ. Sci. Technol. 47, 4967–4983. doi:10.1021/es305071v

Emili, A., Acquavita, A., Koron, N., Covelli, S., Faganeli, J., Horvat, M., Žižek, S., Fajon, V., 2012. Benthic flux measurements of Hg species in a northern Adriatic lagoon environment (Marano and Grado Lagoon, Italy). Estuar. Coast. Shelf Sci. 113, 71–84. doi:10.1016/j.ecss.2012.05.018

Emili, a, Carrasco, L., Acquavita, a, Covelli, S., 2014. A laboratory-incubated redox oscillation experiment to investigate Hg fluxes from highly contaminated coastal marine sediments (Gulf of Trieste, Northern Adriatic Sea). Environ. Sci. Pollut. Res. Int. 21, 4124–33. doi:10.1007/s11356-013-2225-5

Faganeli, J., Hines, M.E., Horvat, M., Falnoga, I., Covelli, S., 2014. Methylmercury in the gulf of trieste (Northern Adriatic sea): From microbial sources to seafood consumers. Food Technol. Biotechnol. 52, 188–197.

Faganeli, J., Horvat, M., Covelli, S., Fajon, V., Logar, M., Lipej, L., Cermelj, B., 2003. Mercury and methylmercury in the Gulf of Trieste (northern Adriatic Sea). Sci Total Env. 304, 315–326. doi:S0048-9697(02)00578-8 [pii]\r10.1016/S0048-9697(02)00578-8

Fantozzi, L., Ferrara, R., Frontini, F.P., Dini, F., 2007. Factors influencing the daily behaviour of dissolved gaseous mercury concentration in the Mediterranean Sea. Mar. Chem. 107, 4–12. doi:10.1016/j.marchem.2007.02.008

Fantozzi, L., Manca, G., Ammoscato, I., Pirrone, N., Sprovieri, F., 2013. The cycling and sea-air exchange of mercury in the waters of the Eastern Mediterranean during the 2010 MED-OCEANOR cruise campaign. Sci. Total Environ. 448, 151–162. doi:10.1016/j.scitotenv.2012.09.062

Gårdfeldt, K., Sommar, J., Ferrara, R., Ceccarini, C., Lanzillotta, E., Munthe, J., Wängberg, I., Lindqvist, O., Pirrone, N., Sprovieri, F., Pesenti, E., Strömberg, D., 2003. Evasion of mercury from coastal and open waters of the Atlantic Ocean and the Mediterranean Sea. Atmos. Environ. 37, 73–84. doi:10.1016/S1352-2310(03)00238-3

Gencarelli, C.N., De Simone, F., Hedgecock, I.M., Sprovieri, F., Yang, X., Pirrone, N., 2015. European and Mediterranean mercury modelling: Local and long-range contributions to the deposition flux. Atmos. Environ. 117, 162–168. doi:10.1016/j.atmosenv.2015.07.015

Gerbig, C.A., Kim, C.S., Stegemeier, J.P., Ryan, J.N., Aiken, G.R., 2011. Formation of nanocolloidal metacinnabar in mercury-DOM-sulfide systems. Environ. Sci. Technol. 45, 9180–9187. doi:10.1021/es201837h

Giani, M., Rampazzo, F., Berto, D., Maggi, C., Mao, A., Horvat, M., Emili, A., Covelli, S., 2012. Bioaccumulation of mercury in reared and wild Ruditapes philippinarum of a Mediterranean lagoon. Estuar. Coast. Shelf Sci. 113, 116–125. doi:10.1016/j.ecss.2012.05.031

Graham, A.M., Aiken, G.R., Gilmour, C.C., 2012. Dissolved organic matter enhances microbial mercury methylation under sulfidic conditions. Environ. Sci. Technol. 46, 2715–2723. doi:10.1021/es203658f

Guédron, S., Huguet, L., Vignati, D.A.L., Liu, B., Gimbert, F., Ferrari, B.J.D., Zonta, R., Dominik, J., 2012. Tidal cycling of mercury and methylmercury between sediments and water column in the Venice Lagoon (Italy). Mar. Chem. 130–131, 1–11. doi:10.1016/j.marchem.2011.12.003

Hammerschmidt, C.R., Bowman, K.L., 2012. Vertical methylmercury distribution in the subtropical

North Pacific Ocean. Mar. Chem. 132–133, 77–82. doi:10.1016/j.marchem.2012.02.005

Hammerschmidt, C.R., Fitzgerald, W.F., 2006. Bioaccumulation and Trophic Transfer of Methylmercury in Long Island Sound. Arch. Environ. Contam. Toxicol. 51, 416–424. doi:10.1007/s00244-005-0265-7

Hammerschmidt, C.R., Fitzgerald, W.F., Lamborg, C.H., Balcom, P.H., Visscher, P.T., 2004. Biogeochemistry of methylmercury in sediments of Long Island Sound. Mar. Chem. 90, 31–52. doi:10.1016/j.marchem.2004.02.024

Han, S., Obraztsova, A., Pretto, P., Choe, K.-Y., Gieskes, J., Deheyn, D.D., Tebot, B.M., 2007. Biogeochemical factors affecting mercury methylation in sediments of the Venice Lagoon, Italy. Environ. Toxicol. Chem. 26, 655–63. doi:10.1897/06-392R.1

Han, S., Obraztsova, A., Pretto, P., Deheyn, D.D., Gieskes, J., Tebo, B.M., 2008. Sulfide and iron control on mercury speciation in anoxic estuarine sediment slurries. Mar. Chem. 111, 214–220. doi:10.1016/j.marchem.2008.05.002

Heimbürger, L.-E., Cossa, D., Marty, J.-C., Migon, C., Averty, B., Dufour, A., Ras, J., 2010. Methyl mercury distributions in relation to the presence of nano- and picophytoplankton in an oceanic water column (Ligurian Sea, North-western Mediterranean). Geochim. Cosmochim. Acta 74, 5549–5559. doi:10.1016/j.gca.2010.06.036

Heimbürger, L.-E., Sonke, J.E., Cossa, D., Point, D., Lagane, C., Laffont, L., Galfond, B.T., Nicolaus, M., Rabe, B., van der Loeff, M.R., 2015. Shallow methylmercury production in the marginal sea ice zone of the central Arctic Ocean. Sci. Rep. 5, 10318.

Hines, M.E., Poitras, E.N., Covelli, S., Faganeli, J., Emili, A., Žižek, S., Horvat, M., 2012. Mercury methylation and demethylation in Hg-contaminated lagoon sediments (Marano and Grado Lagoon, Italy). Estuar. Coast. Shelf Sci. 113, 85–95. doi:10.1016/j.ecss.2011.12.021

Hollweg, T.A., Gilmour, C.C., Mason, R.P., 2010. Mercury and methylmercury cycling in sediments of the mid-Atlantic continental shelf and slope. Limnol. Oceanogr. 55, 2703–2722. doi:10.4319/lo.2010.55.6.2703

Hollweg, T.A., Gilmour, C.C., Mason, R.P., 2009. Methylmercury production in sediments of Chesapeake Bay and the mid-Atlantic continental margin. Mar. Chem. 114, 86–101. doi:10.1016/j.marchem.2009.04.004

Horowitz, H.M., Jacob, D.J., Amos, H.M., Streets, D.G., Sunderland, E.M., 2014. Historical Mercury Releases from Commercial Products : Global Environmental Implications. Environ. Sci. Technol. 48, 10242–10250. doi:dx.doi.org/10.1021/es501337j

Horvat, M., Degenek, N., Lipej, L., Snoj Tratnik, J., Faganeli, J., 2014. Trophic transfer and accumulation of mercury in ray species in coastal waters affected by historic mercury mining (Gulf of Trieste, northern Adriatic Sea). Environ. Sci. Pollut. Res. 21, 4163–4176. doi:10.1007/s11356-013-2262-0

Hsu-Kim, H., Kucharzyk, K.H., Zhang, T., Deshusses, M.A., 2013. Mechanisms regulating mercury bioavailability for methylating microorganisms in the aquatic environment: A critical review. Environ. Sci. Technol. 47, 2441–2456. doi:10.1021/es304370g

Jonsson, S., Mazrui, N.M., Mason, R.P., 2016. Dimethylmercury Formation Mediated by Inorganic and Organic Reduced Sulfur Surfaces. Sci. Rep. 6, 27958. doi:10.1038/srep27958

Jonsson, S., Skyllberg, U., Nilsson, M.B., Westlund, P., Shchukarev, A., Lundberg, E., Björn, E., 2012. Mercury Methylation Rates for Geochemically Relevant HgII Species in Sediments. Environ. Sci. Technol. 46, 11653−11659.

Kim, M.-K., Won, A.-Y., Zoh, K.-D., 2014. The production of dissolved gaseous mercury from methylmercury photodegradation at different salinity. Desalin. Water Treat. 1–10. doi:10.1080/19443994.2014.986829

Kocman, D., Horvat, M., Pirrone, N., Cinnirella, S., 2013. Contribution of contaminated sites to the global mercury budget. Environ. Res. 125, 160–170. doi:10.1016/j.envres.2012.12.011

Koron, N., Faganeli, J., Falnoga, I., Kovac, N., 2011. Interaction of Macroaggregates and Hg in Coastal Waters (Gulf of Trieste, Northern Adriatic Sea). Geomicrobiol. J. 28, 615–624. doi:10.1080/01490451.2011.576165

Kotnik, J., Horvat, M., Ogrinc, N., Fajon, V., Žagar, D., Cossa, D., Sprovieri, F., Pirrone, N., 2015. Mercury speciation in the Adriatic Sea. Mar. Pollut. Bull. 96, 136–148. doi:10.1016/j.marpolbul.2015.05.037

Kotnik, J., Horvat, M., Tessier, E., Ogrinc, N., Monperrus, M., Amouroux, D., Fajon, V., Gibičar, D., Žižek, S., Sprovieri, F., Pirrone, N., 2007. Mercury speciation in surface and deep waters of the Mediterranean Sea. Mar. Chem. 107, 13–30. doi:10.1016/j.marchem.2007.02.012

Kucharzyk, K.H., Deshusses, M.A., Porter, K.A., Hsu-Kim, H., 2015. Relative contributions of mercury bioavailability and microbial growth rate on net methylmercury production by anaerobic mixed cultures. Environ. Sci. Process. Impacts 17, 1568–1577. doi:10.1039/C5EM00174A

Lalonde, J.D., Amyot, M., Kraepiel, A.M.L., Morel, F.M.M., 2001. Photooxidation of Hg (0) in Artificial and Natural Waters. Environ. Sci. Technol. 35, 1367–1372.

Lalonde, J.D., Amyot, M., Orvoine, J., Morel, F.M.M., Auclair, J.-C., Ariya, P.A., 2004. Photoinduced Oxidation of Hg0(aq) in the Waters from the St. Lawrence Estuary. Environ. Sci. Technol. 38, 508–514. doi:10.1021/es034394g

Lamborg, C.H., Hammerschmidt, C.R., Bowman, K.L., 2016. An examination of the role of particles in oceanic mercury cycling. Philos. Trans. R. Soc. A Math. Phys. Eng. Sci. 374, 20150297. doi:10.1098/rsta.2015.0297

Lamborg, C.H., Yiğiterhan, O., Fitzgerald, W.F., Balcom, P.H., Hammerschmidt, C.R., Murray, J., 2008. Vertical distribution of mercury species at two sites in the Western Black Sea. Mar. Chem. 111, 77–89. doi:10.1016/j.marchem.2007.01.011

Lehnherr, I., St. Louis, V.L., Hintelmann, H., Kirk, J.L., 2011. Methylation of inorganic mercury in polar marine waters. Nat. Geosci. 4, 298–302. doi:10.1038/ngeo1134

Liu, B., Schaider, L. a., Mason, R.P., Shine, J.P., Rabalais, N.N., Senn, D.B., 2015. Controls on methylmercury accumulation in northern Gulf of Mexico sediments. Estuar. Coast. Shelf Sci. 159, 50–59. doi:10.1016/j.ecss.2015.03.030

Marvin-DiPasquale, M., Agee, J., McGowan, C., Oremland, R.S., Thomas, M., Krabbenhoft, D., Gilmour, C.C., 2000. Methyl-Mercury Degradation Pathways: A Comparison among Three Mercury-Impacted Ecosystems. Environ. Sci. Technol. 34, 4908–4916. doi:10.1021/es0013125

Mason, R.P., Choi, A.L., Fitzgerald, W.F., Hammerschmidt, C.R., Lamborg, C.H., Soerensen, A.L., Sunderland, E.M., 2012. Mercury biogeochemical cycling in the ocean and policy implications. Environ. Res. 119, 101–117. doi:10.1016/j.envres.2012.03.013

Melaku Canu, D., Rosati, G., Solidoro, C., Heimbürger, L.-E., Acquavita, A., 2015. A comprehensive assessment of the mercury budget in the Marano–Grado Lagoon (Adriatic Sea) using a combined observational modeling approach. Mar. Chem. 177, 742–752. doi:10.1016/j.marchem.2015.10.013

Merritt, K.A., Amirbahman, A., 2009. Mercury methylation dynamics in estuarine and coastal marine environments - A critical review. Earth-Science Rev. 96, 54–66. doi:10.1016/j.earscirev.2009.06.002

Monperrus, M., Tessier, E., Amouroux, D., Leynaert, A., Huonnic, P., Donard, O.F.X., 2007a. Mercury methylation, demethylation and reduction rates in coastal and marine surface waters of the Mediterranean Sea. Mar. Chem. 107, 49–63. doi:10.1016/j.marchem.2007.01.018

Monperrus, M., Tessier, E., Point, D., Vidimova, K., Amouroux, D., Guyoneaud, R., Leynaert, A., Grall, J., Chauvaud, L., Thouzeau, G., Donard, O.F.X., 2007b. The biogeochemistry of mercury at the sediment-water interface in the Thau Lagoon. 2. Evaluation of mercury methylation potential in both surface sediment and the water column. Estuar. Coast. Shelf Sci. 72, 485–496. doi:10.1016/j.ecss.2006.11.014

Morel, F.M.M., Kraepiel, A.M.L., Amyot, M., 1998. The chemical cycle and bioaccumulation of mercury. Annu. Rev. Ecol. Syst. 29, 543–566. doi:10.1146/annurev.ecolsys.29.1.543

Muresan, B., Cossa, D., D., J., Prévot, F., Kerbellec, S., 2007. The biogeochemistry of mercury at the sediment-water interface in the Thau lagoon. 1. Partition and speciation. Estuar. Coast. Shelf Sci. 72, 472–484. doi:10.1016/j.ecss.2006.11.015

Ogrinc, N., Monperrus, M., Kotnik, J., Fajon, V., Vidimova, K., Amouroux, D., Kocman, D., Tessier, E., Žižek, S., Horvat, M., 2007. Distribution of mercury and methylmercury in deep-sea surficial sediments of the Mediterranean Sea. Mar. Chem. 107, 31–48. doi:http://dx.doi.org/10.1016/j.marchem.2007.01.019

Ortiz, V.L., Mason, R.P., Evan Ward, J., 2015. An examination of the factors influencing mercury and methylmercury particulate distributions, methylation and demethylation rates in laboratory-generated marine snow. Mar. Chem. 177, 753–762. doi:10.1016/j.marchem.2015.07.006

Qureshi, A., O'Driscoll, N.J., Macleod, M., Neuhold, Y.M., Hungerbühler, K., 2010. Photoreactions of mercury in surface ocean water: Gross reaction kinetics and possible pathways. Environ. Sci. Technol. 44, 644–649. doi:10.1021/es9012728

Ravichandran, M., Aiken, G.R., Reddy, M.M., Ryan, J.N., 1998. Enhanced dissolution of cinnabar (mercuric sulfide) by dissolved organic matter isolated from the Florida Everglades. Environ. Sci. Technol. 32, 3305–3311. doi:10.1021/es9804058

Ravichandran, M., Aiken, G.R., Ryan, J.N., Reddy, M.M., 1999. Inhibition of precipitation and aggregation of metacinnabar (HgS) by humic substances isolated from the Florida Everglades. Abstr. Pap. Am. Chem. Soc. 217, 105–ENVR. doi:10.1021/es9811187

Rolfhus, K.R., Fitzgerald, W.F., 2004. Mechanisms and temporal variability of dissolved gaseous mercury production in coastal seawater. Mar. Chem. 90, 125–136. doi:10.1016/j.marchem.2004.03.012

Rolfhus, K.R., Fitzgerald, W.F., 2001. The evasion and spatial/temporal distribution of mercury species\rin Long Island Sound, CT-NY. Geochim. Cosmochim. Acta 65, 407–418.

Salvagio Manta, D., Bonsignore, M., Oliveri, E., Barra, M., Tranchida, G., Giaramita, L., Mazzola, S., Sprovieri, M., 2016. Fluxes and the mass balance of mercury in Augusta Bay (Sicily, southern Italy). Estuar. Coast. Shelf Sci. 181, 134–143. doi:10.1016/j.ecss.2016.08.013

Schaefer, J.K., Morel, F.M.M., 2009. High methylation rates of mercury bound to cysteine by Geobacter sulfurreducens. Nat. Geosci 2, 123–126.

Schaefer, J.K., Rocks, S.S., Zheng, W., Liang, L., Gu, B., Morel, F.M.M.M., Zhang, W., Liang, L., Gu, B., Morel, F.M.M.M., 2011. Active transport, substrate specificity, and methylation of

Hg(II) in anaerobic bacteria. Proc. Natl. Acad. Sci. U. S. A. 108, 8714–8719. doi:10.1073/pnas.1105781108

Schartup, A.T., Balcom, P.H., Mason, R.P., 2014. Sediment-porewater partitioning, total sulfur, and methylmercury production in estuaries. Environ. Sci. Technol. 48, 954–960. doi:10.1021/es403030d

Schartup, A.T., Balcom, P.H., Soerensen, A.L., Gosnell, K.J., Calder, R.S.D., Mason, R.P., Sunderland, E.M., 2015a. Freshwater discharges drive high levels of methylmercury in Arctic marine biota. Proc. Natl. Acad. Sci. 112, 11789–11794. doi:10.1073/pnas.1505541112

Schartup, A.T., Mason, R.P., Balcom, P.H., Hollweg, T. a., Chen, C.Y., 2013. Methylmercury production in estuarine sediments: Role of organic matter. Environ. Sci. Technol. 47, 695–700. doi:10.1021/es302566w

Schartup, A.T., Ndu, U., Balcom, P.H., Mason, R.P., Sunderland, E.M., 2015b. Contrasting effects of marine and terrestrially derived dissolved organic matter on mercury speciation and bioavailability in seawater. Environ. Sci. Technol. 49, 5965–5972. doi:10.1021/es506274x

Sharif, A., Monperrus, M., Tessier, E., Bouchet, S., Pinaly, H., Rodriguez-Gonzalez, P., Maron, P., Amouroux, D., 2014. Fate of mercury species in the coastal plume of the Adour River estuary (Bay of Biscay, SW France). Sci. Total Environ. 496, 701–713. doi:10.1016/j.scitotenv.2014.06.116

Sharif, A., Tessier, E., Bouchet, S., Monperrus, M., Pinaly, H., Amouroux, D., 2013. Comparison of Different Air–Water Gas Exchange Models to Determine Gaseous Mercury Evasion from Different European Coastal Lagoons and Estuaries. Water, Air, Soil Pollut. 224, 1606. doi:10.1007/s11270-013-1606-1

Skyllberg, U., 2008. Competition among thiols and inorganic sulfides and polysulfides for Hg and MeHg in wetland soils and sediments under suboxic conditions: Illumination of controversies and implications for MeHg net production. J. Geophys. Res. 113, 1–14. doi:10.1029/2008JG000745

Slowey, A.J., 2010. Rate of formation and dissolution of mercury sulfide nanoparticles: The dual role of natural organic matter. Geochim. Cosmochim. Acta 74, 4693–4708. doi:http://dx.doi.org/10.1016/j.gca.2010.05.012

Soerensen, A.L., Jacob, D.J., Schartup1, A.T., Fisher, J.A., Lehnherr, I., St. Louis, V.L., Heimbürger, L.-E., Sonke, J.E., Krabbenhoft, D.P., Sunderland, E.M., 2016a. A mass budget for mercury and methylmercury in the Arctic Ocean. Global Biogeochem. Cycles 30, 560–575. doi:10.1002/2015GB005280.Received

Soerensen, A.L., Mason, R.P., Balcom, P.H., Sunderland, E.M., 2013. Drivers of Surface Ocean Mercury Concentrations and Air–Sea Exchange in the West Atlantic Ocean. Environ. Sci. Technol. 47, 7757–7765. doi:10.1021/es401354q

Soerensen, A.L., Schartup, A.T., Gustafsson, E., Gustafsson, B.G., Undeman, E., Björn, E., 2016b. Eutrophication Increases Phytoplankton Methylmercury Concentrations in a Coastal Sea—A Baltic Sea Case Study. Environ. Sci. Technol. acs.est.6b02717. doi:10.1021/acs.est.6b02717

Soerensen, A.L., Sunderland, E.M., Holmes, C.D., Jacob, D.J., Yantosca, R.M., Skov, H., Christensen, J.H., Strode, S. a., Mason, R.P., 2010. An improved global model for air-sea exchange of mercury: High concentrations over the North Atlantic. Environ. Sci. Technol. 44, 8574–8580. doi:10.1021/es102032g

Sunderland, E.M., Gobas, F.A.P.C., Branfireun, B.A., Heyes, A., 2006. Environmental controls on the speciation and distribution of mercury in coastal sediments. Mar. Chem. 102, 111–123.

doi:10.1016/j.marchem.2005.09.019

Sunderland, E.M., Krabbenhoft, D.P., Moreau, J.W., Strode, S.A., Landing, W.M., 2009. Mercury sources, distribution, and bioavailability in the North Pacific Ocean: Insights from data and models. Global Biogeochem. Cycles 23, 1–14. doi:10.1029/2008GB003425

Ullrich, S.M., Tanton, T.W., Svetlana, A., 2001. Mercury in the Aquatic Environment : A Review of Factors Affecting Methylation 31, 241–293.

Waples, J.S., Nagy, K.L., Aiken, G.R., Ryan, J.N., 2005. Dissolution of cinnabar (HgS) in the presence of natural organic matter. Geochim. Cosmochim. Acta 69, 1575–1588. doi:10.1016/j.gca.2004.09.029

Whalin, L., Kim, E.-H., Mason, R., 2007. Factors influencing the oxidation, reduction, methylation and demethylation of mercury species in coastal waters. Mar. Chem. 107, 278–294. doi:10.1016/j.marchem.2007.04.002

Wool, T.A., Ambrose, R.B., Martin, J.L., Comer, E.A., 2001. Water Quality Analysis Simulation Program (WASP) Version 6.0: User's Manual.

Zhang, T., Kim, B., Levard, C., Reinsch, B.C., Lowry, G. V., Deshusses, M.A., Hsu-Kim, H., 2012. Methylation of mercury by bacteria exposed to dissolved, nanoparticulate, and microparticulate mercuric sulfides. Environ. Sci. Technol. 46, 6950–6958. doi:10.1021/es203181m

Zhang, T., Kucharzyk, K.H., Kim, B., Deshusses, M.A., Hsu-Kim, H., 2014. Net Methylation of Mercury in Estuarine Sediment Microcosms Amended with Dissolved, Nanoparticulate, and Microparticulate Mercuric Sulfides. Environ. Sci. Technol. 48, 9133–9141. doi:10.1021/es500336j

Zhang, Y., Jacob, D.J., Dutkiewicz, S., Amos, H.M., Long, M.S., Sunderland, E.M., 2015. Biogeochemical drivers of the fate of riverine mercury discharged to the global and Arctic oceans. Global Biogeochem. Cycles 29, 854–864. doi:10.1002/2015GB005124

Zhang, Y., Jaeglé, L., Thompson, L., 2014. Natural biogeochemical cycle of mercury in a global three-dimensional ocean tracer model. Global Biogeochem. Cycles 28, 553–570. doi:10.1002/2014GB004814

Chapter 2 – A comprehensive assessment of the mercury budget in the Marano-Grado Lagoon (Adriatic Sea) using a combined observational – modelling approach

Part of this chapter has been published as:

Melaku Canu, D., Rosati, G., Solidoro, C., Heimbürger, L.-E., Acquavita, A., 2015. A comprehensive assessment of the mercury budget in the Marano-Grado Lagoon (Adriatic Sea) using a combined observational modeling approach. Mar. Chem. 177, 742–752.

2.1 Introduction

Mercury (Hg) is a persistent pollutant of global concern, mainly emitted as the volatile elemental form Hg^0 from anthropogenic and natural sources. Upon oxidation to Hg^{2+}, Hg deposits on land and oceans where it can undergo multiple biotic and abiotic transformations, such as photochemical and microbial reduction as well as microbial methylation to organic methylmercury (MeHg) (Sonke et al., 2013). Biological MeHg production (methylation) and degradation (demethylation) in coastal environments occur predominantly in sediment (Monperrus et al., 2007a, Merritt and Amirbahman, 2009 and references therein). However, there is increasing evidence of MeHg biotic production in oxic surface water, especially during or after periods of high productivity when heterotrophic activity is elevated (Bouchet at al., 2013, Heimbürger et al. 2015, Heimbürger et al. 2010, Lehnherr et al., 2011, Monperrus et al., 2007a, Monperrus et al., 2007b, Sharif et al., 2014).

MeHg is assimilated by living organisms and tends to bioaccumulate and biomagnify along freshwater and marine trophic webs (Watras et al., 1998, Cossa et al., 2012). Human MeHg exposure can subsequently occur through fish intake (Black et al., 2012, Fitzgerald et al., 2007, Mason et al., 2012, Sunderland et al. 2009). The health risk for human and wildlife posed by chronic exposure to MeHg and its related socio-economics consequences have led to an increase in attention to this issue, such as those agreed upon by the United Nation Environment Programme (UNEP) during the Minamata Convention. These global efforts to reduce anthropogenic Hg emissions highlight the importance of this issue and there has been a concerted effort among researchers to quantify the concentrations and flux of Hg species and understand Hg transformations. We now have abundant field observations that can be modeled in an effort to develop predictive models to assess long-term ecological impacts and to better focus future research efforts.

Hg is a pollutant of great concern in the North Adriatic Sea, particularly in the Marano-Grado Lagoon, where high productivity, occurrence of seasonal anoxia, and shallow conditions could promote the transformation of Hg into bio-available compounds, as previously observed in

other shallow lagoon systems (Bloom et al., 2004; Monperrus et al., 2007a, 2007b). To date, the dynamics of Hg species in the benthic compartment of the lagoon have been investigated in some detail (Acquavita et al., 2012a; Brambati, 1997; Covelli et al., 2012; Covelli et al., 2008; Emili et al., 2012; Giani et al., 2012; Hines et al., 2012; Piani et al., 2005), although a limited number of sampling stations have been considered in most cases and emerging data are fragmented. Less is known regarding the fate of Hg species in the water column. In this medium several transformations can occur (i.e. photo-reduction, photo-oxidation, photo-demethylation and possibly biotic methylation and demethylation), which can increase Hg evasion, deposition or bioaccumulation rates. The water column is also where bioconcentration by phytoplankton takes place (i.e. the first step of Hg biomagnification in the pelagic trophic web). Therefore, collating and integrating the available information into a common framework would be timely and useful for enhancing our current understanding of Hg pollution, identifying possible gaps, and informing effective management policies.

Characterizing Hg speciation and fluxes among environmental compartments is difficult, expensive and time consuming. Consequently, even in environmental hot spots, dataset are often incomplete, and robust measurement assessments are often unavailable. Moreover, quantifying the transfer of Hg from environmental matrices to biota is a challenging task. Simple correlations cannot give a correct assessment of bioaccumulation, because environmental parameters influence the transfer kinetics. Modelling approaches may help overcome some of these limitations, and are highly encouraged (Sonke et al., 2013; Black et al., 2012) although the lack of comprehensive data sets often hinder the development and application of models (Black et al., 2012).

Currently a few attempts have been made to model the budget and biogeochemical cycling of total Hg in the marine environments at global, regional and subregional scales (Amos et al., 2015, Soerensen et al., 2014, Sunderland et al., 2009), including the Mediterranean Sea (Rajar et al., 2007; Žagar et al., 2007). However, additional efforts are needed to model MeHg budget in coastal areas (Bloom et al., 2004), where more accurate quantification of pollutant sources, transformation, and transport would be required.

Hg cycling in the Marano-Grado Lagoon has been previously modelled with the 0-D model SERAFM (Melaku Canu et al., 2012) to compile an initial overview of the processes that govern Hg fluxes into and out of the lagoon and to assess the relative importance of different contamination sources. However, this model lacked the ability to resolve spatial and temporal trends/characteristics.

Incorporating finer spatial and temporal resolutions into the model would generate a better representation of local characteristics such as biogeochemical and transport processes and would improve the Hg model to provide a better assessment of the fluxes of Hg species among the compartments. However, this would also require more information on the spatial distribution of chemical and biogeochemical parameters and processes, as well as detailed information on the hydrology, and solid transport within the system. Therefore, a sensible trade-off is needed. Here, we decided to model Hg dynamics by subdividing the lagoon into 21 boxes, and the transport between boxes was modelled using a high-resolution hydrodynamic model.

In this study, we collated available information on the Hg cycle in the Marano-Grado Lagoon, estimated missing information through an extensive literature review, and implemented the dynamic Hg module of WASP7 (Water Analysis Simulation Program, US EPA, 1988) to investigate Hg dynamics and establish a mass balance. We also aimed to determine whether and to what extent the lagoon could represent a site of net MeHg production and a secondary source of bioavailable Hg contamination to the Adriatic.

2.1.1 Study area

The Marano-Grado Lagoon (Northern Adriatic Sea, Italy) is a large wetland environment in the Mediterranean area (Figure 1). It covers an area of 160 km^2 and provides important ecosystem services, which sustain economic, touristic, and fishery activities. The watershed supports around 32,000 inhabitants (Pirastu et al., 2014). The lagoon is an optimal recruitment zone for some fish species and shelter to many bird colonies. It has been recognized as a Special Area of Conservation (SAC — IT3320037) by the EU Habitat Directive 92/43/EEC.

The lagoon dynamically exchanges water and matter with the Northern Adriatic Sea through six inlets, namely Lignano, S.Andrea, Buso, Morgo, Grado and Primero (Figure 1). An increasing salinity gradient occurs from the inland regions of the lagoon toward the inlets. Due to its shallowness, the lagoon also experiences strong seasonal fluctuations in water temperature spanning from approximately 0 to 30 °C. The western and the eastern sectors, also called the Marano and Grado Lagoons, exhibit some different physico-chemical features: the Marano Lagoon receives a greater input of freshwater from its tributaries (Stella, Turgnano, Zellina, Cormor, Corno–Aussa rivers) and is characterized by lower salinity and higher nutrient concentrations compared with the Grado Lagoon, which receives small freshwater inputs from the Natissa River (Figure 1). The Grado Lagoon is shallower, and presents weaker hydrodynamics and more complex morphologies such as saltmarshes and a tidal flat.

The Marano-Grado Lagoon acts as a sink for various contaminants released from different anthropogenic activities, including large amounts of Hg compounds that have lead to high total Hg (Hg_T) concentrations of the lagoon sediments (2.49 – 69.8 nmol/g; Acquavita et al., 2012; Regional Protection Agency-Friuli Venezia Giulia-ARPAFVG), pore-waters (Covelli et al., 2008; Emili et al., 2012) and local biota (Brambati, 1997; Giani et al,, 2012). Sediment values are 10 to 280 times higher than those in the open Mediterranean Sea (Heimbürger et al., 2012).

The historic source of Hg was the Idrija cinnabar mine in western Slovenia, which operated from the 16th century until 1994. Dizdarevič (2001) estimated that approximately 37,000 tons of Hg (equivalent to $1.84 \cdot 10^5$ kmol of Hg) were discharged during the lifetime of the mine. Much of the released Hg persists in the Soča/Isonzo River banks and is slowly released into the Gulf of Trieste (the northern part of Adriatic Sea), especially during flooding events. Once Hg reaches the Gulf of Trieste, it is transported through general water circulation and in the sediment. When the river plume is diverted to the SW under the influence of E–NE winds, the tidal flux carries particulate Hg (Hg_P), which is mostly inorganic, into the Grado Lagoon (Covelli et al., 2007). The second most relevant Hg source is a chlor-alkali plant (see Figure 1) that dumped approximately 190 tons of Hg (equivalent to $9.5 \cdot 10^2$ kmol) directly into the lagoon through the Aussa–Corno River (Acquavita et al., 2012a, 2012b) during its 45 years of operation.As a result of historical and more recent Hg contamination, it has been estimated that 251 t of Hg (equivalent to $1.25 \cdot 10^3$ kmol) are buried in the sediments of the lagoon (Covelli et al., 2012). Therefore, the lagoon sediment, together with the sediment stored in the Aussa–Corno River and in the Gulf of Trieste, has the potential to act as a secondary source of Hg.

Figure 1. The Marano-Grado Lagoon with its six sub-basins (yellow lines) and their corresponding inlets (double arrows). Light blue arrows indicate transport by water masses. The two main sources of contaminations are shown as well.

2.2 Materials and Methods

In order to investigate Hg cycle dynamics and estimate Hg species fluxes in the Marano-Grado Lagoon ecosystem, we implemented the water quality model WASP7, released by the US EPA and publicly available at the website http://www2.epa.gov/exposure-assessment-models/surface-water-models (last visit 13/01/2015).

2.2.1 The WASP model

TheWASP7model is a dynamic process-based water quality model made of different sub-models, including one for Hg (MERC7). This model can reproduce the temporal and spatial evolution of three Hg species (Hg^{II}, MeHg, Hg^0) concentrations in water, pore-water and sediments, accounting for their partition into dissolved phases (Hg_D and $MeHg_D$,which include both the ionic form and the DOC-complexed fraction) and particulate phases (Hg_P and $MeHg_P$, which include silt, sand and organic matter sorbed fractions), as illustrated in Figure 2.

The model allows users to discretize a water body in one, two or three dimensions, by means of interconnected zero dimensional boxes, which represent water or sediment compartments. The overall equation (equation 1.1) of the mass conservation of the state variables in each water box, includes terms for advection (U in m/sec) and diffusion (E in m^2/day) in the three dimensions (x, y, z). It also accounts for direct or diffusive loads (S_L in g/m^3 day), exchanges with the boundaries or the sediment (S_B in g/m^3 day) as well as the biochemical or photochemical transformation of Hg species (S_{rx} in g/m^3 day):

$$\frac{dC}{dt} = -\frac{d(U_x \cdot C)}{dx} - \frac{d(U_y \cdot C)}{dy} - \frac{d(U_Z \cdot C)}{dz} + \frac{d}{dx}\left(E_x \frac{dC}{dx}\right) + \frac{d}{dy}\left(E_y \frac{dC}{dy}\right) + \frac{d}{dz}\left(E_z \frac{dC}{dz}\right) + S_L + S_B + S_{rx} \qquad eq.\ 1.1$$

Hence, the exchanges of water, Hg species and suspended particulate matter between water boxes - as well as the ones between boxes and boundaries - depend on advection and dispersion processes. While it is being subjected to transport, Hg species can undergo several biotic or light-mediated transformations (i.e. microbial methylation and demethylation, dark oxidation, photo-reduction, photo-oxidation and photo-demethylation). Dissolved elemental Hg (Hg^0) is exchanged between the surface water boxes and the overlying atmosphere (Hg^0_{atm}) with a rate *Ae* that depends on the water and air concentrations of elemental Hg (Hg^0 and Hg^0_{atm} in mg/L), Henry's Law constant *H*, the Universal Gas constant *R,* the temperature value in degrees Kelvin, and the volatilization rate constant (K_{vol} *in* 1/d).

$$A_e = k_{vol} \cdot (Hg^0 - \frac{Hg^0_{atm}}{H/T}) \qquad eq.\ 1.2$$

Movements of Hg species from the sediment layer to the water - and *vice versa* – are controlled by deposition and resuspension rates of organic and inorganic solids as well as by pore-water diffusion.

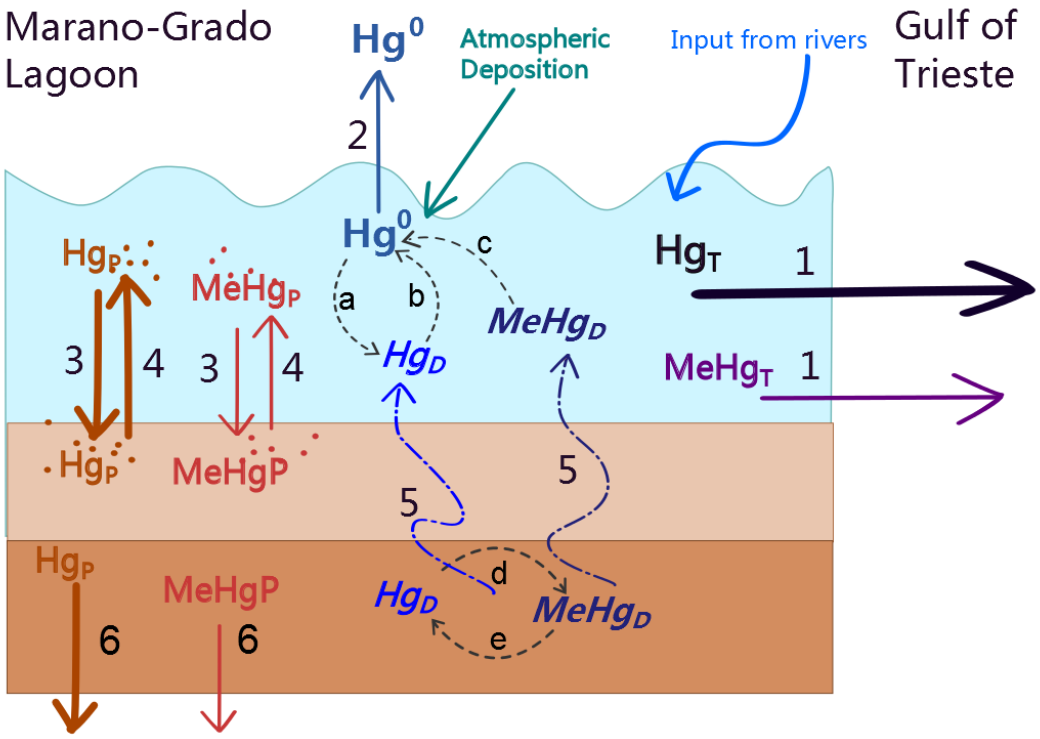

Figure 2. Main transport (1-*Exchange with the Sea*, 2-*Volatilization*, 3-*Deposition*, 4-*Resuspension*, 5-*Pore water diffusion*, 6-*Burial*) and transformation (a-*Photo-oxidation*, b-*Photo-reduction*, c-*Photo-demethylation*, d-*Methylation*, e-*Demethylation*) processes included in the WASP model. Hg_T is total Hg (Hg^{II} + Hg^0 + MeHg in dissolved and particulate phase), $MeHg_T$ is total MeHg (dissolved and particulate phase of MeHg), Hg_P and $MeHg_P$ are particulate-bounded Hg^{II} and MeHg, whilst Hg_D and $MeHg_D$ are the dissolved forms of Hg^{II} and MeHg.

Two kinds of sediment box are assumed in the model implementation: an uncompacted surface sediment box, and one sub-surface compacted sediment box Wool et al., (2001). In surface sediment boxes, the variation of concentration S (g/m^3) of a solid k (silt, POM or sand) in the j box ($\frac{S_k^j}{dt}$; Equation 1.3) is computed as the sum of fluxes owing to deposition of suspended particulate matter from water ($D^w = v_d \cdot S_k^w$, g/m^{2}d), sediment resuspension ($R^j = v_{rs} \cdot S_k^j$, g/m^{2}d) and burial from the sediment box itself to the lower sediment box ($B^j = v_b \cdot S_k^j$, g/m^{2}d). The burial velocity v_b (m/d) depends on the balance between D and R ($v_{b,j} = (D - R)/S_k^j$). When deposition exceeds resuspension ($D^w > R^j;\ B^j > 0$), sediment and Hg mass are added to the surface box, which increases in volume. The volume of the box is compressed to the original value and sediment are pushed toward the sub-surface sediment box (z), part of which is buried out of the model domain at a rate B^z ($B^z = B^j \cdot S_k^z$, g/m^{2}d),

causing losses of Hg from the sub-surface sediment box (Equation 1.4). When resuspension exceeds deposition ($R^j > D^w;\ B^j < 0$), the volume of the surface box decreases, and if the upper layer erodes completely, the sub-surface sediment box is exposed to scour.

$$d\frac{m_k^j}{dt} = D^w - \left(R^j + B\right) \qquad \textit{eq. 1.3}$$

$$d\frac{m_z^j}{dt} = B^z \qquad \textit{eq. 1.4}$$

In each water box, the concentration of the adsorbed fraction of a Hg species *i* on the solid *k*, $C^w_{i,k}$ varies according to the Hg species concentration, the solid dynamics described above and the fraction $f_{i,k}$ of the chemical species adsorbed, which depends on the partition coefficients (K_D, L/kg) of each species between water and solids.

Sediment deposition and resuspension are governed by the shear stress according to equations 1.5 and 1.6. In equation 1.5, the deposition velocity (v_d) is computed from: the Stokes's settling velocity ($v_s,\ m/d$), the probability of deposition (α_D), the bed shear stress ($\tau_b, \mathrm{N/m^2}$), and the lower and upper critical stress thresholds for deposition (τ_{c1} and τ_{c2}). Depending on the value of τ_b, α_D varies between 1 and 0 within the range from $\tau_{c1}(\approx 0)$ to $\tau_{c2}(\approx 0.01\ -\ 0.2\ \mathrm{N/m^2})$.

$$v_d = v_s \cdot \alpha_D \qquad \begin{matrix}\alpha_D = 1\ if\ \tau_b \le \tau_{c1} \\ \alpha_D = 0\ if\ \tau_b \ge \tau_{c2}\end{matrix} \qquad \textit{eq. 1.5}$$

The resuspension velocity v_{rs} (equation 1.6) depends on the ratio between the entertainment flux E (g/m^2sec) and the particle density ρ_D (~2.6 kg/m^3). The entertainment flux E (equation 1.7) depends on the fraction of cohesive sediment, the multiplier *M* (0.1 to 100 g/m^2sec, set to 3 g/m^2sec in the model implementation), and the bed shear stress (τ_b) and the critical stress for erosion (τ_{ce} = 0.12 for silt and 0.04 for POM, model default).

$$v_{rs} = \frac{E}{\rho_D} \qquad \textit{eq. 1.6}$$

$$E = (f_{silt} + f_{POM}) \cdot M \cdot \frac{\tau_b - \tau_{ce}}{\tau_{ce}} \qquad \textit{eq. 1.7}$$

The bed shear stress ($\tau_b, \mathrm{N/m^2}$) is computed by the model (equation 1.8) from water density ($\rho, kg/m^3$), the square of the water velocity ($u^2, m/s$), the water depth (z, m), and the equivalent roughness height (k_s, m) that is 4 times the median diameter of sediment (D_{50}).

$$\tau_b = \frac{\rho u^2 \frac{0.24}{log_2(\frac{12z}{k_S})}}{8} \qquad \textit{eq. 1.8}$$

Further details on the equations used in the model are provided by Wool et al. (2001).

2.2.2 Available data and model implementation

We implemented the WASP7 model using site-specific data, complemented by literature values obtained from similar environments, as summarized in Supplemental Material. Although many research studies focusing on the Hg cycle have been carried out in the lagoon, a comprehensive investigation has never been performed. We therefore augmented our seasonal database with additional information obtained from projects carried out by the Regional Environmental Protection Agency (ARPA FVG) at the University of Trieste in the Friuli Venezia Giulia Region, and the National Institute of Oceanography and Experimental Geophysics (OGS). We gathered data on meteo-climatic conditions, suspended particulate matter and Hg species concentrations at the lagoon boundaries (i.e., the water/air interface, the river mouths and the lagoon inlets), as well as data regarding Hg distribution, transport processes and transformation rates within the Marano-Grado Lagoon (Table 1) and similar environments (Table 2).

Considering the spatial resolution of available Hg data and the major features of the lagoon environment, the model was implemented starting from the hydrological classification defined by Dorigo (1965). Therefore we represented the lagoon (Figure 1) with 6 water boxes, each representing a lagoon sub-basin, and 12 sediment boxes, i.e. a surface sediment layer (0 – 2 cm depth) and a subsurface sediment layer (3 – 10 cm depth) for each sub-basin. Additionally, there were 3 more water boxes representing the 3 major tributaries. Cross sectional areas between boxes were estimated using the hydrodynamic model. The cross sectional areas between the marine boundaries and the lagoon (i.e., the inlet sections) are given in Fontolan et al. (2007). Gross bulk water exchanges (m^3/s) between the 6 water boxes and the marine boundaries were computed using the 2D hydrodynamical model described in Ferrarin et al. (2010) and were then included in the WASP7 model. Following indications from theWASP7 model (US EPA 1988, US EPA, 2009 and http://epa.gov/athens/wwqtsc/courses/wasp7/index.html last access 04/12/2014) and calibration results, we set the dispersion between water boxes at 10 m^2/s.

The model requires the initial conditions for each of the 21 boxes to be defined. The Hg species concentrations in sediment were initialized according to Acquavita et al., 2012a, 2012b.We discriminated between cinnabar mercury (HgS) and the more recent Hg that originated from the chlor-alkali plant by setting different partition coefficient (K_D) values (Table 3). In agreement with this choice, the cinnabar form was less susceptible to transformations. Initial concentrations of silt-clay, sand and POM in sediment boxes (g/m^3) were computed from the percent distributions of silt-clay, sand and OC (Acquavita et al., 2012a, Table 1), respectively.

Initial conditions in water components were obtained by running the model for 21 years under a cyclically repeating 3-year time series of the boundary conditions, and by letting the model adjust to such external forcing to achieve a pseudo-stable condition. This adjustment is usually referred to as model spin-up. We performed 3-year simulations after the spin up. The hydrodynamic model was forced by actual data of tidal levels at the inlets, river discharge data, wind forcing and thermal fluxes. Actual meteorological data (i.e., daily light intensity, daylight hours, monthly water temperature and average air temperature; Table 1) were used as external forcing for biogeochemical processes such as organic solid production and degradation, photoreactions and microbial transformations of Hg species. All of the forcing data refer to data obtained during 2009–2011 and were provided by ARPA-FVG. The time course of Hg_D concentration at the inlets was prescribed in agreement with monthly measurements (see Table 1), and the time series of Hg_T concentrations (not measured) were estimated by multiplying the Hg_D time series by a correction factor of 1.5 that was derived from experimental information on the Hg_T/Hg_D in the Gulf of Trieste (Faganeli et al., 2014, Table 1). As a safety measure, we verified that the average values of the reconstructed Hg_T series were in agreement with the values reported by Horvat et al. (2003) and Faganeli et al. (2003) for the Gulf of Trieste (Table 1).

No information on the seasonal dynamics of MeHg at the sea boundaries was available, so we adopted the constant value of 0.22 pM used by Horvat et al. (2003) for the Gulf of Trieste. Monthly values of particulate organic matter (POM) in the north- ern Adriatic Sea were prescribed at the sea boundaries. Hg inputs from the Stella and Natissa rivers were estimated using measured time series of Hg_D (ARPAFVG, Table 1), and by assuming that Hg_D was 60% of HgT; these values were in accordance with previous studies on the Aussa–Corno river (Covelli et al., 2009), and literature on similar rivers (Sharif et al., 2014; Buckman et al., 2015). We also estimated MeHg in the river to be 5% of HgT, in accordance with previous studies on temperate rivers (Balogh et al., 2003; Paller et al., 2004; Sharif et al., 2014). The concentrations of Hg^0 at the atmospheric boundary were set conservatively and were equal to the average value of total gaseous Hg (TGM) measured in the lagoon watershed (Acquavita et al., 2012b). Deposition of Hg over the surface of the lagoon was treated as an external input, and the average deposition rate (kg/m^2) was set using estimates from Žagar et al. (2007) for the Mediterranean Sea (Table 2). The SPM concentration at the river boundaries was given by ARPAFVG measurements at the Aussa–Corno River. The POM concentration in the river boundary was calculated from available monthly SPM data (Table 1) according to Covelli et al., 2009 and Sutherland, 1998, assuming the POM fraction was 12.7% of the total SPM

	Measured Variable	*Sampling Year*	*Sampling*	*Notes*	*Value (average)*	*Unit*	*Reference*
Atmospheric boundary	Solar irradiation and fraction of daylight	*2009 - 2011*	*One year series; hourly samplings*	*Lignano weather station*	*339*	*langley/day*	*ARPAFVG*
	Total gaseous mercury (TGM)	*2001*	*January - February*	*n=731*	*19.9*	*pmol/m^3*	*Acquavita et al., 2012b*
Marine boundaries	Hg_D	*From Aug '09 to Jul '10*	*One year series; Monthly sampling*	*Gulf of Trieste nearby the lagoon*	*22.8*	*pM*	*ARPAFVG*
	Hg_T, MeHg	*1999*	*June*	*Provide average value from previously collected data*	*Hg_T = 29.5 MeHg = 0.22*	*pM*	*Horvat et al. 2003*
	Hg_T, Hg_D, $MeHg_T$, $MeHg_D$	*June, Mar, Aug, Sep '95 and '98*	*Occasional sampling*	*Considered their stations AA, CZ, A4, A20, A29, F2*	*Hg_T = 27 MeHg = 0.22*	*pM*	*Faganeli et al., 2003*
	SPM	*2010 - 2011*	*One year series; monthly sampling*	*Lignano and Grado inlets*	*Lignano = 9.6 Grado = 11.6*	*mg/L*	*Regione FVG, 2013*
Riverine boundaries	Hg_P	*2005 - 2010*	*Occasional sampling*	*Aussa-Corno River. Hg_P data used as Hg_T in the model*	*139*	*pM*	*Present work*
	Hg_D	*2009 - 2010*	*One year series; monthly sampling*	*Cormor and Stella rivers. Hg_D data used as Hg_T in the model*	*10.5*	*pM*	*Present work*
	SPM	*2009 - 2011*	*One year series; monthly sampling*	*All rivers but Natissa*	*8*	*mg/L*	*ARPAFVG*

Lagoon Water Lagoon Water	Temperature	*2009 - 2011*	*One year series; monthly sampling*	*17 sampling stations*	*16*	*°C*	*ARPAFVG*
	DOC	*2008 - 2009*	*April and November 2008, March 2009*	*21 sampling stations*	*0.33*	*mM*	*ARPAFVG*
	Hg_D	*Aug '09 - to Aug '10*	*Monthly sampling*	*17 sampling stations*	*31.4*	*pM*	*Present work*
	MeHg	*Oct '08 and Jul '09*	*2 sampling stations out of the benthic chamber (MB, MC)*	*Lignano and Buso sub-basins*	*0.29*	*pM*	*Emili et al., 2012*
	DGM	*Oct '08 and Jul '09*	*2 sampling stations out of the benthic chamber (MB, MC)*	*Lignano and Buso sub-basins*	*1.03*	*pM*	*Emili et al., 2012*
Lagoon Sediment (initial conditions)	Hg_T, HgS, MeHg	*Jun - Jul '08*	*16 sampling stations*	-	*Hg_T = 21.9 HgS = 8.9 MeHg = 0.01*	nmol/ g	*Acquavita et al., 2012a*
	% silt, sand, C org	*Jun - Jul '08*	*16 sampling stations*	-	*silt = 70 sand = 27 Corg = 1.2*	*%*	*Acquavita et al., 2012a*
Lagoon Pore water	Hg_T	*Oct '08, Feb and Jul '09*	*2 sampling stations (MB, MC)*	-	*493*	*pM*	*Emili et al., 2012*
	MeHg	*Oct '08, Feb and Jul '09*	*2 sampling stations (MB, MC)*	-	*3.9*	*pM*	*Emili et al., 2012*

Hg Transformations and transport in lagoon sediment	Hg Methylation	*Oct '08, Feb and Jul '09*	*4 sampling stations (MA, MB, MC, GD)*	*Average value adjusted to 20 °C According to WASP equations*	*MB= 9 10^{-3} MA= 1.7 10^{-2} MC= 8.3 10^{-3} GD = 1.4 10^{-2}*	*1/day*	*Hines et al., 2012*
	Hg Demethylation	*Oct '08, Feb and Jul '09*	*4 sampling stations (MA, MB, MC, GD)*	*Average value adjusted to 20 °C According to WASP equations*	*MB= 2.4 10^{-1} MA= 9.2 10^{-2}; MC=2.6 10^{-1}; GD = 9.7 10^{-2}*	*1/day*	*Hines et al., 2012*
	Hg and MeHg benthic fluxes	*Jun and Oct '03, Feb '04*	*2 sampling stations (BAR, ART)*	*Grado Lagoon*	*Hg = 91 MeHg = 4*	*nmol/ m^2d*	*Covelli et al. 2008*
	Hg and MeHg benthic fluxes	*Oct '08, Feb and Jul '09*	*2 sampling stations (MB, MC)*	*Marano lagoon*	*Hg = 23 MeHg = 0.6*	*nmol/ m^2d*	*Emili et al. 2012*

Table 1 Site-specific data from regional projects and literature sources used to model the mercury cycle in the Marano-Grado Lagoon.

2.2.3. Mercury dynamics, Partition coefficients and Transformations

Transformation rate constants and transport coefficients were obtained from the literature on studies conducted in the Marano-Grado Lagoon, when available, or in other similar environments. The partition coefficient (K_D in L/kg) is defined as the ratio between the concentration of a substance into the solid phase and the concentration of the substance in the enveloping aqueous phase (Hammerschmidt and Fitzgerald, 2004).

The WASP7 model uses K_D values constant in space and time, which were chosen according to the calibration results (Table 3) and based on site-specific values provided by Covelli et al. (2008a, 2008b) and Hines et al. (2012).

Methylation and demethylation rate constants in sediment were derived from seasonal values reported by Hines et al., 2012 standardized to 20°C, according to the equations implemented inWASP7 and assuming only the dissolved fractions of Hg and MeHg were subjected to methylation and demethylation. Because studies on photo-reactions (e.g., photo-demethylation, photo-reduction and photo-oxidation) for the Marano-Grado Lagoon water column are missing, we parameterized these processes in agreement with Monperrus et al. (2007a, 2007b) and Whalin et al. (2007). The former explored seasonal variations in methylation, demethylation, reduction rates and photo-demethylation in the Thau Lagoon and in the open Mediterranean Sea. The latter measured photo-reduction and photo-oxidation rates at different salinities and environmental conditions and investigated the occurrence of methylation and photo- demethylation in seawater (Table 2). Given the light intensity at which the reactions were measured, photo-demethylation rates were internally adjusted by the model for the light conditions of the system. We assumed that these reactions were driven by UV-A and UV-B radiation (Vost et al., 2012) and that only the DOC-complexed fractions of HgII and MeHg were prone to photo- reactions (Vost et al., 2012; Whalin et al., 2007). The movement of Hg species from pore water to the water column depends on diffusion processes. We averaged the molecular diffusion coefficients (D_t in m^2/s) for Hg and MeHg at 25 °C and adjusted the value to the water temperature of each box, according to Rothenberg et al. (2008) (Table 2). Bioturbation was then taken into account by increasing the D_t 10 times from May to September to accommodate more intense biological activity. The average D_t for the whole year was $8.5 \cdot 10^{-9}$ m^2/s and was in the acceptable range reported by Schnoor et al. (1987) for bioturbated sediments.

The biotic solid production rate (g/m^3day) R_{pp} was set in agreement with Sorokin et al. (1996) and Blasutto et al. (2005) for water boxes and for benthic boxes, respectively. The organic matter degradation rate constant -$K_{deg\text{-}POM}$ - (1/day) was calibrated to match US EPA (1995) values. Sediment deposition, erosion and burial were computed by the model depending on the value of the shear stress induced by the currents. The particulate fraction of Hg and MeHg (Hg_P and $MeHg_P$) follows the fate

of the sediment, whilst the dissolved fraction (Hg_D, Hg^0 and $MeHg_D$) is transported by the current flow and by pore-water diffusion. Average values of deposition and resuspension rates were 1.3 m/day and $9.6 \cdot 10^{-7}$ m/day (corresponding to $1.2 \cdot 10^3$ g/m^{2}day and $3.8 \cdot 10^2$ g/m^{2}y of settled and resuspended particles), respectively, which is in agreement with the value of the resuspension rate of $4.2 \cdot 10^2$ g/m^{2}y given by Bloom et al. (2004) for the southern basin of the Venice Lagoon. The highest value of the modelled resuspension rate was $2.8 \cdot 10^{-4}$ g/m^{2}s, which was lower than the rates measured by Brand et al. (2010) in the South San Francisco Bay. The average burial rate was 0.11 g/cm^{2}y and was comparable to the rates estimated in three stations of the Marano-Grado lagoon by Covelli et al., 2012.

	Measured Variable	***Sampling Year***	***Value (or average***	***Unit***	***Reference***
Transport	Hg deposition	-	*9.24*	*ug/m^{2}y*	*Zagar et al., 2007*
	Molecular diffusion coefficient	-	*$Hg_{(25^\wedge)}$= 9.5E-6 $MeHg_{(25^\wedge)}$= 1.08E-5*	*cm^2/s*	*Rothenberg et al. 2008*
	Dispersion coefficient	-	*10*	*m^2/s*	*WASP manual*
Transformations	Photo-reduction	*Aug and Nov 2004*	*6.5 10^{-4}*	*1/s*	*Whalin et al., 2007*
	Photo-oxidation	*Aug and Nov 2004*	*4 10^{-4}*	*1/s*	*Whalin et al., 2007*
	Photo-demetylation	*May and Oct '03; Jan, Apr, Jul '04*	*6 10^{-7}*	*1/s*	*Monperrus et al., 2007*

Table 2. Literature mercury transport and transformation parameters used for the model implementation.

	Hg^{II}	***HgS***	***MeHg***	***Hg^0***
K_D Silts and Fines	10^5	9 10^5	10^5	--
K_D Sands	10	1 10^5	--	--
K_D Organic Solids	7 10^5	10	7 10^5	--
K_D DOC	3 10^4	10^3	10^5	--

Table 3 Partition coefficients (K_D) [L/kg] used in the model for Hg^{II}, HgS, MeHg and Hg^0.

2.3. Results and Discussion

2.3.1 Model-Data comparison

Model output was compared with an independent data set of Hg_D in the Marano-Grado Lagoon water (ARPAFVG) and MeHg in sediment (Acquavita et al. 2012, Table 1). We compared the WASP7 model output of each box with the average, minimum and maximum concentration of Hg_D in the corresponding month and at the corresponding sampling stations (Figure 3A). The model was able to reproduce the temporal variability through the year and the spatial variability between the boxes. However, spatial variability was underestimated. The misfit, computed from the monthly values of all the boxes, was 34% which is a rather good result for this type of model, especially given the complexity of the phenomena described. A closer analysis of the data-model comparison indicated that a large fraction of the misfit was related to the months of September and November. Without these values, the fit would have improved significantly. We suspect the inconsistency between the model and field data for these months is due to the low resolution of the field data, which was collected once each month and may not be representative of average conditions; importantly, these data could also reflect the occurrence of atypical events. Conversely, the boundary conditions which drove the model referred to typical average conditions. Incidentally, this is why all models typically underestimate observed variabilities. Finally, the description of the domain did not take into account some of the local processes that affected the dynamics of the Hg species, including local tidal oscillations, desorption induced by changeable redox conditions and other effects induced by variable bathymetry such as variable thermal inertia. Several authors (Bloom et al., 2004; Bouchet et al., 2013, Guédron et al., 2012) reported substantial variations of Hg species concentrations due to the effects of tidal movements. Bloom et al. (2004) found that Hg_T in the water column of a channel of the Venice Lagoon was inversely correlated with tide height, while MeHg varied only slightly. Again in the Venice Lagoon, Guédron et al. (2012) found increased $MeHg_D$ and Hg_D levels at the sediment–water interface and, to a lesser extent, in the water column during late tidal flooding. The authors concluded that in Venice, the release of dissolved Hg species from the salt marshes during tidal flushing affected Hg concentrations in the water column. Tidal flooding enhances shear stress along the lagoon sediments, which, in turn, could cause oxygen penetration and redox oscillations leading to enhanced $MeHg_D$ and Hg_D release from sediments by promoting diffusion and MeHg production. Bouchet et al. (2013) found $MeHg_D$ and Hg_D levels in a channel of the Arcachon Bay to be related to tidal movements and turbidity peaks, with maxima recorded during ebb tide.

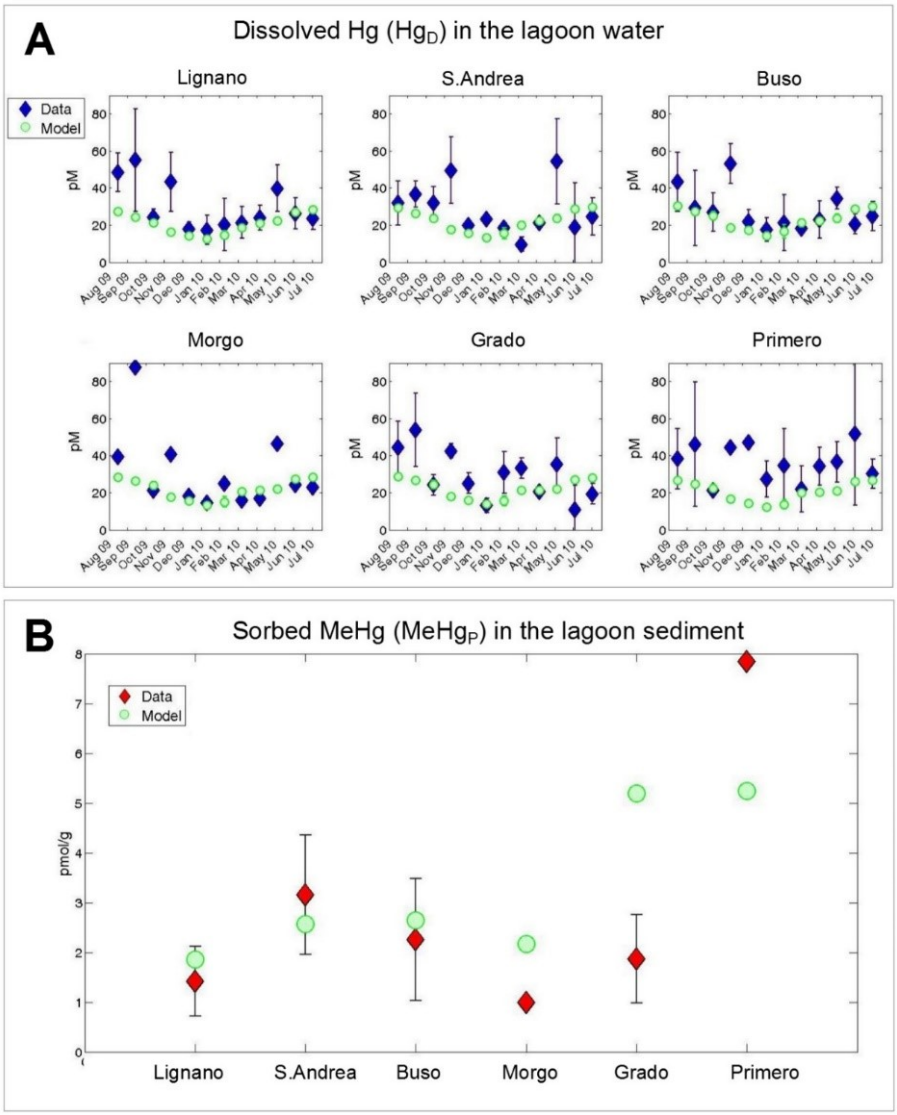

Figure 3. A) Comparison between modelled (green circle) and observed (blue diamonds) dissolved Hg (Hg_D<0.45 μm) concentrations in the lagoon water for the six sub-basins in each month. B) Comparison between modelled (green circle) and observed (red diamonds) sorbed MeHg ($MeHg_P$) concentrations in the lagoon sediment for the six sub-basins.

The modelled Marano-Grado Lagoon surface sediment $MeHg_P$ contents averaged 15.4 pmol/g, which was in satisfactory agreement with the average measured concentration of 13.6 pmol/g (Acquavita et al., 2012a) as shown in detail for each box in Figure 3B. Agreements with experimental estimates varied in space and were extremely good for the Buso sub-basin; the Grado sub-basin had a larger, but still acceptable, misfit. The differences, however, point to the need for more accurate information on the spatial variability of methylation and demethylation constants, and possibly on the relationships between methylation rates and sediment properties or biological substrata. Indeed, three out of four measurements of methylation and demethylation rates (Hines et al., 2012) concern the Marano Lagoon (Lignano, S.Andrea and Buso sub-basins), while only one site was sampled in the Grado Lagoon. Moreover, in our model we assumed high partition coefficients (k_D) for the HgS fraction that is

therefore unavailable to methylation. However, the presence of dissolved organic matter (DOM) in the lagoon pore-water may reduce the stability of $HgS_{(s)}$ complexes favoring their dissolution and bioavailability to methylation (Ravichandran et al., 1998).

In the model, Hg transformation rates change with time and depend on temperature, solar radiation, and water fluxes. For example, Figure 4 shows that over the course of a year, the methylation, demethylation, photo-reduction, photo-oxidation and photo-demethylation processes for the 6 sub-basins exhibits temporal variation which we attribute to seasonal fluctuations in the parameters that influence Hg transformations. Therefore, net fluxes between Hg species vary accordingly in space and in time, depending on Hg concentration and transformation rates.

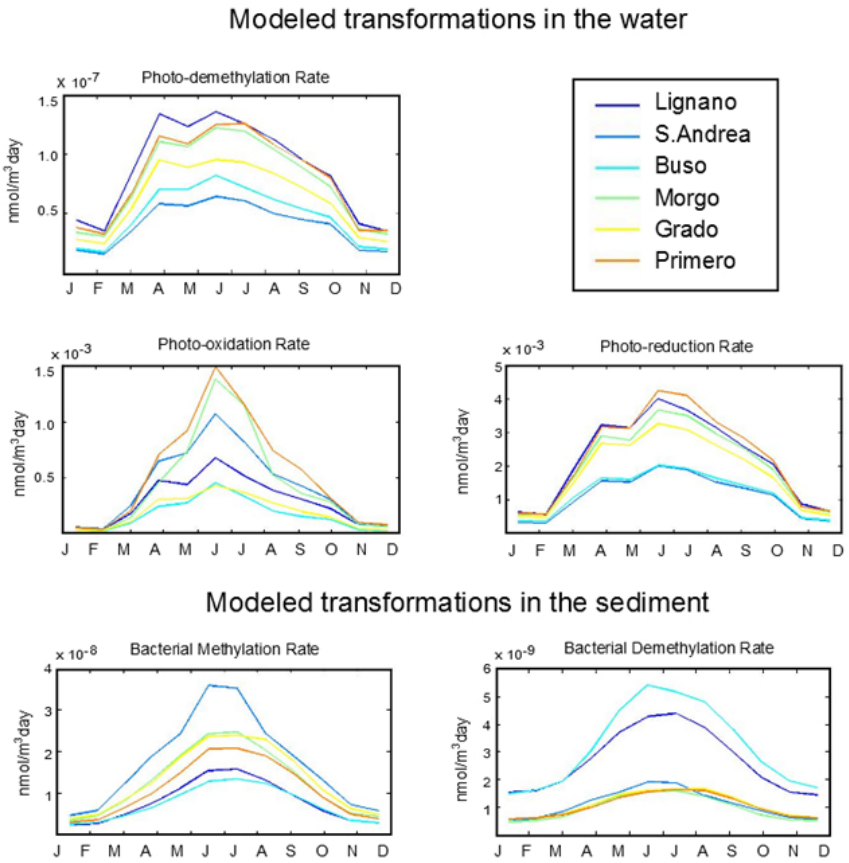

Figure 4. Time evolution of photo-demethylation, photo-oxidation, photo-reduction, methylation and demethylation, rates modulated by the model during the three years, as a function of the environmental parameters.

2.3.2. Mercury budget in the Marano-Grado Lagoon

The model provides an estimate of three Hg species (Hg_T, MeHg and Hg^0) concentrations and fluxes in the water column and sediment of the Marano-Grado Lagoon in a 21 box representation. The advantage of the model application lies in its ability to reproduce the Hg dynamics of the system at each time step, and as a function of environmental variables (i.e. water and air temperatures, light intensity, sediment resuspension, water fluxes, organic matter). This offers an advantage over purely statistical analyses of environmental measurements. Furthermore, the model allows the user to quantify the exchanges among sub-basins and with the adjoining systems (Adriatic Sea, rivers, atmosphere), a process that is difficult to assess through direct measurements. The model was used to compute the mass balance of Hg in the Marano-Grado Lagoon, considering time-variable river loads, exchanges with the Adriatic Sea, atmospheric deposition, the initial sediment Hg_T content and HgS fraction.

Modelled fluxes between environmental compartments of total Hg (Hg_T), MeHg, Hg^0, particulate Hg (Hg_P) and MeHg ($MeHg_P$) as well as dissolved Hg and MeHg (Hg_D, $MeHg_D$) are shown in Figure 5A, together with the average concentration of each compartment. Similar information for each sub-basin is reported in Table 3. Finally, the net exchanges of Hg_T and Me Hg_T between the 6 lagoon boxes and between each box and the sea are reported in Figure 5B. The simulated average Hg_T concentration in the water column was 39 pM (range 11.4 – 75.3 pM), while Hg^0 was 0.3 pM (approximately 0.7% of Hg_T) and $MeHg_D$ was 0.25 pM (0.6% of Hg_T). This indicates that the lagoon water concentrations of Hg_T and MeHg were 11% and 13% higher than the concentrations in incoming water from the Adriatic Sea, respectively. Hg_T and MeHg concentrations in the water column were slightly higher in the Marano Lagoon (40 and 0.26 pM) compared to the Grado Lagoon (38 and 0.23 pM), while Hg^0 was higher in the Grado Lagoon (0.32 pM) than in the Marano Lagoon (0.27 pM). Model estimates of Hg^0 and MeHg were coherent with the experimental findings in Emili et al. (2012). The highest Hg_T concentrations in the water of Marano Lagoon may be due to the effect of water circulation that induce transport of Hg from east to west (see below) and to lower deposition rates of suspended solids in the eastern sector.

The model predicted that water column Hg_T and MeHg occurred primarily in the dissolved phase. Dissolved (<0.45 μm) Hg_T and MeHg comprised 57% and 62% of the total concentration, respectively. These ratios were similar to those reported for the Thau Lagoon (Monperrus et al., 2007a, 2007b), where Hg_D ranged from 61 to 81% and $MeHg_D$ from 52 to 74%. The ratios were also comparable with the data of the Gulf of Trieste (mean Hg_D is 42%, range 6–90%; Faganeli et al., 2003). In contrast, the ratios were much higher than those reported for the Venice Lagoon by Bloom et al. (2004), where Hg_D was 15% on average (range 4–39%) and $MeHg_D$ was 35% (range 23–56%). These discrepancies may

be due to high resuspension levels of contaminated sediment in Venice. The model predicts that the lagoon is a net source of Hg species for the Adriatic Sea, exporting 559 mol/y of HgT of which 4.1 mol/y is MeHg. The percentage of MeHg (0.73%) is comparable to the average values reported in Venice Lagoon (0.65%, Bloom et al., 2004), which is another site that is heavily impacted by direct industrial pollution.

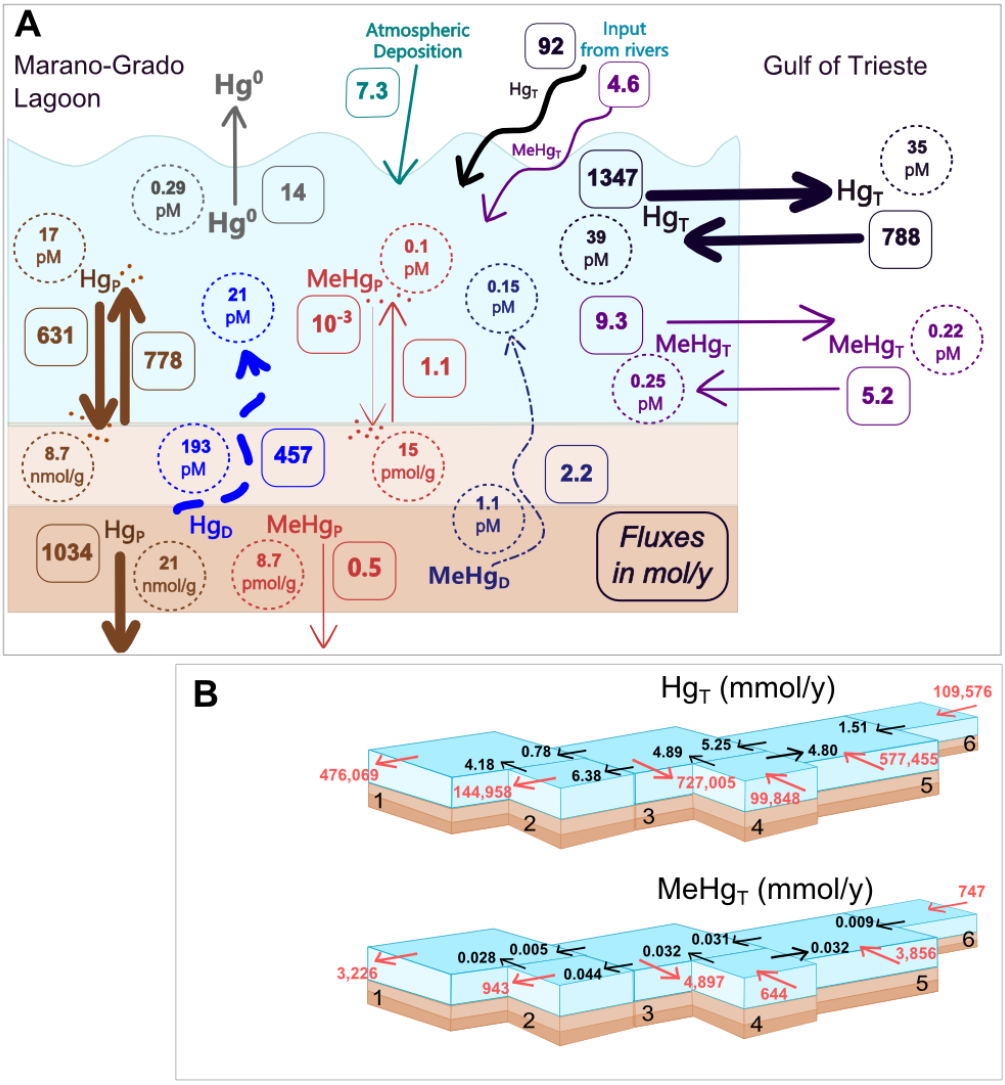

Figure 5. A) Modelled concentrations (circles) and fluxes (squares) of Hg species in the Marano-Grado Lagoon. Hg_T is total Hg (Hg^{II} + Hg^0 + MeHg in dissolved and particulate phase), $MeHg_T$ is total MeHg (dissolved and particulate phases of MeHg), Hg_P and $MeHg_P$ are particulate-bounded Hg^{II} and MeHg, whilst Hg_D and $MeHg_D$ are the dissolved phases of Hg^{II} and MeHg. All fluxes are in mol/y and the width of the arrows is proportional to the square root of the magnitude of the flux. B) 3D framework of the modelled lagoon, net exchanges of Hg_T and $MeHg_T$ between the boxes of the lagoon (black arrows) and between each box and the sea (red arrows). All fluxes are in mmol/y.

Sub-basin		**Lignano**	**S. Andrea**	**Buso**	**Morgo**	**Grado**	**Primero**	***Total***	***DB (-31%)***	***IB (+100%)***
Surface	m^2	$5.1\ 10^7$	$2.2\ 10^7$	$3.6\ 10^7$	$2.9\ 10^6$	$3.3\ 10^7$	$1.4\ 10^7$	**$1.6\ 10^8$**		
1 - Exchange with the Sea	Hg_T	-475	-145	-727	100	578	110	**-559**	**-1.39%**	**+4.06%**
	$MeHg_T$	-3.30	-0.97	-5.02	0.64	3.81	0.74	**-4.1**	**-0.18%**	**+0.53%**
2 - Input from rivers	Hg_T	23.7	--	68.5	--	0.09	--	**92**	**--**	**--**
	$MeHg_T$	1.18	--	3.43	--	$4\ 10^{-3}$	--	**4.6**	**--**	**--**
3 - Atmospheric deposition	Hg_T	2.34	0.99	1.64	0.14	1.53	0.63	**7.3**	**--**	**--**
4 - Volatilization	Hg^0	4.02	2.84	3.66	0.37	3.51	1.90	**14**	**-20.9%**	**+68.2%**
5 - Deposition	Hg_P	149	138	132	61.4	124	151	**631**	**-29.5%**	**+88.3%**
	$MeHg_P$	$3\ 10^{-4}$	$1.4\ 10^{-4}$	$3\ 10^{-4}$	$2\ 10^{-5}$	$2\ 10^{-4}$	$7\ 10^{-5}$	**$1\ 10^{-3}$**	**-0.01%**	**--**
6 - Resuspension	Hg_P	145.05	29.55	351.15	0.01	251.97	10.28	**778**	**-1.99%**	**+5.92%**
	$MeHg_P$	0.22	0.10	0.35	0.00	0.39	0.02	**1.1**	**-1.18%**	**+3.50%**
7 - Pore Water diffusion	Hg_D	-93.87	-31.59	-119	-4.39	-154	-57.6	**-457**	**-1.41%**	**+4.23%**
	$MeHg_D$	-0.37	-0.28	-0.37	-0.04	-0.80	-0.35	**-2.2**	**-1.50%**	**+4.53%**
8 - Burial	Hg_P	--	207	--	93.9	222	511	**1034**	**-0.38%**	**+1.13%**
	$MeHg_P$	--	$1.5\ 10^{-1}$	--	$7.3\ 10^{-2}$	$6.8\ 10^{-2}$	$2.1\ 10^{-1}$	**0.5**	**-0.77%**	**+2.30%**
a - Photo-oxidation		2.44	2.52	1.57	0.22	1.12	1.30	**7.9**	**-21.0%**	**+68.9%**
b - Photo-reduction		33.1	12.4	21.2	1.92	19.9	10.4	**83**	**-28.2%**	**+84.5%**
c - Photo-demethylation		$1\ 10^{-3}$	$4\ 10^{-4}$	$7\ 10^{-4}$	$1\ 10^{-4}$	$6\ 10^{-4}$	$3\ 10^{-4}$	**$3\ 10^{-3}$**	**-**	**-**
d - Methylation		0.71	0.68	1.24	0.10	1.61	0.77	**5.06**	**-1.45%**	**+4.36%**
e - Demethylation		0.04	0.03	0.05	0.00	0.04	0.02	**0.18**	**-0.76%**	**+2.60%**

Table 3. Model estimates of mercury cycle fluxes for the six sub-basins and for the total lagoon under reference conditions. All fluxes are given in mol/y. The last columns report changes influxes for the total lagoon under the two additional scenarios obtained by decreasing (DB) or increasing (IB) Hg concentration at the marine boundaries. Numbers and letters related to processes are the same as in Figure 2. Numbers in bold refer to the whole lagoon.

Approximately 788 mol/y of Hg_T and 5.2 mol/y of $MeHg_T$ enters the lagoon from the eastern inlets (Primero, Grado, Morgo) and 1347 mol/y of Hg_T and 9.3 mol/y of $MeHg_T$ exit from the western inlets (Buso, S. Andrea, Lignano). In agreement with our calculations, Hg_T export from the Marano-Grado Lagoon is higher than the export from other contamination hot- spots such as the Augusta basin (159 mol/y, Sprovieri et al., 2011) and the Aveiro Lagoon (209–383 mol/y, Pereira et al., 2009). Our estimation of Hg export is one order of magnitude less than that provided by Bloom et al. (2004) for the Venice lagoon (5533mol/y exported to the Adriatic Sea). However, caution should be taken when comparing budgets obtained with different methods because this may lead to incorrect conclusions. In fact, Hg budgets are sometimes given as a first order assessment, in which time dynamics are not considered and fluxes are computed simply as the product of average concentrations and time average boundary flows without considering mixing processes and concentration variations in time (Bloom et al., 2004; Pereira et al., 2009 and Sprovieri et al., 2011). Furthermore, some budget measurements only refer to a part of a larger system or to a period of the year and are then extrapolated to the whole, again neglecting space and time variability. In other cases, different assumptions or limited data sets are used. As an example, Melaku Canu et al. (2012), used a simplified physical representation of the system and only assessed the Hg_D fraction of the Hg budget. Oversimplification of the data occurs frequently, which surely affects final assessments and emphasizes the need of great caution in comparison exercises. Other output terms in our budget are the evasion of Hg^0 toward the atmosphere and the burial of contaminated sediments. Modelled volatilization of Hg^0 from the water column represented a loss term of 14 mol/y, corresponding to an average evasion rate equal to 0.098 μmol/m^2y, which was comparable with the rates reported for the Adriatic Sea (Andersson et al., 2007). The figure was comparable with, but lower than, the rates measured in the heavily polluted Augusta basin (mean in June: 0.52 μmol/m^2y, range 0.31–0.78 and mean in November: 1.74 μmol/m^2y, range 0.62–3.14; Bagnato et al., 2013). The average volatilization rate was slightly higher in the Grado Lagoon (0.1 μmol/m^2y) than in the Marano Lagoon (0.09 μmol/m^2y), but the total amount of evaded Hg^0 was higher in the latter (9.1 vs 4.9 mol/y) due its greater surface area.

Our results suggest that the major pathways for the natural attenuation of Hg_T concentrations in Marano-Grado Lagoon sediment are burial (1 kmol/y) and diffusion from the sediment to the water column (457 mol/y, of which 0.48% is MeHg). MeHg tends to move from sediment mainly via pore water diffusion (2.2 mol/y) and resuspension of $MeHg_P$ (1.1 mol/y). Both burial and diffusion processes are more intense in the Grado Lagoon relative to the Marano Lagoon, while resuspension is higher in the Marano Lagoon mainly due to differences in morphological and hydrodynamic features of the two lagoon systems. Indeed, the more intense circulation of water in the Marano Lagoon favors resuspension, while in the shallower Grado Lagoon the lower hydrodynamic energy

favors Hg deposition and accumulation into the sediment. The amount of Hg_P and $MeHg_P$ buried is equal to 206 mol/y and 0.15 mol/y in the Marano Lagoon, respectively, and 825 mol/y and 0.34 mol/y in the Grado Lagoon, respectively. Hg_T is buried more efficiently than MeHg because of its higher affinity to sediment (i.e. higher K_D for Hg_T than MeHg).

The annual export of Hg_D and $MeHg_D$ diffusing from the pore water is 243 and 1 mol/y in the Marano Lagoon, respectively, and 214 and 1.2 mol/y in the Grado Lagoon. These correspond to diffusion rates of 2.2 μmol/m^2y for Hg_D, and 0.01 μmol/m^2y for MeHg in the Marano Lagoon, and diffusion rates of 3.4 μmol/m^2y for Hg_D and 0.02 μmol/m^2y for MeHg in the Grado Lagoon. Modelled diffusion rates of pore water are lower than the estimates provided by Emili et al. (2012) based on seasonal benthic fluxes in the Marano-Grado lagoon. The authors calculated average Hg_T fluxes to be 8.4 μmol/m^2y (for the Marano Lagoon) and 19.9 μmol/m^2y (for the Grado Lagoon, Primero station) and MeHg fluxes to be 0.23 (for the Marano Lagoon) and 0.84 μmol/m2y (for the Grado Lagoon, Primero station). Intense Hg transformations occurred in water, with 83 mol/y of Hg0 produced by photo-reduction and 7.9 mol/y of Hg^{II} produced by photo-oxidation. Due to the higher sediment concentrations of Hg_D compared to $MeHg_D$ (193 vs 1.1 pM), the model computed a net production of MeHg via microbial methylation. Approximately 0.2 mol/y of Hg_D was produced by demethylation and 5 mol/y of $MeHg_D$ was produced by methylation. More than half of the MeHg produced in the sediment moved to the water as a consequence of pore-water diffusion (2.2 mol/y) and resuspension of the particle-bound fraction (1.1mol/y). Approximately 10% of the MeHg produced each year was buried (0.5 mol/y), and only a small amount was reduced to Hg^0 by photo-demethylation (0.003 mol/y). The remaining amount of MeHg (1.2mol/y), together with the MeHg coming from riverine sources (4.6mol/y), was partially exported to the Adriatic Sea (4.1mol/y) or remained in the lagoon water (1.7mol/y). An analysis of additional simulations performed after changing model Hg concentrations at the boundary enabled us to assess the sensitivity of model outputs to changes in the marine boundary. This type of assessment is usually used to assess the robustness of model results, to understand the relationships between input and output variables in a complex system, or to indicate focus areas for future measurement efforts. Melaku Canu et al. (2012) already showed that the Hg cycle in the Marano-Grado Lagoon is a little sensitive to riverine input, because there are 2 other sources of Hg which are more important, namely the Hg exchanged at the inlets (i.e. input from the sea) and the Hg exchanged at the sediment/water interface (i.e. input from the sediment). The most important input is the input from the sea, possibly because: a) the Hg concentration in sea water is anomalously high, because of the impact of the Soča/Isonzo River; b) the water volume exchanged at the inlets is higher than the water mass that comes from the rivers. In fact, the time required by the river flow to flush the entire lagoon is around 30 days, while the flushing time computed considering

both the river inputs and the inlets exchanges is about 7 days. Here we explored the model response, in terms of Hg species concentrations and overall budgets, to two hypothetic scenarios in which HgT concentrations at the lagoon inlets were significantly higher or lower. The results indicated that a hypothetic doubling (+100%) of Hg concentration at the marine boundary would induce an average increase of Hg_T andHg0 in the lagoon water by 80% and 70%, respectively, a 12% increase of HgT in the sediment compartment, and a negligible increase of MeHg. Conversely, a sharp decrease (−30%) in the Hg concentration at the marine boundary would cause a decrease of 20% of Hg_T and Hg^0 in the lagoon water and a decrease of 3% of Hg_T in the sediment compartment. Accordingly, the evasion flux would increase by 68% (or decrease of 21%) with an increase (or decrease) in concentration. The export flux to the sea was less sensitive to changes in Hg_T and Hg^0 concentrations at the marine boundary and varied by −1.4%, and +4% in the increasing and decreasing scenarios, respectively. Therefore, an increase in Hg concentration at the inlets would generally increase the Hg fluxes, but the responses are not linear and some processes are likely to be more affected than others. In particular, an estimation of the Marano-Grado Lagoon's contribution to the Hg input of the Mediterranean Sea is only slightly affected by changes in the marine boundary concentration. This result also adds robustness to our estimates. In addition to the budget quantification, another important output of this application lies in its ability to suggest knowledge gaps that need to be addressed to reduce the level of uncertainty of the model responses, and, in particular to address future field efforts. Current legislation mainly focuses on assessments of Hg_T, due to analytical challenges in Hg speciation measurements. However, a complete synoptic set of measurements of Hg_D, Hg_P, and MeHg in water, even if maintained for a limited time period, would provide useful information to assess the performance of models and to calibrate the model for use in planning and evaluating environmental management scenarios. Moreover, MeHg measurements in water would also be needed considering that these species are of major interest due to public and ecosystem health concerns. Additionally, special efforts should be made to assess photo-transformation rates such as of photo-reduction, photo-oxidation and photo-demethylation.

2.4. Conclusions

Models, such as the one developed and presented in this study, are valuable tools that link a plethora of disconnected field studies and enable investigations on system behaviors. In this application, a model was used to assess Hg export to the Mediterranean Sea. However, this model could be used to investigate other aspects, too, such as long-term responses to environmental changes related to long-term climate variations, land use changes or morphological changes that could alter lagoon dynamics. The model has room for improvement, for instance, in aspects such as increases in spatial resolution that would allow for a better representation of spatial variability. This

would require, concurrently, the availability of additional measures. Another aspect that deserves further investigation and effort is the representation of dynamics at the sediment layer, and, in particular, the dynamic modelling of the relationship between organic matter re-mineralization and Hg_D release to pore water, and the implementation of empirical diffusion functions. Sediment processes are very important in shallow water environments and play an especially crucial role in MeHg budgets. This work provides a first comprehensive overview of the Hg cycle in the Marano-Grado Lagoon, by integrating Hg data and other environmental parameters with literature values of Hg kinetic processes into a model framework specifically developed for Hg modelling. The model was able to reproduce the average measured Hg_T and MeHg values and was used to quantify the Hg budgets between the Marano-Grado Lagoon and its surrounding environments. During its residence in the Marano-Grado Lagoon, Hg underwent several transformations, which led to a net MeHg production of 5mol/y (1 kg/y) within the sediment compartment.

The estimated net export of Hg_T from the Lagoon to the Adriatic Sea was 0.56 kmol/y (i.e., approximately 115 kg/y) for Hg_T, and 4.1 mol/year for MeHg. The Hg_T export corresponded to almost 6% of the Hg_T load to the Mediterranean basin (10 kmol/y) estimated by Rajar et al. (2007), thus confirming that the Marano-Grado Lagoon is an important source of Hg for the Mediterranean Sea. Results also demonstrated that the Marano-Grado Lagoon was a net emitter of Hg0 to the atmosphere. Information on Hg inputs to the Adriatic and to the atmosphere therefore appears to be crucial when assessing Hg budgets at a regional scale. Finally, our results also indicated that the most critical shortcoming of the currently available data sets is the lack of complete synoptic measurements and suggest that future experimental efforts should also include information on the photo-transformation rates.

Acknowledgments:

This research was carried out with contributions from the RITMARE flagship project and EU-SHAPE project. We would like to thank Isabella Scroccaro from ARPA-FVG for sharing unpublished data. We would like to thank Robert Ambrose for his support with the WASP code.

2.5 References

Acquavita, A., Covelli, S., Emili, A., Berto, D., Faganeli, J., Giani, M., Horvat, M., Koron, N., Rampazzo, F., 2012 (a). Mercury in the sediments of the Marano and Grado Lagoon (northern Adriatic Sea): Sources, distribution and speciation. Estuar. Coast. Shelf Sci. 113, 20-31.

Acquavita, A., Grahonja, R., Mattassi, G., Skert, N., 2012 (b). Biomonitoraggio di mercurio aerodisperso tramite licheni come bioccumulatori nella Laguna di Marano e Grado e basso bacino scolante. XXV Convegno della Società Lichenologica Italiana, Roma, 3-5 Ottobre.

Andersson, M.E., Gårdfeldt, K., Wängberg, I., Sprovieri, F., Pirrone, N., Lindqvist, O., 2007. Seasonal and daily variation of mercury evasion at coastal and off shore sites from the Mediterranean Sea. Mar. Chem. 104, 214-226.

Amos H.M., Sonke J.E., Obrist D., Robins N., Hagaìn N., Horowitz H.M., Mason R.P., Witt M., Hedgecock I.M., Corbitt E.S., Sunderland E.M. 2015. Environmental Science and Technology. Vol. 49, Issue 7: 4036-4047.

Bagnato, E., Sproveri, M., Barra, M., Bitetto, M., Bonsignore, M., Calabrese, S., Di Stefano, V., Oliveri, E., Parello, F., Mazzola, S., 2013. The sea–air exchange of mercury (Hg) in the marine boundary layer of the Augusta basin (southern Italy): Concentrations and evasion flux. Chemosphere 93, 2024-2032.

Black, F.J., Conaway, C.H., Flegal, R.A., 2012. Mercury in the marine environment, in Bank, M.S. (Ed.), Mercury in the Environment. Pattern and Process., University of California press ed. Bank, Michel S., Berkley and Los Angeles, pp. 167-178.

Blasutto, O., Cibic, T., De Vittor, C., Umani, S.F., 2005. Microphytobenthic primary production and sedimentary carbohydrates along salinity gradients in the Lagoons of Grado and Marano (Northern Adriatic Sea). Hydrobiologia 550, 47-55.

Bloom, N.S., Moretto, L.M., Scopece, P., Ugo, P., 2004. Seasonal cycling of mercury and monomethyl mercury in the Venice Lagoon (Italy). Mar. Chem. 91, 85-99.

Bouchet, S., Amouroux, D., Rodriguez-Gonzalez, P., Tessier, E., Monperrus, M., Thouzeau, G., Clavier, J., Amice, E., Deborde, J., Bujan, S., Grall, J., Anschutz, P., 2013. MMHg production and export from intertidal sediments to the water column of a tidal lagoon (Arcachon Bay, France). Biogeochemistry 114, 341-358.

Bramabati, A., 1996. Metalli Pesanti Nelle Lagune Di Marano e Grado. Regione Autonoma Friuli-Venezia Giulia, Trieste.

Castaño, A., Cutanda, F., Esteban, M., Pärt, P., Navarro, C., Gómez, S., Rosado, M., López, A., López, E., Exley, K., Schindler, B.K., Govarts, E., Casteleyn, L., Kolossa-Gehring, M., Fiddicke, U., Koch, H., Angerer, J., Hond, E.D., Schoeters, G., Sepai, O., Horvat, M., Knudsen, L., Aerts, D., Joas, A., Biot, P., Joas, R., Jiménez-Guerrero, J.A., Diaz, G., Pirard, C., Katsonouri, A., Cerna, M., Gutleb, A.C., Ligocka, D., Reis, F.M., Berglund, M., Lupsa, I., Halzlová, K., Charlier, C., Cullen, E., Hadjipanayis, A., Krsková, A., Jensen, J.F., Nielsen, J.K., Schwedler, G., Wilhelm, M., Rudnai, P., Középesy, S., Davidson, F., Fischer, M.E., Janasik, B., Namorado, S., Gurzau, A.E., Jajcaj, M., Mazej, D., Tratnik, J.S., Larsson, K., Lehmann, A., Crettaz, P., Lavranos, G., Posada, M., Fish consumption patterns and hair mercury levels in children and their mothers in 17 EU countries. Environ. Res.

Clarkson, T.W., Magos, L., 2006. The Toxicology of Mercury and Its Chemical Compounds. Crit. Rev. Toxicol. 36, 609-662.

Cossa, D., Harmelin-Vivien, M., Mellon-Duval, C., Loizeau, V., Averty, B., Crochet, S., Chou, L., Cadiou, J.-., 2012. Influences of Bioavailability, Trophic Position, and Growth on Methylmercury in Hakes (Merluccius merluccius) from Northwestern Mediterranean and Northeastern Atlantic. Environ. Sci. Technol. 46, 4885-4893.

Covelli, S., Faganeli, J., De Vittor, C., Predonzani, S., Acquavita, A., Horvat, M., 2008. Benthic fluxes of mercury species in a lagoon environment (Grado Lagoon, Northern Adriatic Sea, Italy). Appl. Geochem. 23, 529-546.

Covelli, S., Faganeli, J., De Vittor, C., Predonzani, S., Acquavita, A., Horvat, M., 2008. Benthic fluxes of mercury species in a lagoon environment (Grado Lagoon, Northern Adriatic Sea, Italy). Appl. Geochem. 23, 529-546.

Covelli, S., Acquavita, A., Piani, R., Predonzani, S., De Vittor, C., 2009. Recent contamination of mercury in an estuarine environment (Marano lagoon, Northern Adriatic, Italy). Estuar. Coast. Shelf Sci. 82, 273-284.

Covelli, S., Langone, L., Acquavita, A., Piani, R., Emili, A., 2012. Historical flux of mercury associated with mining and industrial sources in the Marano and Grado Lagoon (northern Adriatic Sea). Estuar. Coast. Shelf Sci. 113, 7-19.

Covelli, S., Piani, R., Acquavita, A., Predonzani, S., Faganeli, J., 2007. Transport and dispersion of particulate Hg associated with a river plume in coastal Northern Adriatic environments. Mar. Pollut. Bull. 55, 436-450.

De Vittor, C., Faganeli, J., Emili, A., Covelli, S., Predonzani, S., Acquavita, A., 2012. Benthic fluxes of oxygen, carbon and nutrients in the Marano and Grado Lagoon (northern Adriatic Sea, Italy). Estuar. Coast. Shelf Sci. 113, 57-70.

Díez, S., Montuori, P., Pagano, A., Sarnacchiaro, P., Bayona, J.M., Triassi, M., 2008. Hair mercury levels in an urban population from southern Italy: Fish consumption as a determinant of exposure. Environ. Int. 34, 162-167.

Dizdarevič, T., 2001. The influence of mercury production in Idrija mine on the environment in the Idrija region and over a broad area. RMZ - Materials and geoenvironment 48, 56-64.

Dorigo, L., 1965. La laguna di Grado e le sue foci. Ufficio Idrografico del Magistrato della Acque 155.

Emili, A., Acquavita, A., Koron, N., Covelli, S., Faganeli, J., Horvat, M., Žižek, S., Fajon, V., 2012. Benthic flux measurements of Hg species in a northern Adriatic lagoon environment (Marano and Grado Lagoon, Italy). Estuar. Coast. Shelf Sci. 113, 71-84.

Faganeli, J., Hines, M.E., Horvat, M., Falnoga, I., Covelli, S., 2014. Methylmercury in the Gulf of Trieste (Northern Adriatic Sea): From Microbial Sources to Seafood Consumers. Food Technology and Biotechnology 52 (2), 188-197.

Faganeli, J., Horvat, M., Covelli, S., Fajon, V., Logar, M., Lipej, L., Cermelj, B., 2003. Mercury and methylmercury in the Gulf of Trieste (northern Adriatic Sea). Sci. Total Environ. 304, 315-326.

Fitzgerald, W.F., Lamborg, C.H., Hammerschmidt, C.R., 2007. Marine biogeochemical cycling of mercury. Chem. Rev. 107, 641-662.

Fontolan, G., Pillon, S., Delli Quadri, F., Bezzi, A., 2007. Sediment storage at tidal inlets in northern Adriatic lagoons: Ebb-tidal delta morphodynamics, conservation and sand use strategies. Estuar. Coast. Shelf Sci. 75, 261-277.

Fontolan, G., Pillon, S., Bezzi, A., Villalta, R., Lipizer, M., Triches, A., D'Aietti, A., 2012. Human impact and the historical transformation of saltmarshes in the Marano and Grado Lagoon, northern Adriatic Sea. Estuar. Coast. Shelf Sci. 113, 41-56.

Giani, M., Rampazzo, F., Berto, D., Maggi, C., Mao, A., Horvat, M., Emili, A., Covelli, S., 2012. Bioaccumulation of mercury in reared and wild Ruditapes philippinarum of a Mediterranean lagoon. Estuar. Coast. Shelf Sci. 113, 116-125.

Gilmour, C.C., Podar, M., Bullock, A.L., Graham, A.M., Brown, S.D., Somenahally, A.C., Johs, A., Hurt, R.A., Bailey, K.L., Elias, D.A., 2013. Mercury Methylation by Novel Microorganisms from New Environments. Environ. Sci. Technol. 47, 11810-11820.

Guédron, S., Huguet, L., Vignati, D.A.L., Liu, B., Gimbert, F., Ferrari, B.J.D., Zonta, R., Dominik, J., 2012. Tidal cycling of mercury and methylmercury between sediments and water column in the Venice Lagoon (Italy). Mar. Chem. 130-131, 1-11.

Heimbürger L.E., Cossa D., Marty J.C., Migon C., Averty B., Dufour A., Ras J., 2010. Methylmercury distributions in relation to the presence of nanoandpicophytoplankton in an oceanic water column (LigurianSea, North-western Mediterranean). Geochim. et Cosmochim. Acta 74, 5549–5559.

Heimbürger LE, Cossa D, Thibodeau B, Khripounoff A, Mas V, Chiffoleau J-F, Schmidt S, Migon C. 2012. Natural and anthropogenic trace metals in sediments of the Ligurian Sea (Northwestern Mediterranean). Chem Geo 291(0): 141-151.

Heimbürger L.E., Sonke J.E., Cossa D., Point D., Lagane C., Laffont L., Galfond B., Nicolaus M., Rabe B., van der Loeff M.,R. 2015. Shallow methylmercury production in the marginal sea ice zone of the central Arctic Ocean. Scientific Reports. DOI: 10.1038/srep10318.

Hammerschmidt, C.R., Fitzgerald, W.F., 2004. Geochemical Controls on the Production and Distribution of Methylmercury in Near-Shore Marine Sediments. - Environ. Sci. Technol. 38, 1487-1495.

Hines, M.E., Poitras, E.N., Covelli, S., Faganeli, J., Emili, A., Žižek, S., Horvat, M., 2012. Mercury methylation and demethylation in Hg-contaminated lagoon sediments (Marano and Grado Lagoon, Italy). Estuar. Coast. Shelf Sci. 113, 85-95.

Horvat, M., Kotnik, J., Logar, M., Fajon, V., Zvonarić, T., Pirrone, N., 2003. Speciation of mercury in surface and deep-sea waters in the Mediterranean Sea. Atmos. Environ. 37, Supplement 1, 93-108.

Hrubá, F., Strömberg, U., Černá, M., Chen, C., Harari, F., Harari, R., Horvat, M., Koppová, K., Kos, A., Krsková, A., Krsnik, M., Laamech, J., Li, Y., Löfmark, L., Lundh, T., Lundström, N., Lyoussi, B., Mazej, D., Osredkar, J., Pawlas, K., Pawlas, N., Prokopowicz, A., Rentschler, G., Spěváčková, V., Spiric, Z., Tratnik, J., Skerfving, S., Bergdahl, I.A., 2012. Blood cadmium, mercury, and lead in children: An international comparison of cities in six European countries, and China, Ecuador, and Morocco. Environ. Int. 41, 29-34.

Kocman, D., Horvat, M., Pirrone, N., Cinnirella, S., 2013. Contribution of contaminated sites to the global mercury budget. Environ. Res. 125, 160-170.

Lamborg, C.H., Hammerschmidt, C.R., Bowman, L.L., Swarr, G.J., Munson, K.M., Ohnemus, D.C., Lam P.J., Heimbürger, L.E., Rijkenberg M.J.A., Saito, M.A. 2014. A global ocean inventory of anthropogenic mercury based on water column measurements. Nature Vol 15, 65.

Mason, R.P., Choi, A.L., Fitzgerald, W.F., Hammerschmidt, C.R., Lamborg, C.H., Soerensen, A.L., Sunderland, E.M., 2012. Mercury biogeochemical cycling in the ocean and policy implications. Environ. Res. 119, 101-117.

Melaku Canu, D., Acquavita, A., Knightes, C.D., Mattassi, G., Scroccaro, I., Solidoro, C., 2012. Modeling the Mercury Cycle in the Marano-Grado Lagoon (Italy) in Jordan, Jorgensen (Eds.), Models of the Ecological Hierarchy: From Molecules to the Ecosphere, 1st Edition ed. Elsevier, pp. 239-257.

Monperrus, M., Tessier, E., Amouroux, D., Leynaert, A., Huonnic, P., Donard, O.F.X., 2007. Mercury methylation, demethylation and reduction rates in coastal and marine surface waters of the Mediterranean Sea. Mar. Chem. 107, 49-63.

Pereira, M.E., LillebÃ¸, A.I., Pato, P., VÃ¡lega, M., Coelho, J.P., Lopes, C.B., Rodrigues, S., Cachada, A., Otero, M., Pardal, M.A., Duarte, A.C., 2009. Mercury pollution in Ria de Aveiro (Portugal): a review of the system assessment. Environ. Monit. Assess. 155, 39-49.

Piani, R., Covelli, S., Biester, H., 2005. Mercury contamination in Marano Lagoon (Northern Adriatic sea, Italy): Source identification by analyses of Hg phases. Appl. Geochem. 20, 1546-1559.

Pirastu, R., Comba, P., Conti, S., Iavarone, I., Fazzo, L., Pasetto, R., Zona, A., Crocetti, E., Ricci, P., 2014. Mortality, cancer incidence and hospital discharges. Epidemiologia e prevenzione 38.

Rajar, R., Četina, M., Horvat, M., Žagar, D., 2007. Mass balance of mercury in the Mediterranean Sea. Mar. Chem. 107, 89-102.

Ravichandran, M., Aiken, G.R., Reddy, M.M., Ryan, J.N., 1998. Enhanced dissolution of cinnabar (mercuric sulfide) by dissolved organic matter isolated from the Florida Everglades. Environ. Sci. Technol. 32, 3305–3311. doi:10.1021/es9804058

Rothenberg, S.E., Ambrose, R.F., Jay, J.A., 2008. Mercury cycling in surface water, pore water and sediments of Mugu Lagoon, CA, USA. Environmental Pollution 154, 32-45.

Saltelli A, Tarantola S and Campolongo F (2000) Sensitivity analysis as an ingredient of modelling. Statistical science 15(4), 377-395.

Schnoor JL, Sato C, McKechnie D, Sahoo D. Processes, Coefficients, and Models for Simulating Toxic Organics and Heavy Metals in Surface Waters. 1987U.S. EPA, Athens, GA. EPA/600/3-87-015.

Soerensen A.L., Mason R.P., Balcom P.H., Jacob D.J., Zhang Y., Kuss J., Sunderland E.M.. 2014. Elemental mercury concentrations and fluxes in the tropical atmosphere and Ocean. Environmental Science and Technology. Vol. 48, Issue 19: 11312-11319.

Sonke, J.E., Heimbürger, L., Dommergue, A., 2013. Mercury biogeochemistry: Paradigm shifts, outstanding issues and research needs. Comptes Rendus Geoscience 345, 213-224.

Sorokin, Y.I., Sorokin, P.Y., Giovanardi, O., Dalla Venezia, L., 1996. Study of the ecosystem of the lagoon of Venice, with emphasis on anthropogenic impact. Mar. Ecol. Prog. Ser. 141, 247-261.

Sprovieri, M., Oliveri, E., Di Leonardo, R., Romano, E., Ausili, A., Gabellini, M., Barra, M., Tranchida, G., Bellanca, A., Neri, R., Budillon, F., Saggiomo, R., Mazzola, S., Saggiomo, V., 2011. The key role played by the Augusta basin (southern Italy) in the mercury contamination of the Mediterranean Sea. J. Environ. Monit. 13, 1753-1760.

Sunderland E.M., Krabbenhoft D.P., Moreau J.W., Strode S.A., Landing W.M. 2009. Mercury sources, distribution, and bioavailability in the North Pacific Ocean: Insights from data and models. Global Biogeochemical Cycles. Vol. 23 Issue 2.

Sutherland, R., 1998. Loss-on-ignition estimates of organic matter and relationships to organic carbon in fluvial bed sediments. Hydrobiologia 389, 153-167.

Thibodeaux, L.J., Matisoff, G., Reible, D.D., 2011. Bioturbation and Other Sorbed-Phase Transport Processes in Surface Soils and Sediments, in Thibodeaux, L.J., Mackay, D. (Eds.), Chemical Mass Transport in the Environment. Taylor and Francis Group, LLC, pp. 359-388.

USEPA, 1988 Water quality Simulation program, v. 5. manual. (Ambrose R.)

US EPA. 1995 Total Maximum Daily Load (TMDL) for Settleable Solid Residues in the Waters of Akutan Harbor, Alaska. Environmental Protection Agency, Seattle, WA. Region X. (Appendix A).

US EPA (2001) Sensitivity analysis: how do we know what's important? RAGS Volume 3, Part A - Process for Conducting Probabilistic Risk Assessment, Appendix A http://www.epa.gov/oswer/riskassessment/rags3adt/pdf/appendixa.pdf

US EPA 2009 Water Quality Simulation Program v. 6. manual. Wool T. A., Ambrose R. B., Martin J.L., Comer E. A.

Vost, E.E., Amyot, M., O'Driscoll, N.J., 2012. Photoreactions of mercury in aquatic systems, in Liu, G., Cai, Y., O'Driscoll, N. (Eds.), Environmental Chemistry and Toxicolgy of Mercury, Wiley ed. JOHN WILEY & SONS, INC., pp. 193-218.

Watras, C.J., Back, R.C., Halvorsen, S., Hudson, R.J.M., Morrison, K.A., Wente, S.P., 1998. Bioaccumulation of mercury in pelagic freshwater food webs. Sci. Total Environ. 219, 183-208.

Whalin, L., Kim, E., Mason, R., 2007. Factors influencing the oxidation, reduction, methylation and demethylation of mercury species in coastal waters. Mar. Chem. 107, 278-294.

Wool, T.A., Ambrose, R.B., Martin, J.L., Comer, E.A., 2001. Water Quality Analysis Simulation Program (WASP) Version 6.0: User's Manual.

Žagar, D., Petkovšek, G., Rajar, R., Sirnik, N., Horvat, M., Voudouri, A., Kallos, G., Četina, M., 2007. Modelling of mercury transport and transformations in the water compartment of the Mediterranean Sea. Mar. Chem. 107, 64-88.

Chapter 3 - Long-term scenarios of mercury budgeting and exports for a Mediterranean hot spot (Marano-Grado Lagoon, Adriatic Sea)

Part of this chapter has been published as:
Canu, D., Rosati, G., 2017. Long-term scenarios of mercury budgeting and exports for a Mediterranean hot spot (Marano-Grado Lagoon, Adriatic Sea). Estuar. Coast. Shelf Sci. 1–11.

3.1. Introduction

Mercury is a persistent pollutant of global concern that can accumulate in organisms and that can have adverse health effects. Its presence is mainly a result of past human activities such as mining and industrial dumping that have severely altered the state of mercury concentrations in several transitional systems worldwide. A SCOPUS abstract search based on keywords "mercury", "contamination", and "estuaries" retrieved 153 papers published from 1985, 65 of which are focused on "lagoons". The number of studied sites and their global distributions highlight the relevance of this issue also because estuarine and transitional environments play a crucial role in the production of MeHg, a central driver of mercury bioaccumulation in pelagic organisms (Balcom et al., 2015).The quantification of mercury export contributions from coastal lagoons and estuaries is, therefore, relevant for the assessment of mercury budgets at the global and regional scales. Several budget analysis and modelling efforts are being pursued to this end to evaluate and inter-compare Hg fluxes such as evasion fluxes (Sharif et al., 2013), transfer to food webs (Balcom et al., 2015), riverine inputs (Amos et al., 2014), and transfer to seas and oceans (Zagar et al., 2006, Pato et al., 2008, Bloom et al., 2004, Canu et al., 2012, Melaku Canu et al., 2015 Sprovieri et al., 2011).

Mathematical models are also suitable tools for addressing long-term trajectories under different conditions, including changes in boundary inputs and climate changes (Harley et al., 2006). Scenario analyses are often used to explore system trends and responses according to different assumptions based on direct and indirect effects of human interventions; explore long term trends under semi-stationary conditions, such as climate change effects on marine biogeochemistry (Cossarini et al., 2008, Lazzari et al., 2014, Solidoro et al., 2009) or on persistent pollutants (Dalla Valle et al., 2007); and to explore the effectiveness of management responses (Canu et al., 2010, Melaku Canu et al., 2001, Thompson and Flower, 2009).

In this work, a mercury model already formulated and tested for the Marano-Grado Lagoon (Melaku Canu et al., 2015) is used to evaluate long-term mercury contamination trends in the lagoon under alternative scenarios.

The Marano–Grado Lagoon (Italy) is a coastal lagoon in the Mediterranean Sea (Figure 1) of roughly 160 km^2 that receives freshwater inputs from rivers and marine inputs from the Northern Adriatic Sea. Tidally driven water exchange with the Adriatic Sea is bidirectional and occurs through six inlets (i.e., Lignano, S. Andrea, Buso, Morgo, Grado and Primero, Figure 1) after which the 6 sub-basins were named (Dorigo, 1965). Riverine effects, given the strong seasonal variations in salinity, have been identified in the western section of the lagoon while the eastern section is more marine driven (Ferrarin et al., 2010).

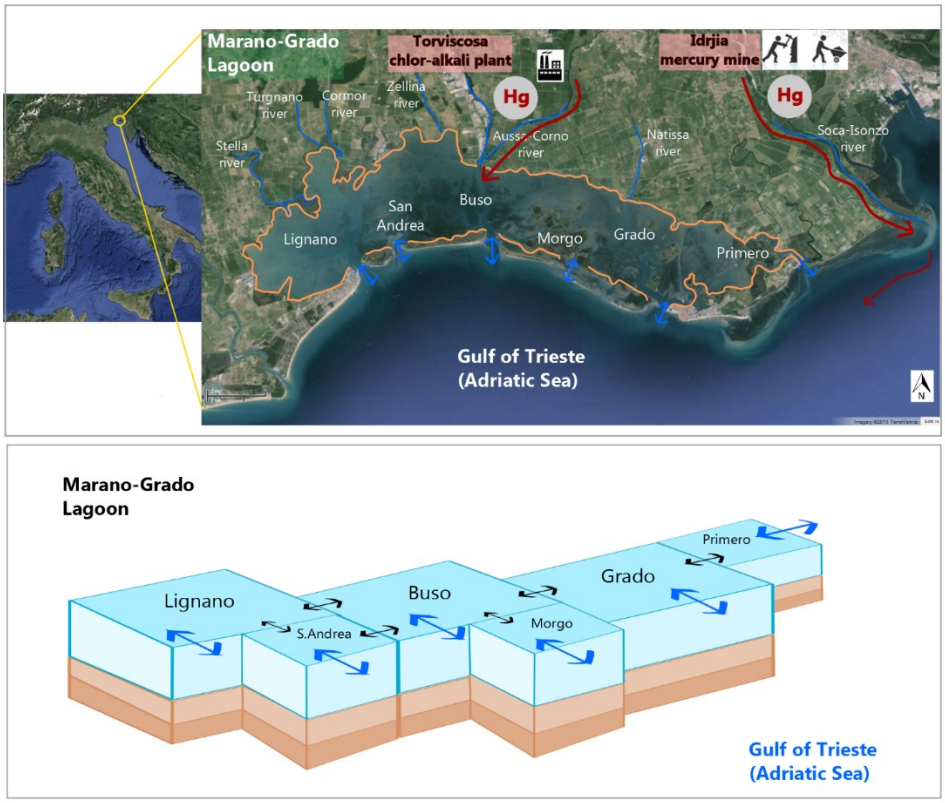

Figure 1. The upper panel is a satellite image of the Marano-Grado lagoon. The lagoon boundary is highlighted in orange, riverine inputs and marine exchanges are represented in blue, local anthropogenic Hg inputs are shown in red. The lower panel shows the box model representation in 6 boxes each formed by a water layer, and two sediment layers (surface and subsurface).

The lagoon is a hot spot of mercury contamination (Covelli et al., 2012) as a consequence of mining and industrial activities that have caused the release of large amounts of mercury compounds into the environment. As Hg is pervasively present in the lagoon sediment, diffuse reclamation is not feasible. The historical source of Hg is the Idrija cinnabar mine (Slovenia), which has been estimated to have released 37,000 tons of Hg over 500 years of activity (Dizdarevič, 2001). The Hg extraction in the Idrija mine reached a maximum at the end of the 19th century, followed by a gradual decrease in the following decades. The ore dumping in the environment followed a similar pattern, until 1970, when the direct dumping into the river was finally prohibited. At the end of the 1980's the Hg production was 1/10 of the peak's production reached in 1890. (Gnamuš and Horvat, 1999, Ĉar and Dizdarevič,

2004). This material has been transported by the Soča-Isonzo River and delivered to the Gulf of Trieste (Zagar et al., 2006). While most particulate Hg deposits are found close to riverbanks, prevailing currents also drive suspended and dissolved materials further south towards the Marano-Grado Lagoon. Currently, average sediment concentrations reach 721 ppm downstream from the mine (Gosar and Teršič, 2015), 40 ppm at the Soča-Isonzo River mouth (Gosar and Teršič, 2015), 1 ppm in the central Gulf of Trieste (Faganeli et al., 2014) and 4.4 ppm in the Marano-Grado Lagoon, thus ranging from 0.6 to 10 ppm (Acquavita et al., 2012). Higher levels in the sediment of the Marano-Grado Lagoon compared to those in the open Gulf of Trieste are attributable to the following different processes: 1) the direction of currents; 2) the lagoon as a more confined environment; and 3) the presence of an additional source of contamination.

In addition to inputs from the mining site, the lagoon has been receiving direct inputs of Hg through its Aussa-Corno River tributary from a former chlor-alkali plant that has dumped roughly 190 tons of Hg over 45 years (Acquavita et al., 2012). Historically, the lagoon has acted as a sink for Hg transported from the Gulf of Trieste and the chlor-alkali plant, accumulating roughly 251 tons of Hg in its sediments (Covelli et al., 2012). A mass balance study showed that under present conditions, outputs from the lagoon exceed inputs (Melaku Canu et al., 2015), and, thus, in the long-term, a natural decontamination of Hg stored in the lagoon's environmental compartment is expected. Here, we explore the time scale for the natural recovery of sediment and the relevance of different inputs and forcings to mercury dynamics in the lagoon using different future scenarios to take into account effects of environmental variability and climate change projections on mercury biogeochemistry dynamics and fluxes.

3.2. The model structure and its application

The dynamic and spatially resolved water quality model was applied using the Water Quality Analysis Simulation Programme (WASP7, v7.3) (as described in Melaku Canu et al., 2015).

As described by Wool et al. (2001), the model simulates the dynamic evolution of three mercury species over time: divalent inorganic mercury (Hg^{II}), methylmercury (MeHg) and elemental mercury (Hg^0) and three solids types (silt, sand, and biotic solids) in a discretized box system.

The overall equation for the mass conservation of generic state variable C (representative of a mercury species) in each water box includes terms for advection (U in m/sec) and diffusion (E in m^2/d) in the three dimensions (x, y, z) and reads as equation 1.1. The equation also accounts for the biogeochemical transformation of Hg species (S_{rx} in g/m^3d), direct and diffusive loads (SL in g/m^3d), and exchanges with boundaries or sediment (S_B in g/m^3d):

$$\frac{dC}{dt} = -\frac{d(U_x \cdot C)}{dx} - \frac{d(U_y \cdot C)}{dy} - \frac{d(U_Z \cdot C)}{dz} + \frac{d}{dx}\left(E_x \frac{dC}{dx}\right) + \frac{d}{dy}\left(E_y \frac{dC}{dy}\right) + \frac{d}{dz}\left(E_z \frac{dC}{dz}\right) + S_L + S_B + S_{rx} \qquad eq.\ 1.1$$

Advective and diffusive processes are responsible for the exchange of water, particles and solutes between water boxes and between boxes and their boundary systems including the atmosphere, deep sediments, and marine boundaries. While transported, Hg species are partitioned between dissolved and particulate phases.

Hg^0 is assumed only in its dissolved form while Hg^{II} and MeHg are modelled as sorbing to sand, silts, and biotic solids and as being complexed with dissolved organic carbon (DOC).

The model addresses the bioaccumulation of mercury in biota simply by dynamically modelling primary production and degradation processes of the 'organic solids' variable, which is subjected to production and dissolution. Production (equation 1.2) is parameterised based on a rate k_{pp} (g/m^3d) corrected by the temperature value ($\theta_{PP}^{T-20} X_t$) and it can be variable in space and time (using the X_{box} multiplier). In a similar way, degradation (equation 1.3) is parameterized based on a rate k_{deg} (1/d) that can be temperature-corrected and that is multiplied by the concentration of organic solids (COM) in that box:

$$Production = k_{PP} * \theta_{PP}^{T-20} * X_t * X_{box} \qquad [g\ dw/m^3 d] \qquad eq.\ 1.2$$

$$Degradation = k_{deg} * \theta_{deg}^{T-20} * X_t * X_{box} * C_{OM} \qquad [g\ dw/m^3 d] \qquad eq.\ 1.3$$

The model dynamically simulates transformations (S_{rx}, equation 1.1) by means of first order rate constants. The main processes included in the model are represented in Figure 2. The modelled transformation processes include the following: the photo-oxidation of Hg^0 into Hg^{II}, the photo-reduction of Hg^{II} into Hg^0, the photo-degradation of MeHg into Hg^0 in water, the biotic methylation of Hg^{II} into MeHg in water and sediments, the biotic demethylation of MeHg into Hg^{II} in water and sediments.

Mercury: 1) is transported through water fluxes in dissolved and particulate forms; 2) is diffused in interface water/sediment in its dissolved form; 3) volatilises at the water/air interface; and 4) is sedimented or resuspended at the sediment/water interface in particulate from.

Hg^0 exchange between surface water boxes and the overlying atmosphere is dependent on water and air concentrations of elemental Hg (Hg^0_w and Hg^0_{atm} in mg/L) and temperatures following Henry's law. Hg species exchange at the sediment layer/water interface is controlled by deposition and resuspension rates of organic and inorganic solids and pore water diffusion.

Resuspension and the settling of mercury species bounded to organic and inorganic solids are simulated dynamically in time at the sediment/water interface as a function of flow velocity, shear stress, and particle size (see Chapter 1, equations 1.3 - 1.8). As velocity decreases the shear stress

along the underlying sediment decreases, thereby decreasing the suspension velocity and increasing the settling velocity.

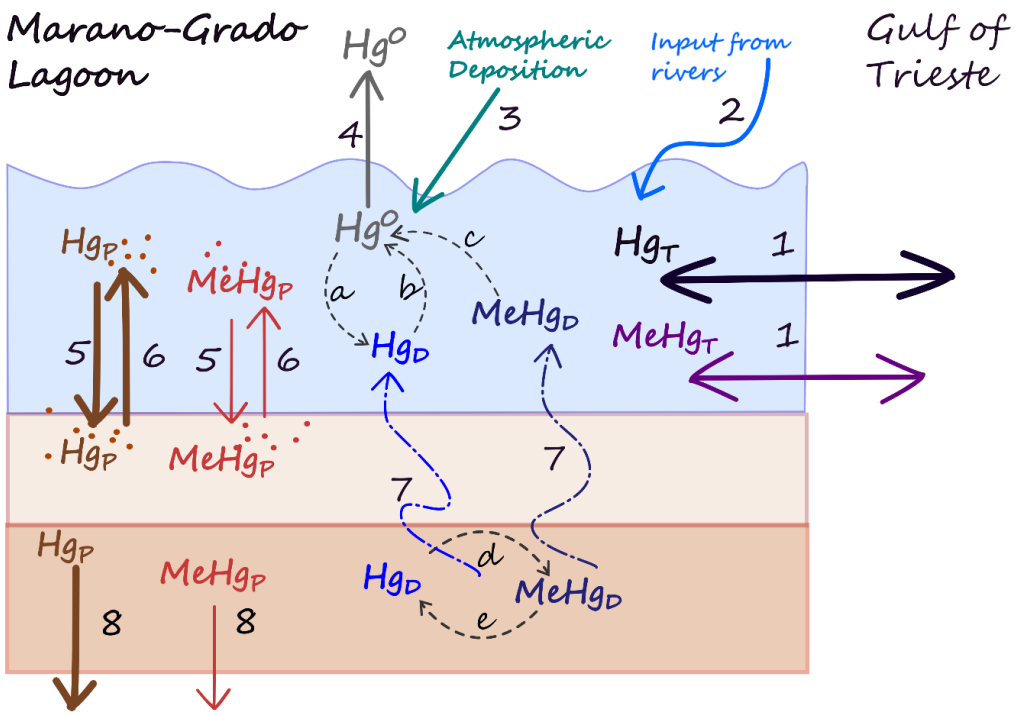

Figure 2. Main transport (1-*Exchange with the Sea*, 2-*Volatilization*, 3-*Deposition*, 4-*Resuspension*, 5-*Pore water diffusion*, 6-*Burial*) and transformation (a-*Photo-oxidation*, b-*Photo-reduction*, c-*Photo-demethylation*, d-*Methylation*, e-*Demethylation*) processes included in the WASP model. Hg_T is total Hg (Hg^{II} + Hg^0 + MeHg in dissolved and particulate phase), $MeHg_T$ is total MeHg (dissolved and particulate phase of MeHg), Hg_P and $MeHg_P$ are particulate-bounded Hg^{II} and MeHg, whilst Hg_D and $MeHg_D$ are the dissolved forms of Hg^{II} and MeHg.

The lagoon system is represented as an 18-box system with 3 water boxes representing riverine systems that are divided into 6 sub-basins (Lignano, S.Andrea, Buso, Morgo, Grado and Primero) according to the hydraulic zonation configuration proposed by Dorigo (1965). Each sub-basin is represented in the model as including the following three layers: a water layer, a surface sediment layer (0-2 cm depth) and a subsurface sediment layer (3-10 cm depth). Sub-basins are interconnected as shown in Figure 1b, and each is connected to the marine and overlying atmospheric boundaries. Three of them (Lignano, Buso and Grado) are connected to rivers. Exchanges of water, suspended particulates and Hg species occur at each intersection between sub-basins and boundaries.

Water transport between the 6 lagoon water boxes and with marine boundaries is simulated using prescribed water fluxes. Water fluxes were computed using a validated finite element hydrodynamic model of the Marano-Grado Lagoon (Ferrarin et al., 2010) forced with a 3-year set-up (2009-2011) that includes the following: water levels at marine inlets, meteorological forcings (hourly solar irradiance, precipitation, wind speed and direction) and riverine discharge.

The dynamical evolution of mercury species is modelled as a function of meteo-climatic data and is included in the model as daily forcing functions of light intensity, daylight hours, and monthly water temperature. The model can, therefore, reproduce the temporal variability of methylation-demethylation and photo-reactions (photo-demethylation, photo-reduction and photo-oxidation) while the partitioning of mercury species (Hg_T and MeHg) occurs at constant rates in time and space. Transport coefficients and transformation rate constants were selected according to studies conducted in the Marano-Grado Lagoon (Covelli et al., 2008 and by Hines et al., 2012) and other similar environments when local information was not available (Hammerschmidt and Fitzgerald, 2004, Monperrus et al., 2007, Rothenberg et al. 2008, Sorokin et al. 1996, Whalin et al., 2007, Vost et al., 2012, US EPA 1988, USEPA 2009).

Marine exchange with the Adriatic Sea was simulated through the advection of dissolved and particulate Hg (Hg_D and Hg_P) and MeHg ($MeHg_D$ and $MeHg_P$) according to the prescribed water flux variable in time and space, and according to monthly variable concentrations of particulate matter (SPM). This information was derived from our dataset (Horvat et al., 2003 and Regione FVG, 2013) as explained in Melaku Canu et al., (2015).

River inputs are given as unidirectional inputs of water, as dissolved and particulate Hg and as MeHg. Hg is input at the atmospheric boundary via deposition using the seasonal values given by Zagar et al., (2007).

The model was set up in agreement with Melaku Canu et al. (2015) using the three-year scenario set-up for 2009-2011, the time frame for which a complete series of dissolved mercury concentrations in the lagoon water and meteorological data are available. The model was initialised using spatially variable field data of sediment compositions (silt, sand and OC) and mercury sediment concentrations (Hg_T, HgS and MeHg) according to Acquavita et al., (2012). Concentrations in the water column were set to 0. Additional information on the model's implementation, parameter selection methods, and comparisons between experimental data on Hg_D and deposition, erosion and burial rates are given by Melaku Canu et al., (2015). Despite the model's simple spatial discretization, data comparisons confirm the model's capacity to reproduce the selected processes. Average sediment deposition values, erosion values and burial rates computed from the model based on values of shear stress induced by currents are in agreement with experimental values measured by Bloom et al. (2004) and Covelli et al. (2012).

The baseline scenario, Reference simulation (Ref), was used here to assess the recovery time of surface sediment under the assumption that external conditions remain as they are now (i.e., recursively applying the three-year set-up of forcing and boundary conditions). At the marine boundary, the concentration of dissolved mercury (Hg_D) and of mercury bounded to suspended

sediments (Hg_P) is mainly related to inputs delivered by the Isonzo River (Covelli et al., 2012, Rajar et al., 2000) and discharged into the Adriatic Sea in the Gulf of Trieste (see Figure 1a). Even though Hg_T at the marine boundary is expected to decrease in the future, as a consequence of the mine's closure in 1996, according to Covelli et al., 2012 in the short term, such a decrease is unlikely to occur. Gosar (2008) noted that mercury concentrations in river sediments in the Idrijca and Isonzo-(Soca) Rivers have not decreased over the past 15 years since mining activities have stopped due to the extent of historical discharge still present along the rivers banks. Therefore, we applied a precautionary approach by maintaining existing Hg_T input values throughout the whole simulation. In addition, we explored uncertainties in changes in forcing and boundary conditions by applying the following three additional scenarios: a) the increase in water temperature according to climatic change (CC) scenarios, b) the sea level rise High water Level scenario (HwL) and c) the removal of mercury inputs from the riverine boundaries (NoR). All of these simulations were run for 100 years and then compared.

The CC scenario was applied according to Lazzari et al., (2014), who modelled the effects of climate change on the biogeochemistry of the Mediterranean Sea following the IPCC's SRES A1B scenario conditions (Nakicenovic and Swart, 2000). For 2070-2100, they predicted a warming of Northern Adriatic Sea surface water of 2.5 °C both in the winter and summer. This temperature increase was, therefore, applied to the water temperature time series while all other forcings and parameters were the same as those used in the Ref simulation.

The HwL scenario was applied by introducing changes in water fluxes in agreement with the results of the hydrodynamic model simulation of a sea level rise scenario. The sea level rise scenario was simulated by increasing sea level values at marine boundaries of 0.315 m in agreement with Lambeck et al., 2011.

Moreover, the sediment recovery time was assessed through a long-term simulation by running the baseline Ref simulation until surface and subsurface sediment met the legislative limit of 0.3 ppm. This result was compared with results obtained from running a simulation that excluded mercury inputs from the Adriatic Sea while setting the sea Hg_T to 0 as an extreme case of mercury input reduction.

3.3. Results

After 100 years, the Ref simulation shows a general decrease in Hg_T concentrations along the Lagoon surface (Figure 3) and subsurface sediments (Figure 4). The average reduction in the two sediment layers of the whole lagoon is -63% with more pronounced decreasing trends found in the Primero (-86%) and Morgo (-93%) sub-basins, where depositional processes are more intense.

After an initial increase at the start of the simulation, MeHg tends to decrease and stabilize with asymptotic behaviour, on average increasing at the end by 43% in surface sediment and by 1.2% in the water column as shown in Tab. 1. At the end of the simulation, concentrations decrease in S.Andrea and Primero by -20% and -64% in surface sediments, respectively, and increase in the Lignano, Buso Morgo and Grado sub-basins by 102%, 81%, 22%, and 139%, respectively.

The increase or decrease of MeHg concentrations in each basins depends on several factor, among which:

1. the local ratio between potential methylation and demethylation rates;
2. the availability of substrate for methylation (i.e. Hg_D), which in the model depends on the sediment composition (silt, POM, sand), on the K_D, and on the fraction of HgS/Hg_T;
3. the mobility of MeHg that is affected by its partitioning between $MeHg_D$ and $MeHg_P$, depending on the sediment composition;
4. the current velocity and the residence time of water that determine the rate of sediment deposition and burial, and/or resuspension, erosion and transport to other sub-basins or across boundaries.

MeHg concentrations tend to increase in subsurface sediment (Figure 4, Tab. 1), reaching a pseudo-stable value in some sub-basins (S.Andrea, Primero and Morgo) and maintaining an increasing trend towards the end of the simulation for the others.

In response to high frequency signals (e.g., tidal exchanges and solar radiation), Hg_T concentrations in lagoon water (Figure 5) show higher levels of intra-annual variability than sediment concentrations. With time evolution (Table 1), an overall (statistically significant ($p<0.05$, Wilcoxon rank sum test)) decrease of -13% is observed for all sub-basins with minimal decrease found in Primero (-8%) and maximum decrease found in Grado (-15%). Water MeHg increases overall at a statistically significant level ($p<0.5$, Wilcoxon rank sum test) by 1.2% in all of the sub-basins.

Compartment	**Water**		**Surface Sediment**		**Subsurface Sediment**	
Depth	Average 1 m		0 – 2 cm		2 – 10 cm	
Mercury species	Hg	MeHg	Hg	MeHg	Hg	MeHg
	-13%	+1.2%	-80%	+43%	-45%	+420%

Table 1. Summary of the average percentage of variations (from the initial state) of Hg species concentrations in water, surface sediment and subsurface sediment by the end of the 100 years simulations scenario (Ref).

A scenario analysis was carried out at the sub-basin scale by comparing the evolution of total mercury (Hg_T) and methylmercury (MeHg) concentrations in surface sediments (0 – 2 cm), subsurface sediments (3 – 10 cm) and the water column as shown in Figures 3, 4, 5. The percentage of the variation in mercury (Hg) concentrations in each scenario with respect to Ref conditions was computed for each sub-basin and then averaged for the whole lagoon as shown in Tab. 2.

The NoR simulation scenario was explored to address the effect of Hg riverine inputs on the recovery of lagoon sediment. Computed concentrations of the NoR scenario at the end of the 100-year simulation were compared with the Ref, revealing a small decrease in Hg_T at the surface (1.24%, Figure 3) and subsurface sediment (0.4%, Figure 4) and a decrease of Hg_T in water of 2.6% (Figure 5). Effects of the absence of riverine inputs on MeHg concentrations are more pronounced, leading to a -12.5% reduction in the water column and decreases of 6.6% and 2.9% in the surface and subsurface sediment layers, respectively. The impact of riverine input removal is more intense in the Marano Lagoon (22% in the Buso sub-basin, 14% in the Lignano and S.Andrea sub-basins) that receive most of freshwater inputs, and it is progressively less important moving eastward (13%, 8% and 3% in the Grado, Morgo and Primero sub-basins)

Compartment	**Water**		**Surface Sediment**		**Subsurface Sediment**	
Depth	Average 1 m		0 – 2 cm		2 – 10 cm	
	Hg	**MeHg**	**Hg**	**MeHg**	**Hg**	**MeHg**
NoR	-2.6%	-12.5%	-1.2%	-6.6%	-0.4%	-2.9%
CC	<0.1%	0.4%	(±0.3%) 0.3%	8%	(±0.2%) 0.2%	13%
HwL	9%	(3%, -2.3%) -0.2%	(58%, -21%) 15.2%	(32%, -16%) 6.8%	(26%, -45%) 2%	(26%, -5%) -0.2%

Table 2. Variations in Hg species concentrations in water, surface sediment and subsurface sediment by the end of the 100 years simulations scenario (NoR, CC, and HwL) relative to that of the Ref scenario by the end of the 100-year period. Values in brackets show the range of variation values computed for the six boxes when they have opposite signs.

Under the CC scenario, an average temperature increase of 2.5°C over the whole simulation period has a negligible effect on Hg_T water (<0.1) and sediment concentrations (±0.3%) with respect to Ref (Table 2). Methylation and demethylation processes, however, are more sensitive to temperature changes than to other transformation processes. We, therefore, observed higher MeHg concentrations in the surface (8%) and subsurface sediments (13%) in the CC scenario with respect to the Ref. This effect could have been even more significant if the model had taken into account methylation processes possibly occurring in the water column.

Under the CC scenario, the transfer of MeHg (Figure 6) from sediment to the water column is enhanced due to higher $MeHg_D$ diffusion rates from pore-water (+12%) and higher due to $MeHg_P$ resuspension rates (+11%). This affects the export of MeHg into the Adriatic Sea, which increases by 2.7%. As a consequence, $MeHg_P$ burial in deep sediments increases as well (+11%). Higher temperatures also affect exchanges between surface water and the atmosphere, causing a 1% increase in Hg^0 evasion. Hg_P and Hg_D budget processes are generally less affected than those involving MeHg.

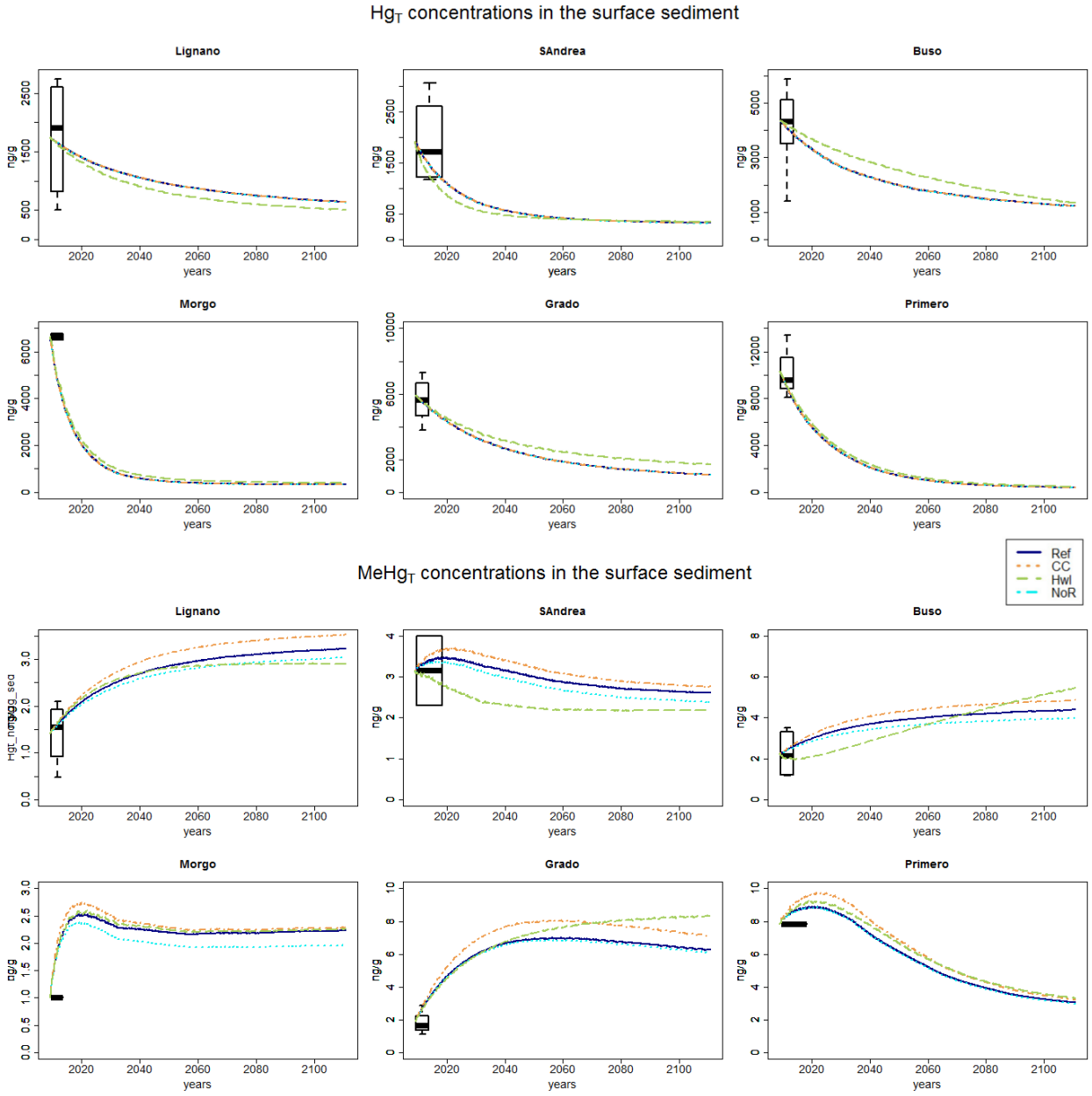

Figure 3. Time evolution of Hg_T (upper panel) and MeHg (lower panel) concentrations in surface sediment layers. Box plot: field data.

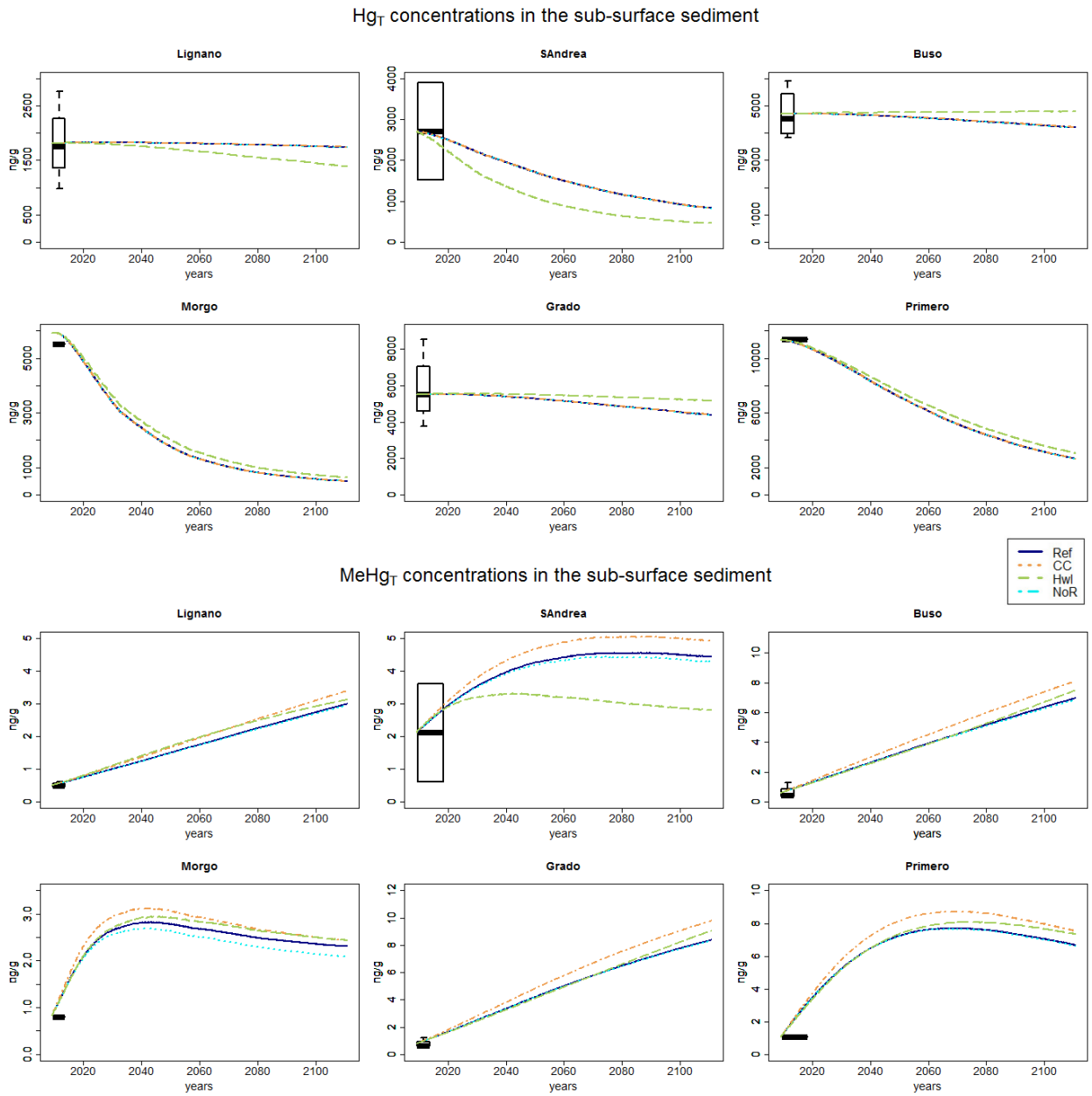

Figure 4. Time evolution of Hg_T (upper panel) and MeHg (lower panel) concentrations in subsurface sediment layers. Box plot: field data.

Under the HwL scenario, water circulation in the lagoon changes: it intensifies in the Grado Lagoon and in the Buso sub-basin increasing the resuspension and transport of sediment, Hg_P and $MeHg_P$; while becoming weaker in the westernmost sub-basins (Lignano and S.Andrea). As a consequence, contrasting changes in the eastern and western sub-basins are observed. A general increase of Hg_T in water is observed in the whole lagoon with respect to Ref (Table 2), varying from 15% in Morgo to 0.5% in Lignano (Figure 5), due to increased sediment resuspension and transport across inlets and sub-basins. Higher Hg_T concentrations in water also result in higher concentrations of Hg_P in settling sediment.

A general increase of Hg_T and MeHg is observed in sediment (up to 58% and 33% for Grado surface sediment Hg_T and MeHg; 20% for Morgo sediment Hg_T; and 10% for Primero sediment MeHg). This pattern is likely due to reduced deposition and burial in the eastern sector (Primero, Grado and Morgo) that slow self-decontamination and favor the cycling between sediment and water. On the contrary, lower sediment concentrations compared to the Ref simulation are observed in the westernmost basins, where deposition and burial are enhanced (about -20% Hg_T for Lignano and S. Andrea surface and subsurface sediment, and -8% and-26% MeHg for Lignano and S.Andrea surface and subsurface sediment, respectively).

Overall, sediment concentrations in the water column are higher in the HwL than in the Ref simulation, promoting Hg and MeHg partitioning into sediment and decreasing Hg^0 evasion (-26% with respect to Ref). In the HwL scenario, the overall mercury budget is changed by a net increase of Hg_T outputs from the lagoon to the sea with respect to Ref (Figure 6).

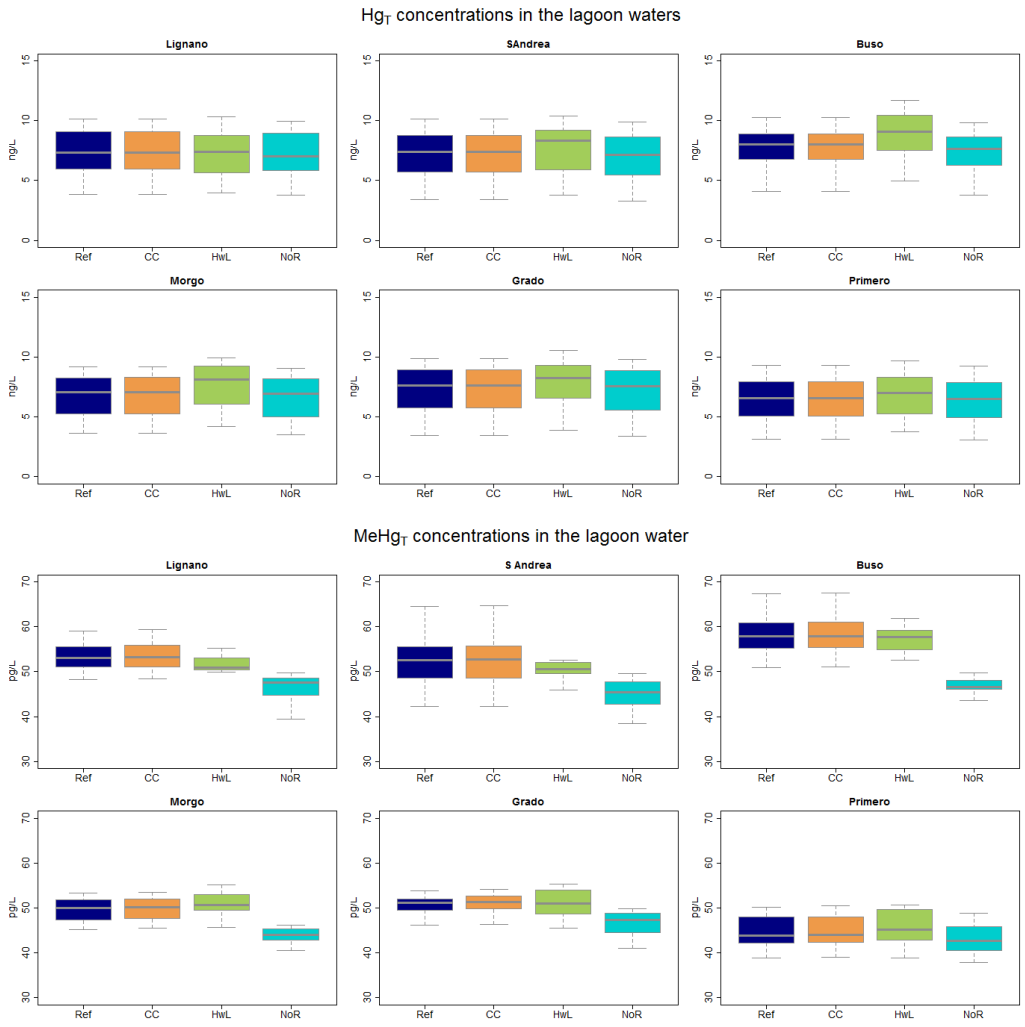

Figure 5. Box plots of concentration of Hg in the water column at the end of the scenario simulations: Hg_T (upper panel) and MeHg (lower panel). The graphs show the median; the 1st and 3rd quartiles; and minimum and maximum values for each simulation.

The sediment recovery time was computed for the Ref simulation (baseline scenario) as the time required for surface sediment to reach the contamination level limit of Hg_T of 0.3 mg/Kg set by Italian legislation under the EU–Water Framework Directive (Ministry of Environment Decree, 28/11/2010 n° 260, WFD 2000/60 EU).

Under baseline conditions, the averaged recovery time for all lagoon surface sediments (weighted over the surface of each box) is 570 years, ranging from 50 years in Morgo to 1,040 years in Buso depending on initial concentrations and on transport and transformation processes acting on each sub-basin. The sub-surface sediment averaged recovery time is much longer (1,250 years) and ranges from 108 years in Morgo to 1,750 years in Lignano and Buso. With the simulation run fully removing Hg inputs at marine boundaries (NoM), 0.3 ppm average concentrations in surface sediment are achieved 5 times faster relative to the Ref scenario, being reached after only 110 years. Conversely, the removal of direct river mercury inputs from the lagoon does not have a significant impact on average sediment recovery times.

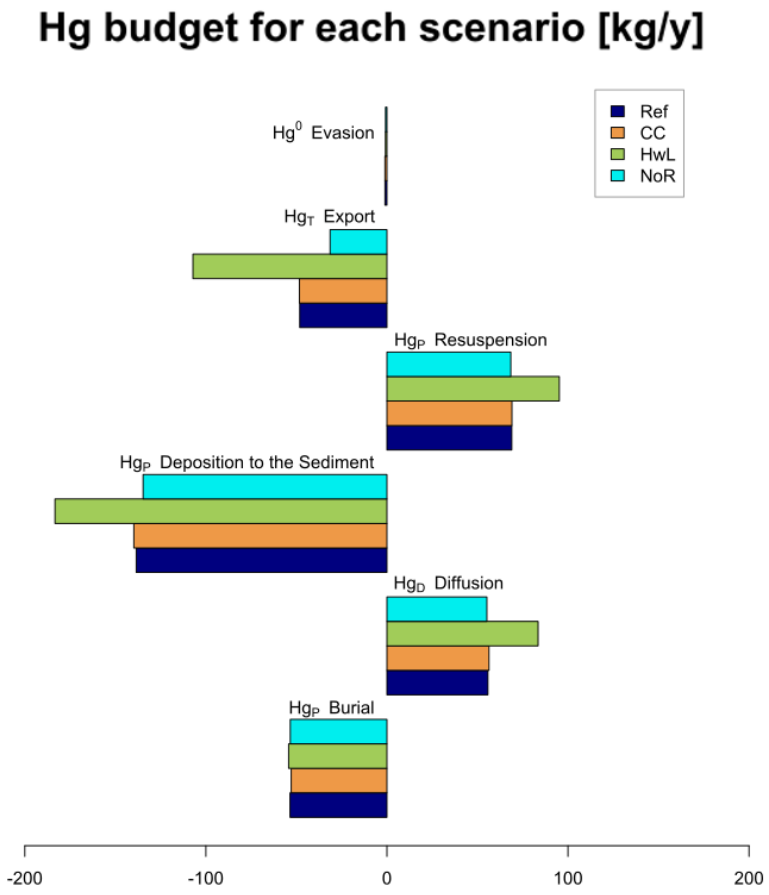

Fig. 6. Mass budget for Hg_T by the end of the 100 years simulations scenario (for the 4 scenarios: Ref, NoR, CC, and HwL).

3.4. Discussion

In this paper, we modelled the evolution of the mercury system in a hot spot of the Northern Adriatic Sea to project this system's evolution over the next 100 years while also considering climate change scenarios. The analysis was performed to contribute insight on relevant processes and on relative contributions of external boundaries and climatic conditions to overall budgets and dynamics. Hg budgets have been computed and compared for the scenarios, as reported in Figure 6. In addition, a long term run was used to estimate the time required to reach sediment concentration values prescribed under environmental legislation.

The model results highlight the relevance of the marine boundary to overall processes and, in particular, to mercury dynamics present in the water column, which are mainly driven by boundary conditions. However, the evolution of sediment concentrations is mainly driven by processes acting within the sediment and at the water/sediment interface. Such processes include sediment resuspension/deposition dynamics and methylation/demethylation processes, which in the model are, respectively governed in large part by water circulation dynamics and environmental conditions, and namely by temperature and solar radiation levels.

The model was applied in a 6-box configuration in the horizontal dimension. This configuration is more efficient than finer scale resolution models used, for instance, for the computation of water fluxes between boxes. It, thus, allows one to perform long-term scenario simulations. Another simplification commonly applied and accepted for model applications (Amos et al., 2014, 2015, Sorensen et al., 2010, Sorensen et al., 2016, Sunderland and Mason, 2007) pertains to the simple representation of Hg uptake by phytoplankton and its bioaccumulation in the trophic chain. Indeed, mechanisms of Hg uptake by phytoplankton are more complex in reality (Le Faucheur et al., 2013). However, Sunderland et al., (2010) have shown that this process only contributes to a small portion of the overall budget in Passamaquoddy Bay. Despite its simplicity, the model allows one to identify major Hg lagoon dynamics and reproduce sediment deposition, erosion and burial processes. Comparisons drawn between monthly measures of dissolved mercury (Hg_D) in the water column and with particulate MeHg ($MeHg_P$) content in surface sediment have shown satisfactory agreement with field data (Melaku Canu et al., 2015).

The model reproduced spatial variability between boxes and year-round temporal variability according to limits set by the model resolution, by the resolution (both in time and space) of field data, and by the time resolution of boundary conditions. Results of the Ref simulation on long-term mercury budget trends in the Marano-Grado Lagoon show that sediment will continue to act as a secondary source of contamination in the long run. However, after 100 years of simulation conducted at the baseline, current Hg_T concentrations in the surface and subsurface sediment levels will

decrease, inducing a net decrease (-77%) in Hg_T export to the sea over time that will change from 112 kg/y of the present state to 48 kg/y over 100 years with a net future MeHg export level of 0.63 kg/y. Hg_T concentrations in surface and subsurface sediment will slowly decrease over time due to transport processes (e.g., burial in the deepest sediment and transferring to the water column followed by export to the Adriatic Sea or volatilization). The model predicts that surface sediment (the first 2 cm) will be recovered in all sub-basins after 1,000 years, but it will be 500 years more before concentrations decline in subsurface sediment (3 to 10 cm in depth). Interestingly, the decreasing trend observed for Hg_T is decoupled from MeHg decontamination. After 100 years, the change in MeHg export will be almost negligible, with its formation and export related to environmental conditions and not limited by the predicted decrease in subsurface sediment Hg_T concentrations.

Recovery times were computed assuming that boundary concentrations and global mercury dynamics do not change in the future. This is clearly an approximation based on the best data currently available and based on data and model collation. This estimate is not meant to be used as an official value but as information useful for determining the extent of historical mercury pollution based on a time-focused perspective. However, an unbridgeable uncertainty regarding boundary and forcing condition values must be taken into account when considering such a long time frame, and such computations have only to be taken as broad indications of timescales of recovery and not as exact estimations of recovery time.

Other set-ups could be developed if global mercury models (projecting overall changes in mercury circulation in a coupled ocean-atmospheric system based on future climatic and socio-economic scenarios) were available. Without such information, we prefer to use existing boundaries instead of drawing subjective assumptions on global trends while remembering that our scenario could be considered as precautionary because in the long run mercury inputs from the Isonzo River through the Adriatic Sea could decline considerably. To apply a minimum (but unrealistic) limit to our computation of recovery time, a NoM simulation was run after removing Hg inputs at marine boundaries; this generated an average recovery time of only 110 years.

Conversely, the removal of direct river mercury inputs to the lagoon (NoR scenario) did not significantly change average sediment recovery times. The simulation allowed us to explore the effects of a hypothetical decontamination intervention on river basins (e.g., mercury capping) as an indication of the benefits of such an intervention for a given system. The model shows that riverine input removal has minimal effects on Hg_T mercury concentrations in surface and subsurface sediments and the water column. Effects on MeHg concentrations are instead more evident in sediments and the water column as shown in Figure 3, 4 and 5. An overall effect, however, is found at the end of the 100-year simulation, with a decrease in mercury exports to the Adriatic Sea for the

Ref (35% for Hg_T and 94% for MeHg) and with a reduction in Hg_T concentrations in surface sediment as described above (exports of Hg_T of 31 kg/y and only of 0.04 kg/y of MeHg).

For the CC scenario, we assessed the effects of temperature increases on mercury dynamics in the Marano-Grado Lagoon without making any other assumptions on changes in Hg_T concentrations at boundaries related to either temperature changes or socio-economic scenarios. The net MeHg sea export level is slightly higher (by 3%) while the Hg_T export level is almost the same. Higher temperatures fuel higher bacterial metabolic rates that enhance methylation (and demethylation) activities. However, methylation prevails over demethylation, resulting in higher MeHg concentrations in surface and sub-surface sediments with potential effects on the trophic chain. Conversely, Hg_T concentrations in sediments and water do not change significantly relative to Ref ones, being mainly driven by marine boundary values. The effects of increasing methylation and demethylation rates are much less significant in water column MeHg concentrations (+0.17%) due to the effects of intense water circulation and exchanges with seawater. However, we speculate that temperature increases can lead to longer periods of stratification in shallow lagoon water, a condition that is known to promote bottom anoxia, to enhance diffusion from pore-water (Emili et al., 2014) and favour optimal zone shifting for methylation from sediments to the water column (Fitzgerald et al., 2007). Moreover, increasing temperatures can induce an increase in MeHg levels in surrounding coastal systems, including at river mouths. Therefore, our set up may underestimate MeHg concentrations in the lagoon. In addition, our representation of sediment-water transport could be somewhat underestimated for all scenarios due to model limitations concerning the following: 1) the use of a partition constant (K_D) fixed in time and space and 2) the use of Fick's law to calculate diffusion processes that often cause underestimations of in-situ fluxes measured within a benthic chamber (Benoit et al., 2009).

When removing boundary inputs, MeHg concentrations in water decrease dramatically (-79% in the NoM scenario, and -12.5% in the NoR scenario), and concentrations in surface and subsurface sediment decrease as well. This allows us to infer that riverine and marine inputs of Hg and MeHg play a key role in the accumulation of MeHg in sediment. In their absence, MeHg produced in sediment should be partly counterbalanced by demethylation and transport to the water column (followed by export, photo-degradation or deposition back to sediment). Marine boundary concentrations are clearly the main drivers shaping mercury dynamics in the Marano-Grado lagoon system and corresponding self-decontamination rates. As shown above, river inputs have a minor effect but are still important, and especially when considering net mercury fluxes between the lagoon and its boundary systems.

The sea level rise and increasing levels of water exchange at inlets tend to intensify all transfer processes directly related to water circulation. By the end of the 100-year run, the HwL shows (with respect to the Ref) an increase in the net Hg_T export towards the sea (+122%), diffusion (+48%), resuspension (+38%) and deposition (+32%). A minor change in burial rates is also observed (2%). Concentrations of MeHg and Hg_T in water increase by 3% and 9% on average, and their levels in sediment increase by 7% and 15%, thus potentially increasing in biota as well. The general increase of concentrations implies a lower self-decontamination timing and is attributable to: higher exchanges at the marine boundary; enhanced sediment dynamic prompting intense cycling of Hg and MeHg between water and sediment; higher fraction of Hg_P and $MeHg_P$ in the water due to higher suspended particulate matter concentrations. As both CC and HwL show an increase in MeHg concentrations in surface sediment, combined effects of sea level rise and temperature increases should reasonably lead to conditions of increased toxicity for local biota.

3.5. Conclusions

The Marano Grado lagoon is a large Mediterranean hot spot for mercury contamination. The lagoon has been receiving mercury discharge for centuries, and even if inputs from anthropogenic sources stopped decades ago, the lagoon's sediments still present high mercury concentrations and act as a secondary source for the whole Mediterranean basin. A scenario analysis performed based on a validated numerical model constrained by available data and information allowed us to assess short- and long-term dynamics of mercury contamination in this system. The model shows that based on the current configuration, 100 years from now, a decrease in Hg_T concentrations is expected in the system. Similarly, there should be an overall decrease in mercury flux within the lagoon system and between the lagoon and its surrounding boundaries. However, a general increase in MeHg is expected, and particularly in sediment. Climate change should worsen this situation, causing increases in MeHg concentrations of up to 87% and 95% of current levels with respect to increasing temperatures (+2.5°C) and sea level rise (0.315 m), respectively. Accordingly, mercury bioaccumulation in biota is expected to increase in the future.

Our simulation suggests that a complete removal of mercury inputs from rivers directly discharging into this lagoon would not substantially affect mercury dynamics besides reducing MeHg concentrations in water (12%) and surface sediments (6%). Interestingly, the reduction in MeHg as a consequence of the total removal of Hg inputs from rivers is of the same order as MeHg increase resulting from an increase in temperature or from sea level rise; therefore, the former may be envisaged as a possible way of mitigating adverse effects of the latter.

The long-term run of the baseline reference simulation indicates that recovery times of lagoon sediments computed as the time required to decrease Hg_T to 0.3 mg/Kg are roughly 600 years for surface sediments and 1,200 years for sub-surface sediments. These lengths of time should be markedly shorter (110 years for sediment) for unrealistic scenarios involving no Hg inputs from the sea. Though unrealistic, such scenarios still offer a timescale for waste remediation measures needed for the system and serve as a framework for understanding this ecosystem service.

Acknowledgments: This research was carried out with contributions from the RITMARE flagship Project and with the contribution from the Friuli Venezia Giulia Regional Protection Agency (ARPA-FVG) in the frame of the EU-SHAPE project activities.

3.6. References

Acquavita, A., Covelli, S., Emili, A., Berto, D., Faganeli, J., Giani, M., Horvat, M., Koron, N., Rampazzo, F., 2012. Mercury in the sediments of the Marano and Grado Lagoon (northern Adriatic Sea): sources, distribution and speciation. Estuar. Coast. Shelf Sci. 113, 20–31.

Amos, H.M., Jacob, D.J., Kocman, D., Horowitz, H.M., Zhang, Y., Dutkiewicz, S., Horvat, M., Corbitt, E.S., Krabbenhoft, D.P., Sunderland, E.M., 2014. Global biogeochemical implications of mercury discharges from rivers and sediment burial. Environ. Sci. Technol. 48, 9514–22.

Balcom P.H., Scartup A.T., Mason R.P., Chen C.Y., 2015. Sources of water column methylmercury across multiple estuaries in the Northeast U.S. Mar. Chem. 177, 721-730.

Bloom, N.S., Moretto, L.M., Scopece, P., Ugo, P., 2004. Seasonal cycling of mercury and monomethyl mercury in the Venice Lagoon (Italy). Mar. Chem. 91, 85-99.

Canu M. D, Solidoro C, Cossarini G, Giorgi F. 2010 Effect of global change on bivalve rearing activity and the need for adaptive management. Clim. Res. 42:13-26.

Canu, D.M., Acquavita, A., Knightes, C.D., Mattassi, G., Scroccaro, I., Solidoro, C., 2012. Modeling the Mercury Cycle in the Marano-Grado Lagoon (Italy). In: Models of the Ecological Hierarchy: From Molecules to the Ecosphere. Elsevier B.V., pp. 239–257.

Ĉar, J. & Dizdareviĉ, T. 2004 Written Reports on the Effects of Mining Activities on the Natural Environment in Idrija in the 19th Century. In: Winkler Prins, C.F. & Donovan, S.K. (eds.), Scripta Geologica Special Issue, 4: 35-44, 6. Leiden.

Cossarini, G., Libralato, S., Salon, S., Gao, X., Giorgi, F., Solidoro, C., 2008. Downscaling experiment for the Venice lagoon. II. Effects of changes in precipitation on biogeo- chemical properties. Clim. Res. 38, 43–59.

Covelli, S., Faganeli, J., De Vittor, C., Predonzani, S., Acquavita, A., Horvat, M., 2008. Benthic fluxes of mercury species in a lagoon environment (Grado Lagoon, Northern Adriatic Sea, Italy). Appl. Geochem. 23, 529–546.

Covelli, S., Langone, L., Acquavita, A., Piani, R., Emili, A., 2012. Historical flux of mercury associated with mining and industrial sources in the Marano and Grado Lagoon (northern Adriatic Sea). Estuar. Coast. Shelf Sci. 113, 7–19. doi:10.1016/j.ecss.2011.12.038

Dalla Valle, M., Codato, E., Marcomini, A., 2007. Climate change influence on POPs distribution and fate: A case study. Chemosphere. Vol 67 (7), pp. 1287-1295

Dizdarevič, T., 2001. The influence of mercury production in Idrija mine on the environment in the Idrija region and over a broad area. RMZ-Mater. Geoenviron. 48, 56–64.

Dorigo, L., 1965. La Laguna di Grado e le sue foci. Ufficio Idrografico del Magistrato della Acque.

Faganeli, J., Hines, M.E., Horvat, M., Falnoga, I., Covelli, S., 2014. Methylmercury in the gulf of Trieste (Northern Adriatic sea): From microbial sources to seafood consumers. Food Technol. Biotechnol. 52, 188–197.

Ferrarin, C., Umgiesser, G., Bajo,M., Bellafiore, D., De Pascalis, F., Ghezzo,M., Mattassi, G., Scroccaro, I., 2010. Hydraulic zonation of the lagoons of Marano and Grado, Italy. A modelling approach. Estuar. Coast. Shelf Sci. 87, 561–572.

Gnamuš, A., Horvat, M., 1999. Mercury in Terrestrial Food Webs of the Idrija Mining Area, in: Ebinghaus, R., Turner, R.R., de Lacerda, L.D., Vasiliev, O., Salomons, W. (Eds.), Mercury Contaminated Sites: Characterization, Risk Assessment and Remediation. Springer Berlin Heidelberg, Berlin, Heidelberg, pp. 281–320. doi:10.1007/978-3-662-03754-6_16.

Golden H.E.,Knightes C.D., Conrads P.A., Feaster T.D., Davis G.M., Benedict S.T., Bradley P.M. 2013. Climate change and watershed mercury export: a multiple projection and model analysis. Environ. Toxicol. Chem. 32(9), 2165–2174.

Gosar M., Mercury in River Sediment, Floodplains and Plants Growing thereon in Frainage Area of Irrija Mine, Slovenia. Polish J. of Environ. Stud. Vol 17, No. 2 (2008), 227-236.

Gosar, M., Teršič, T., 2015. Contaminated sediment loads from ancient mercury ore roasting sites, Idrija area, Slovenia. J. Geochemical Explor. 149, 97–105. doi:10.1016/j.gexplo.2014.11.012

Hammerschmidt, C.R., Fitzgerald, W.F., 2004. Geochemical controls on the production and distribution of methylmercury in near-shore marine sediments. Environ. Sci. Technol. 38, 1487-1495.

Harley CDG, Hughes AR, Hultgren KM, Miner BG and others (2006). The impacts of climate change in coastal marine systems. Ecol. Lett. 9:228–241.

Hines, M.E., Poitras, E.N., Covelli, S., Faganeli, J., Emili, A., Žižek, S., Horvat, M., 2012. Mercury methylation and demethylation in Hg-contaminated lagoon sediments (Marano and Grado Lagoon, Italy). Estuar. Coast. Shelf Sci. 113, 85–95.

Horvat, M., Kotnik, J., Logar, M., Fajon, V., Zvonarić, T., Pirrone, N., 2003. Speciation of mer cury in surface and deep-sea waters in the Mediterranean Sea. Atmos. Environ. 37 (1), 93-108.

Lambeck K., Antonioli, F., Ferranti, L., Leoni, G., Scicchitano, G., Silenzi, S., 2011. Sea level change along the Italian coast during the Holocene and projections for the future. Quat. Int. 232, 250-257.

Lazzari, P., Mattia, G., Solidoro, C., Salon, S., Crise, A., Zavatarelli, M., Oddo, P., Vichi, M., 2013. The impacts of climate change and environmental management policies on the trophic regimes in the Mediterranean Sea: Scenario analyses. J. Mar. Syst. 135, 137-149. doi:10.1016/j.jmarsys.2013.06.005

Melaku Canu, D., Rosati, G., Solidoro, C., Heimbürger, L.-E., Acquavita, A., 2015. A comprehensive assessment of the mercury budget in the Marano–Grado Lagoon (Adriatic Sea) using a combined observational modeling approach. Mar. Chem. 177, 742-752. doi:10.1016/j.marchem.2015.10.013

Monperrus, M., Tessier, E., Amouroux, D., Leynaert, A., Huonnic, P., Donard, O.F.X., 2007. Mercury methylation, demethylation and reduction rates in coastal and marine sur- face waters of the Mediterranean Sea. Mar. Chem. 107, 49-63.

Nakicenovic, N., Swart, R. (Eds.), 2000. Special Report on Emissions Scenarios. A Special Report of Working Group III of the Intergovernmental Panel on Climate Change. Cambridge University Press, Cambridge, UK.

Pato P., Lopes C., Válega M, Lillebø A.I., DiasJ.M, Pereira E., Duarte A.C 2008. Mercury fluxes between an impacted coastal lagoon and the Atlantic Ocean. Estuarine, Coastal and Shelf Science. Volume 76, Issue 4, 1. Pages 787-796

Rajar, R., Žagar, D., Širca, A., Horvat, M., 2000. Three-dimensional modelling of mercury cycling in the Gulf of Trieste. Sci. Total Environ. 260, 109-123. doi:10.1016/S0048-9697(00)00555-6

Regione FVG. 2013. Attività sperimentali di monitoraggio del trasporto sedimentario alle bocche tidali della Laguna di Marano e Grado.

Rothenberg, S.E., Ambrose, R.F., Jay, J.A., 2008. Mercury cycling in surface water, pore water and sediments of Mugu Lagoon, CA, USA. Environ. Pollut. 154, 32-45.

Sharif A., Tessier E., Bouchet S, Monperrus M, Pinaly H, Amouroux D. 2013 Comparison of different air-water gas exchange models to determine gaseous mercury evasion from different european coastal lagoons and estuaries. Water, Air, and Soil Pollution. Volume 224, Issue 7,

Solidoro, C., Cossarini, G., Libralato, S., Salon, S., 2010. Remarks on the redefinition of system boundaries and model parameterization for downscaling experiments. Prog. Oceanogr. 84, 134–137.

Sorokin, Y.I., Sorokin, P.Y., Giovanardi, O., Dalla Venezia, L., 1996. Study of the ecosystem of the lagoon of Venice, with emphasis on anthropogenic impact. Mar. Ecol. Prog. Ser. 141, 247–261 .

Sprovieri, M., Oliveri, E., Di Leonardo, R., Romano, E., Ausili, A., Gabellini, M., Barra, M., Tranchida, G., Bellanca, A., Neri, R., Budillon, F., Saggiomo, R., Mazzola, S., Saggiomo, V., 2011. The key role played by the Augusta basin (southern Italy) in the mercury contamination of the Mediterranean Sea. J. Environ. Monit. 13, 1753-1760.

Thompson, J.R., Flower, R.J.. 2009. Environmental science and management of coastal lagoons in the southern mediterranean region: Key issues revealed by the MELMARINA project. Hydrobiologia. Vol 622, Issue 1, Pages 221-232.

US EPA, 1988. Water quality Simulation program, v. 5. manual. (Ambrose R.).

US EPA, 2009. Water Quality Simulation Program v. 6. manual. Wool T. A., Ambrose R. B., Martin J.L., Comer E. A.

Vost, E.E., Amyot,M., O'Driscoll, N.J., 2012. Photoreactions of mercury in aquatic systems. In: Liu, G., Cai, Y., O'Driscoll, N. (Eds.), Environmental Chemistry and Toxicolgy of Mercury.Wiley ed. John Wiley & Sons, Inc., pp. 193–218

Whalin, L., Kim, E.-H., Mason, R., 2007. Factors influencing the oxidation, reduction, methylation and demethylation of mercury species in coastal waters. Mar. Chem. 107, 278-294.

Wool, T.A., Ambrose, R.B., Martin, J.L., Comer, E.A., 2001.Water Quality Analysis Simulation Program (WASP) Version 6.0: User's Manual.

Zagar, D., Knap, A., Warwick, J.J., Rajar, R., Horvat, M., Cetina, M., 2006. Modelling of mercury transport and transformation processes in the Idrijca and Soca river system. Sci. Total Environ. 368, 149-63. doi:10.1016/j.scitotenv.2005.09.068

Žagar, D., Petkovšek, G., Rajar, R., Sirnik, N., Horvat, M., Voudouri, A., Kallos, G., Četina, M., 2007. Modelling of mercury transport and transformations in the water compartment of the Mediterranean Sea. Mar. Chem. 107, 64-88.

Chapter 4 – Mercury in the Black Sea: new insights from measurements and numerical modelling

This chapter has been submitted (April 2017) to Global Biogeochemical Cycles as:

Rosati G., Heimbürger L.E., Melaku Canu D., Lagane C., Laffont L., Rijkenberg M.J.A., Gerringa L.J.A., Solidoro C., Gencarelli C.N., Hedgecock I. M., De Baar H.J.W., Sonke J.E. Mercury in the Black Sea: new insights from measurements and numerical modelling.

4.1. Introduction

The ubiquitous presence of mercury (Hg) in the environment is a matter of concern due to the transformation of inorganic oxidized Hg (Hg^{II}) into methylmercury (MeHg), which is a biomagnifying neurotoxin (Clarkson and Magos, 2006; Cossa et al., 2012; Fitzgerald et al., 2007; Hammerschmidt and Fitzgerald, 2006). As fish consumption is the main route of human exposure to MeHg (Oken et al., 2012) the understanding of the mechanisms underlying MeHg production, degradation, transport and accumulation in the marine environment is crucial.

Hg methylation is thought to be a mainly a microbial-driven process that occurs in marine sediments (Bouchet et al., 2013; Hammerschmidt et al., 2004; Hollweg et al., 2010, 2009; Monperrus et al., 2007b; Schartup et al., 2013) and in the marine water column (Cossa et al., 2009; Heimbürger et al., 2010; Mason and Fitzgerald, 1990; Sunderland et al., 2009) during remineralization of natural organic matter (NOM). The degradation of NOM prompts the release of Hg^{II} from the solid phases of OM itself (POM) and/or from oxides of Fe and Mn, making it bioavailable to microbes (Cossa et al., 2009; Heimbürger et al., 2010; Muresan et al., 2007; Sunderland et al., 2009). Biogeochemical controls on Hg methylation rates are thus related both to the composition and the activity of the microbial community, and to the speciation and partitioning of Hg^{II} that influence its bioavailability (Cossa et al., 2014; Merritt and Amirbahman, 2009) with a critical role played by redox conditions and NOM availability and quality (Cossa et al., 2014; Schartup et al., 2015b). Previous studies, using equilibrium modeling to explain sedimentary MeHg distribution, proposed that methylation is hindered above sulfide concentrations of ~10 µM, due to a shift of Hg speciation from neutral to charged species that would make it unavailable to microbes (Benoit et al., 2001, 1999a, 1999b). This theory has been questioned as more recent findings have contradicted some of its assumptions, which we will discuss in this paper (see Merritt and Amirbahman, 2009; Hsu-Kim et al., 2013 and refence therein).

The Black Sea is an ideal location to investigate biogeochemical cycles under changing redox conditions, because its waters encompass oxic, suboxic and anoxic conditions (Schijf et al., 1991). The

Black Sea is a deep semi-enclosed basin (Figure 1), with permanently stratified water owing to the hydrological balance between the inflow of water from the Mediterranean Sea via the Marmara Sea-Bosporus system and freshwater inputs. Each year, around 605 km^3 of surface water leaves the Black Sea through the Bosporus Strait, while 305 km^3 of Mediterranean waters enter the Black Sea at depth <50 m. Riverine input (~350 km^3) compensate the imbalance between incoming and outgoing water, and evaporation (~350 km^3) exceed precipitations (~ 300 km^3). The Bosporus inflow mixes with the CIL waters and sinks along the shelf slope, generating horizontal intrusions that cause mixing between coastal and open water (Özsoy and Ünlüata, 1997). Surface circulation is driven by two large cyclonic gyres, in the eastern and western basin, connected to each other by the Rim Current that homogenize surface waters (Murray et al., 2007). Vertical mixing instead is weak, and when oxygen depletion occurs bacterial remineralization of NOM is driven by a sequence of alternative electron acceptors, according to a sequence that is fixed across systems (O_2 > NO_3 > Mn_{Ox} > Fe_{Ox} > SO_4) (Froelich et al., 1979). Hence, the redox progression along the Black Sea water column is similar to the one in sedimentary environments and hypoxic basins worldwide, with the advantage that the redox layers of the Black Sea are quite stable throughout the year and are stretched over a scale of several meters, and thus easier to discern.

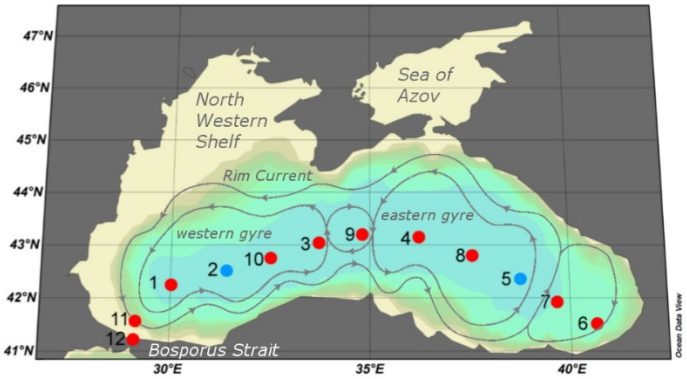

Figure 1. The Black Sea with the 2013 GEOTRACES MedBlack cruise stations (red dots, blue dots indicate high-resolution samples). The Rim Current is shown in grey curves.

The sequence of redox reactions driving NOM remineralization in the water column is mirrored by the concentration profiles of the electron acceptors (Figure 2) and by the stratification of different functional microbial populations (Fuchsman et al., 2011). The oxic layer (OL) includes the euphotic layer (PHOT, ~ 50 m-depth) with high O_2 concentrations (~300 µM) and the aphotic layer, where O_2 is gradually consumed by nitrifying bacteria (oxycline, OXCL), as revealed by increasing NO_3 concentrations (Oguz et al., 2000). Between the lower end of the oxycline (~100 m-depth) and the depth of sulfide onset (~140

m-depth), there is the suboxic layer (SOL), where concentrations of both oxygen and sulfides are extremely low (O_2 < 20 μM, H_2S < 1 μM) and denitrification, chemosynthesis, ammonium and Mn oxidation occur (Murray et al., 2007; Tuğrul et al., 2014; Yakushev and Newton, 2013; Yılmaz et al., 2006). Below, in the anoxic layer (AOL, down to 2200 m-depth), sulfate reduction causes increasing levels of sulfides (Murray et al., 2007). In addition to the redox layers, other layers are identified based on hydrographic properties. At the top of the aphotic layer is the Cold Intermediate Layer (CIL), a mass of cold dense water (T<8°C) which originates in wintertime on the northwest shelf and in the western gyres (Figure 1) (Gregg and Yakushev, 2005; Konovalov and Murray, 2001). The upper part of the AOL (UAOL, <500 m-depth) is ventilated on a shorter timescale than the rest of the deep water, while the last meters of bottom water (benthic bottom layer, BBL, >1775 m-depth) are characterized by uniform salinity, temperature, and density due to geothermal heat flow (Murray et al., 2007; Ozsoy and Ünlüata, 1997). Between the UAOL and the BBL lies the largest portion of the AOL, which we will refer to as the deep anoxic layer (DAOL, 500-1775 m-depth), as in Margolin et al., (2016). The layers occur at variable depths according to the bathymetry and hydrographical region but they are distributed along isopycnals (Konovalov et al., 1997). Therefore, the use of density (σ) as a vertical coordinate is a standard approach in studies dealing with the Black Sea since the early '90s (Konovalov et al., 2004) and the one dimensional (1D) modeling has widely been used to investigate the biogeochemical and ecological features of the basin (Grégoire and Soetaert, 2010; Konovalov et al., 2004; Oguz et al., 2000; Yakushev et al., 2007).

This manuscript aims at understanding Hg speciation along a redox gradient, focusing on Hg methylation and demethylation processes. To achieve our scope, we integrated marine Hg observations, from the 2013 GEOTRACES MEDBlack cruise, with a fate and transport 1D model for Hg species (WASP7 model) (Wool et al., 2001). The model implementation requires a careful compilation of Hg fluxes within the basin, which includes exchanges with the Marmara Sea, rivers and the atmosphere, as well as water-sediment exchanges and burial. We used the model to investigate Hg methylation and demethylation in the Black Sea, parameterizing the concomitant occurrence of the two processes either in the OL, in the SOL or in the AOL, or in multiple layers. We implemented 7 simulations and compared the modeled MeHg profile of each to observations.

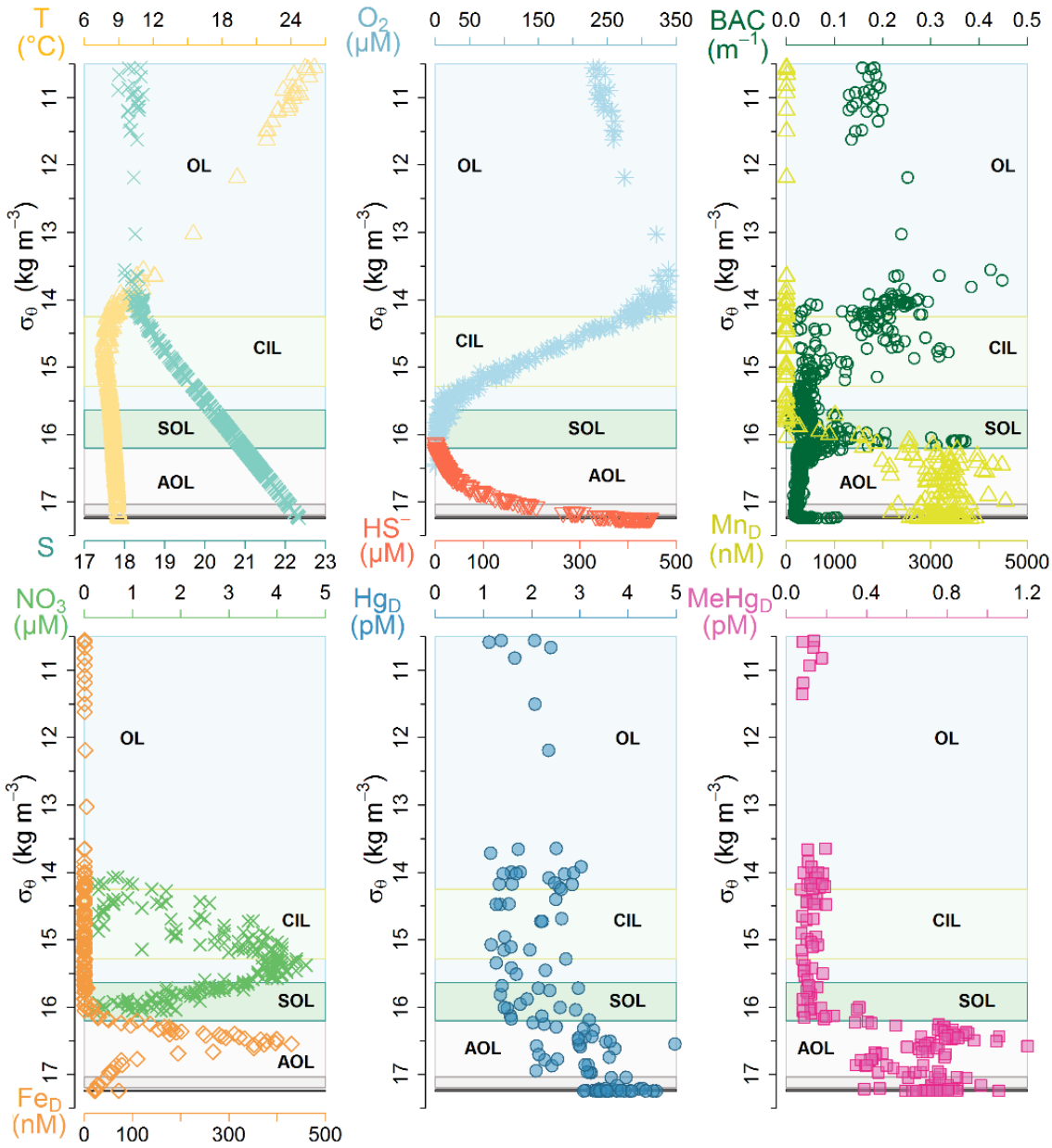

Figure 2. Biogeochemical and hydrographic features of the water column (stations 1-10) illustrated by the observed vertical profiles of temperature (T), salinity (S), Oxygen (O_2), hydrogen sulfide (HS), beam attenuation coefficient (BAC, as a proxy of suspended particulate matter), dissolved manganese (Mn_D), dissolved iron (Fe_D), nitrates (NO_3), dissolved Hg (Hg_D), and MeHg ($MeHg_D$). The potential density anomaly ($\sigma_\theta = \sigma(S,\theta,0)-1000$, kg/m^3) is used as vertical axes to study homogeneous water masses (see main text), the boundaries of the redox layers computed from the cruise dataset are shown in the background as following: oxic layer (OL, light cyan boxes), including the cold intermediate layer (CIL, yellow box), suboxic layer (SOL, green box) and anoxic layer (AOL, grey boxes).

4.2. Materials and Methods

4.2.1 Sampling and laboratory analysis

Samples were acquired during the second leg of the 2013 GEOTRACES MEDBlack (GA04-leg2) cruise in the Black Sea. Research vessel Pelagia occupied 12 full depth stations in the Black Sea along an East-West transect between 13 and 25 July 2013. High resolution vertical profiles were sampled using a titanium ultraclean CTD frame (De Baar et al., 2008) equipped with 24 x 24L PVDF samplers. Samples were filtered (0.2 µm, Sartobran 300), drawn directly into individual pre-cleaned 250 mL PFA Teflon bottles (Savillex Purillex™), acidified to 0.4% (v:v) with double-distilled HCl.

Total Hg_D was measured on a 35 mL aliquot following the USEPA 1631 method. Potassium bromide (Sigma Aldrich, USA) and Potassium Bromate (Sigma Aldrich, USA) were heated for 4 h at 250 °C to remove Hg traces before making up BrCl solution with freshly double-distilled HCl. We used a custom made semi-automatic single gold trap setup coupled to a cold vapor atomic fluorescence spectrometry (Brooks Rand Model III, USA), modified with a mirrored quartz cuvette (Hellma Optics, Germany).

We measured dissolved methylmercury ($MeHg_D$) as the sum of mono- and dimethylmercury (MMHg + DMHg). $MeHg_D$ was analyzed via isotope dilution (ID), using a high sensitivity coupled gas chromatography - sector field ICP-MS (GC-SF-ICP-MS) (Heimbürger et al., 2015). Briefly, enriched spikes of ^{199}iHg and ^{201}MeHg (ISC Science, Spain) were added to a 115 mL aliquot of the seawater samples. After 24h equilibration, pH was adjusted to 3.9 with NH_3 (ULTREX® II Ultrapure Reagent, J.T. Baker, USA) and a buffer solution made up with acetic acid (glacial, ULTREX® II Ultrapure Reagent, J.T. Baker, USA)/sodium acetate (J.T. Baker, USA). Sodium tetra propyl borate (1mL, 1%, v:v; Merseburger Spezialchemikalien, Germany) was then added together with 200 µL hexane (Sigma Aldrich, USA). The glass bottles were hermetically sealed with Teflon-lined caps and vigorously shaken for 15 minutes. The organic phase was recovered and injected in the GC (Thermo Trace Ultra) coupled to the high resolution ICP-MS (Thermo Element XR). Initial results indicated undetectable amounts of MeHg in the anoxic waters. However, we also did not recover the added isotopic spikes, indicating that our method was not appropriate for anoxic samples. Another aliquot was oxygenated for 15 min after the spike addition, and prior to the derivatization step. This allowed for full spike recovery and significant amounts of MeHg detected in all samples. Detection limit was 0.025 and 0.001 pM for Hg_D and $MeHg_D$, respectively.

A GEOTRACES intercalibration sample was taken on July 15th 2013 in the western gyre (31.402°E; 42.521°N), in the oxic waters near the chlorophyll maximum (45 m-depth). Our results compare well with the consensus values, Hg_T = 0.92 ± 0.36 pM, n = 17, $MeHg_T$ = 0.57 ± 0.36 pM, n = 9. We

measured the GEOTRACES intercalibration sample 3 times for Hg_T and obtained 0.98 (10/09/2013), 0.95 (15/12/2013), and 0.96 (30/10/14) pM. We determined 0.091 and 0.063 pM of MeHg on 10/09/2013 and 15/12/2013, respectively.

4.2.2 Vertical discretization of the dataset

As already observed by many authors (e.g. Konovalov and Murray, 2001), depth profiles of a given variable differ between stations whereas density profiles do not (Figure 2). We analyzed the distribution of physical properties, nutrients and metals at 10 deep stations of the 2013 GEOTRACES MEDBlack cruise (Gerringa et al., 2016; Margolin et al., 2016), excluding the stations closest to the Bosporus Strait (11 and 12). The vertical profiles of selected physical and biogeochemical data are shown in Figure 2. To study homogeneous water masses, density is used as vertical coordinate; the density anomaly (σ_t = σ(S, T, 0)-1000, kg/m^3) is a shorthand for density computed from measured temperature (T) and salinity (S) at atmospheric pressure (ρ = 0). However, as depth increases, the adiabatic compression on water particles causes a temperature increase that leads to an apparent decrease of density. Therefore, for deep waters it is recommended to use potential density anomaly (σ_θ = σ(S, θ, 0)-1000, kg/m^3) that is computed from potential temperature (θ) and thus is corrected for adiabatic compression (Talley et al., 2011). To study the evolution of the data along the water column (up to 2160 m-depth; σ_θ = 17.25), we first excluded possible outliers from the Hg and MeHg data discretizing the water column with a fine resolution. This partitioning is appropriate to handle outliers and to define the average concentration profile of metals and nutrients (Figure 3), but it is too detailed for our modeling purpose. The vertical discretization for the model (Table 1) was made in order to decompose the water column into its redox and hydrographic layers (PHOT, CIL, OXCL, SOL, UAOL, DAOL, BBL), further dividing some of the layers to simulate the evolution of the variables of greatest interest (Hg, MeHg and POM). The euphotic part of the OL above the CIL (PHOT) and the UAOL were divided into 2 sub-layers (PHOT1, PHOT2, UAOL1, UAOL2) as were the sediments (SED1, SED2).

Layer	Sublayer	Thickness	Depth	σ_0	O_2	HS^-	Volume	Velocity*	Eddy Diffusivity$^{\Delta}$
		m	*m*		*μM*	*μM*	m^3	*m/s*	m^2/s
OL (oxic layer)	*PHOT1*	20	0 – 20	10.5 – 12.05	246 (229 – 247)	0.00	$5.9\ 10^{12}$	0.25	$1.1\ 10^{-5}$
	PHOT2	20	20 – 40	12.05 – 14.25	315 (269 – 341)	0.00	$5.9\ 10^{12}$	0.5	$1.1\ 10^{-5}$
	CIL	15	40 – 55	14.25 – 15.18	165 (63.2 – 292)	0.00	$4.5\ 10^{12}$	0.5	$9.5\ 10^{-6}$
	OXCL	20	55 – 75	15.18 – 15.64	31.3 (3.60 – 88.2)	0.00	$5.9\ 10^{12}$	-	$9.5\ 10^{-6}$
SOL (suboxic layer)	*SOL*	25	75 – 100	15.64 – 16.2	3.53 (0.00 – 27.8)	0.17 (0.00 - 3.50)	$7.4\ 10^{12}$	-	$9.5\ 10^{-6}$
AOL (anoxic layer)	*UAOL1*	180	100 – 280	16.2 – 16.6	0.00	15 (0.00 – 39.2)	$5.3\ 10^{13}$	-	$1\ 10^{-5}$
	UAOL2	180	280 – 460	16.6 – 17.04	0.00	97 (34.2 – 192)	$5.3\ 10^{13}$	-	$1\ 10^{-5}$
	DAOL	1000	460 – 1460	17.04 – 17.24	0.00	317 (180 - 413)	$2.9\ 10^{14}$	-	$5.5\ 10^{-6}$
	BBL	350	1460 – 1810	17.24 – 17.25	0.00	421 (385 - 446)	$1\ 10^{14}$	-	$8.7\ 10^{-6}$
Sediment	*SED1*	0.03					$8.8\ 10^{9}$	-	-
	SED2	0.07					$2.0\ 10^{10}$	-	-

** Velocity from Murray et al., (2007);*
$^{\Delta}$ Eddy diffusivity from Konovalov et al., (2004)

Table 1. Physico-chemical properties of the water and sediment layers implemented in the WASP7 model.

4.2.3 Model theory

The WASP7 Hg model, MERC7 sub-model (Wool et al., 2001) is a dynamic process-based model designed to simulate the Hg cycle within a system made of well-mixed discrete spatial units (layers) of water and sediment, as well as the exchanges of the system with its boundaries.

Modeled Hg species include dissolved and particulate compounds of oxidized Hg (Hg^{II}), elemental mercury (Hg^0) and MeHg, whereas DMHg) is not explicitly considered. Dissolved species include Hg^0, DOC-complexed species of Hg^{II} and MeHg (i.e. Hg_{DOC}, $MeHg_{DOC}$), and their ionic species ($HgCl_3^-$, $HgCl_4^-$, and MeHgCl in marine environments (Morel et al., 1998). Particulate species involve only oxidized Hg and MMHg that in the model can be adsorbed to POM or silt (Hg_{POM}, $MMHg_{POM}$, Hg_{silt} and $MMHg_{silt}$), where silt represents inorganic particles and POM is used to represent both organic particles and Fe/Mn oxides that are prone to precipitation and dissolution. POM can indeed be produced and degraded within one or more model layers, which is parameterized through production and degradation rates.

Hereafter we will refer to total Hg (Hg_T) and total MeHg ($MeHg_T$) as the sum of all Hg and MeHg species in the dissolved and particulate phases. We will refer to dissolved Hg (Hg_D) to indicate the sum of all dissolved species (Hg^0, Hg_{DOC}, $MeHg_{DOC}$, $HgCl_3^-$, $HgCl_4^{2-}$ and MeHgCl), while dissolved MeHg ($MeHg_D$) will be used to indicate the sum of the solely $MeHg_{DOC}$ and MeHgCl. Likewise, we will refer to particulate Hg (Hg_P) as the sum of all particle-bounded species (Hg_{POM}, $MeHg_{POM}$, Hg_{silt} and $MeHg_{silt}$) and to particulate MeHg ($MeHg_P$) as the sum of $MeHg_{POM}$ and $MeHg_{silt}$.

The main transport (i.e. diffusion, advection, volatilization, deposition, settling, resuspension, burial) and transformation processes (i.e. biotic methylation and demethylation, photo-reduction, photo-oxidation, photo-demethylation) related to the Hg cycle are taken into account in the model. Transport processes are described through advective water fluxes, diffusion coefficients and transport mediated by particles. Hg transformation processes are modeled as first-order kinetics, through a reaction constant (k_r) modulated based on environmental forcing such as temperature and light intensity. Details about the model equations and parameters can be found elsewhere (Canu and Rosati, 2017; Melaku Canu et al., 2015; Wool et al., 2001).

4.2.4 Model implementation: physical and biological setting

We represent the Black Sea as a 1D vertical system made of 9 layers of water and 2 layers of sediment (Table 1). Since we aimed at simulating the dynamics in the offshore basin of the Black Sea, the shelf area was excluded from the analysis (~30% of surface area) (Panin and Jipa, 2002), constraining the model domain to represent 70% of the volume of the upper waters and 100% of deep waters, accounting overall for the 99% of the total volume. The steady-state balance of water masses was arranged according to Özsoy and Ünlüata, (1997), to represent the inflow from Marmara that mix with the CIL, sinks into the suboxic zone and upwell toward the oxic zone (Figure 3a). No water masses flow into the anoxic zone, which is subject only to weak vertical exchange due to eddy diffusion ($5.5\ 10^{-6}$ – $1.1\ 10^{-5}$ cm/s, see Table 1).

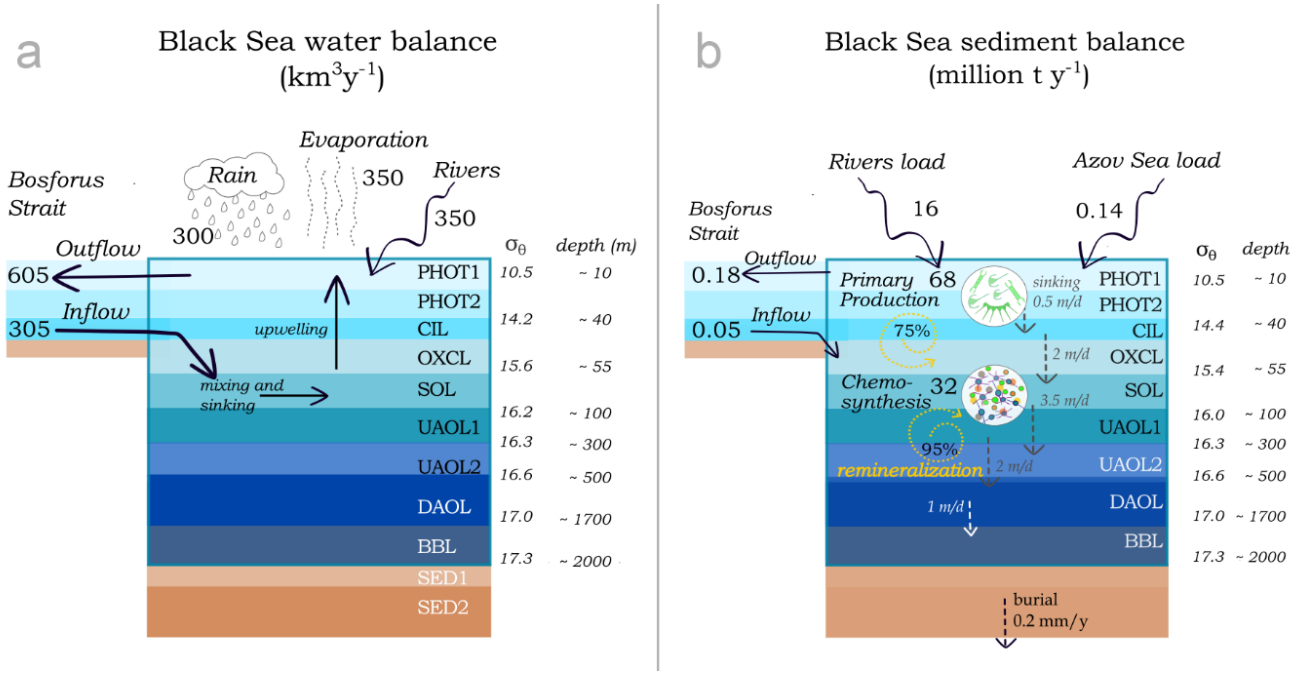

Figure 3. Water (a) and sediment (b) balance of the Black Sea implemented in the model

Monthly averaged data for solar irradiation, day length and sea surface temperature for the year 2013 (Gencarelli et al., 2015; Grell et al., 2005) were used as forcing for photoreactions, biological reactions and volatilization.

To satisfy the sediment balance of the Black Sea (Figure 3b), we considered silt and POM exchanges with the Marmara Sea (Mediterranean Sea), the loadings from rivers and the Azov Sea and the internal production and degradation, including both primary production (Agirbas et al., 2014) and chemosynthesis (Yılmaz et al., 2006).

Concentrations of suspended particulate matter (SPM) in the Marmara Sea subsurface layer, which forms the inflow to the Black Sea, were calculated from beam attenuation coefficients (BAC) at 660 nm measured during the cruise. Coefficient values were converted to SPM according to the regressions equations computed for the Aegean Sea (equation 1 and 2), where $c_{p(\lambda)}$ is the attenuation due to particles at a given wavelength λ:

$$c_{p(670)} = 0.992 * c_{p(660)} - 0.0039 \qquad \textit{eq. 1}$$

(Karageorgis et al., 2008)

$$SPM = 1.09104 * c_{p(670)} + 0.08045 \qquad \textit{eq. 2}$$

(Karageorgis and Anagnostou, 2003)

Through equations 1 and 2, we estimated an average SPM concentration of 150 µg/L, of which ~75 µg/L are of POM, according to POC measurements (Çoban-Yıldız et al., 2006, 2000). The Sea of Azov carries 12-14 km^3/y of water to the Black Sea each year with average SPM concentrations of 11.6 mg/L (Agapov et al., 2012; Ovsienko et al., 2012). Riverine solid load was estimated from the literature (Jaoshvili, 2002; Panin and Jipa, 2002; Tescari et al., 2006), the sediment export beyond estuaries was estimated taking into account the river sediment dispersal typology (Walsh and Nittrouer 2009) and the parameter 'fraction of sediment exported' ($\mathbf{f_{exp}}$) as computed by (Zhang et al., 2015). Depending on the solid load estimated for the Danube (~25 Mt/y, Panin and Jipa (2002); ~51 Mt/y, Jaoshvili (2002), ~63 Mt/y, Tescari et al., (2006)) the total solid load spans from 66 to 100 Mt, around the 20% of which is exported to the open sea (See Table 2). Riverine POM account for the 4% of total solid load (Deuser, 1971) except in the Danube, where POM is the 20-30% of SPM (Berlinsky et al., 2006).

	River type^	f_{exp} *	Solid load	Solid discharge	Hg_P conc.	Hg_P load	Hg_P discharge	Hg_D load	Hg_T discharge
	g/y		10^6 t/y	10^6 t/y	nmol/g	kmol/y	kmol/y	kmol/y	Kmol/y
Danube - lower estimate	PAD	0.2	25 °	5	1.4 ¤	34	6.9	0.21	7.1
Danube - upper estimate	PAD	0.2	63 +	12	2.5 ¤	155	31	0.96	32
Dnestr - lower estimate	PAD	0.2	2 ч	0.3	0.6 §	1	0.2	0.01	0.2
Dnestr - upper estimate	PAD	0.2	2 ч	0.3	2.5 ¤	4.3	0.9	0.03	0.9
Other rivers flowing to the NW shelf	PAD	0.2	0.3 ч	0.2	0.6 §	0.7	0.2	0.00	0.1
Kizil-Irmak	CC	0.6	0.4 ч	0.3	0.6 §	0.3	0.2	0.00	0.2
Other Turkish Rivers	-	0.2	13 ч	3	0.6 §	8	0.8	0.02	0.8
Eastern river	-	0.2	20 ч	4	0.6 §	12	3.6	0.11	3.7
Bulgarian rivers	-	0.2	1 ч	0.2	0.6 §	0.5	<0.1	<0.1	<0.1
Crimean rivers	-	0.2	0.1 ч	<0.1	0.6 §	<0.1	<0.1	<0.1	<0.1
Lower estimate			**62**	**13**		**57**	**12**	**0.4**	**12**
Upper estimate			**99**	**20**		**181**	**37**	**1.1**	**38**
Best estimate			**81**	**16**		**113**	**22**	**0.7**	**23**

^ River type (Walsh and Nittrouer, 2009)
**** Fraction of sediments and Hg_P transported beyond the estuary, after Zhang et al., (2015)***
° Danube load after damming (Panin and Jipa, 2002);
+ Danube load in 2002 (Tescari et al., 2006),
ч compilation of sediment load from all the Black Sea tributary (Jaoshvili, 2002)
***¤ Hg_P concentrations in the Danube River* (Woitke et al., 2003);**
***§ median concentration of Hg_P in rivers worldwide* (Amos et al., 2014)**

Table 2. Estimation of riverine load of sediment, Hg_P and Hg_T, assuming that Hg_P is 97% of Hg_T. The fraction of the load exported by the tributary of the Black Sea (f_{exp}) [*Zhang et al*., 2015] depends on the sediment dispersal system of the river, according to the classification proposed by *Walsh and Nittrouer*, [2009].

Seasonal rates of offshore primary production (PP) were measured in south-eastern Black Sea by Agirbas et al., (2014). Around 80% of the OM produced in the photic zone is respired and recycled within the OL, while the remaining is exported to the AOL, where the degradation is slower but detectable (Deuser, 1971; Grégoire and Soetaert, 2010; Margolin et al., 2016). At the lower end of the SOL, upward fluxes of reduced chemical species from the AOL fuel microbial chemoautotrophic production, which is responsible for 30% to 89% of total water column production and is maximum at the lower end of the redox nepheloid layer (RNL) (Yılmaz et al., 2006). The RNL is composed by a mixture of bacteria, precipitates, organic and inorganic matter and is located at lower end of the SOL where oxygen completely disappears (σ_θ=16.08 in Nyffeler et al., 2007). In the model, 60 Mt of POM are produced each year in the euphotic layer and the 77% is remineralized within the OL and SOL. Chemoautotrophy was parametrized setting POM production within the SOL (as the 30% of total water column production, 32 Mt/y). Nearly all the POM produced in the SOL is degraded in the underlying UAOL1; below the degradation rates of the residual POM are slower. POM sinking velocities along the water column were assumed to vary along the water column, as already done by other authors (Grégoire and Soetaert, 2010; Konovalov et al., 2004; Yakushev et al., 2007). In the euphotic zone (PHOT), where most of the SPM is given by POM, mainly living plankton, we set settling velocities at 0.5 m/d. Below, the settling velocity of POM detritus increases at 2 m/d in CIL and oxycline. Chemosynthetic production in the lower SOL leads to the formation of larger aggregates of organic and inorganic matter, making the average settling speed increase up to 3.5 m/d. Sinking velocities decrease in the AOL (2 m/d) due to the dissolution of Fe/Mn oxides, and decrease further in the lower anoxic layer (1 m/d) due to the formation of smaller sulfidic compounds. As for the sediment compartment, two layers were modeled: a 3 cm deep fluffy layer with porosity ~0.96 (Yücel et al., 2012) on top of a 7 cm deep layer of more consolidated sediment. The resulting burial rate is 0.21 mm/y, comparable to the range reported by Yücel et al., (2012). The modeled SPM profile is shown in Figure 4 along with SPM concentrations estimated from BAC measurements.

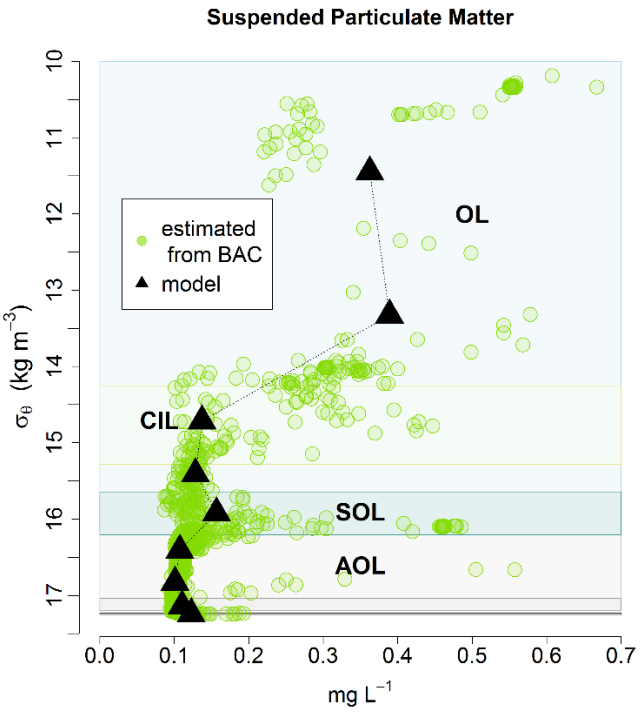

Figure 4. Comparison between modeled SPM profile (black triangles) and observed concentrations, as estimated from the beam attenuation coefficient (BAC, green circles) and equations 1 and 2. Potential density anomaly (σ_θ) is used as vertical axes, the boundary of the redox layers computed from the cruise dataset are shown in the background as following: oxic layer (OL, light cyan boxes), including the cold intermediate layer (CIL, yellow box), suboxic layer (SOL, green box) and anoxic layer (AOL, grey boxes).

4.2.5 Model implementation: mercury biogeochemistry

To simulate Hg dynamics in the Black Sea, we took into account inputs and outputs of the system, transport mediated by water and sediment, and transformation processes. We developed a 1D model of Hg excluding the biotic production and degradation of MeHg within the system, and then used this as the baseline simulation to add in Hg methylation and demethylation processes at different water depths (section 2.6). We gathered information about Hg species loads, boundary concentrations and fluxes for the year 2013 (Tables 2 and 3), however, since the residence time of the deep water has been estimated between 330 and 1500 years (Murray et al., 2007), the present-day concentrations in the deep water must reflect processes that have been occurring over such a long time. Therefore, we estimated the temporal evolution of Hg input from the year 1850 to the year 2013 by scaling the current input according to historical anthropogenic enrichment factors estimated for global emissions and deposition of Hg. Riverine inputs were scaled according to the inventory of global Hg emissions compiled by Horowitz et al., (2014), while atmospheric deposition rates were scaled according to the global Hg atmospheric deposition (Amos et al., 2015). Furthermore, we projected the simulation to the year 2050,

maintaining Hg input relative to the year 2013. The model was initialized without any Hg in the system and run for 200 years.

Input of Hg^{II} and MeHg from the rivers and from the Azov Sea were modeled as constant throughout each year, while atmospheric deposition was modeled as a monthly variable load of Hg^{II}. Upper and lower estimates of riverine Hg load were computed based on Hg_P measurements in the Danube (Woitke et al., 2003) and rivers worldwide (Amos et al., 2014), while the fraction exported to the open sea (Table 2) was assigned according to Walsh and Nittrouer, (2009) and Zhang et al., (2015).

Atmospheric concentrations of Hg^{II} and Hg^0 and deposition rates of Hg^{II} over the Black Sea for the year 2013 were computed with the WRF/Chem-Hg atmospheric model (Gencarelli et al., 2017, 2015, 2014) forced with chemical initial and boundary conditions for Hg species taken from the ECHMERIT model (De Simone et al., 2016, 2014; Jung et al., 2009).

Concentrations data of Hg_D and $MeHg_D$ in the Marmara Sea (Mediterranean Sea) from the 2013 GEOTRACES MEDBlack cruise (GA04-leg1) were used to characterize steady-state boundary conditions. Other model parameters and coefficients (partition constants, diffusion coefficients, photochemical transformations rates) were chosen within literature ranges and are listed in Table 3 (Black et al., 2012; Han et al., 2007b; Hollweg et al., 2010; Lamborg et al., 2016; Liu et al., 2015; Muresan et al., 2007; Schartup et al., 2015a; Whalin et al., 2007).

Boundary concentrations				
Hg_T in Marmara subsurface layer (Black Sea inflow)	1.47	pM	*Assuming that Hg_D is the 90% of Hg_T (Bowman et al., 2015)*	*2013 GEOTRACES MEDBlack (GA04-leg1)*
$MeHg_T$ in Marmara subsurface layer (Black Sea inflow)	0.11	pM	*Assuming that $MeHg_D$ is the 90% of $MeHg_T$ (Bowman et al., 2015)*	*2013 GEOTRACES MEDBlack (GA04-leg1)*
Hg^0 in Marmara subsurface layer (Black Sea inflow)	0.15	pM	*Assuming that Hg^0 is the 10% of Hg_T*	(Fantozzi et al., 2013; Gårdfeldt et al., 2003a; Kotnik et al., 2015; Soerensen et al., 2013)
Atmospheric Hg^0 concentrations	7	$pmol/m^3$	*Used within the model to compute volatilization*	*WRF/Chem atmospheric model*
Direct Loads				
Atmospheric deposition of Hg^{II}	5.3	kmol/y		*WRF/Chem atmospheric model*
Riverine Hg_T	23	kmol/y		*See table 2*
Riverine MeHg	1.2	kmol/y	*MeHg estimated to be 5% of Hg*	Balogh et al. (2003); Paller et al. (2004); Sharif et al. (2014)
Hg Azov Sea	0.42	kmol/y	*MeHg is assumed to be the 5% as it is in our dataset of the Black Sea water*	Chasovnikov et al., (2012)

Parameters and coefficients				
Photo-reduction rate constant	$1.2\ 10^{-6}$	1/s	*Rate for mesohaline water normalized to 1 langley/day*	Whalin et al., (2007)
Photo-oxidation rate constant	$1.4\ 10^{-6}$	1/s	*Rate for mesohaline water normalized to 1 langley/day*	Whalin et al., (2007)
Photo-demethylation rate constant	$3.6\ 10^{-8}$	1/s	*Rate at salinity ~18 normalized to 1 langley/day*	*Black et al., (2012)*
Hg^{II} partition coefficients	$K_{silt} = 3\ 10^3$ $K_{POM} = 5.3\ 10^5$ $K_{DOC} = 3\ 10^3$	L/kg		*(Han et al., 2007; Hollweg et al., 2010; Lamborg et al., 2016; Liu et al., 2015; Muresan et al., 2007; Schartup et al., 2015, 2014)*
MeHg partition coefficients	$K_{silt} = 1\ 10^3$ $K_{POM} = 3.5\ 10^5$ $K_{DOC} = 3\ 10^3$	L/kg		*(Han et al., 2007; Hollweg et al., 2010; Muresan et al., 2007; Schartup et al., 2015)*
Diffusion Coefficient	10^{-5}	cm^2/s		*Hollweg et al., (2010)*
Henry's Law Constant for Hg^0	$7\ 10^{-3}$	atm-m^3/mol		-
Light attenuation coefficient	0.2	1/m		*Agirbas et al., (2014)*
DOC concentrations	1.4 – 2.9	mg/L		*(Ducklow et al., 2007; Margolin et al., 2016)*

Table 3. Synthesis of the data on Hg and MeHg loads, concentrations and parameters used to simulate the Hg cycle in the Black Sea.

4.2.6 Model implementation: setting methylation and demethylation

To investigate MeHg cycling in the Black Sea, we implemented simulations with different set-up by parametrizing Hg methylation and demethylation in different redox layer(s). A compilation of published methylation (k_m) and demethylation rates (k_{dm}) measured in different redox environments (Eckley and Hintelmann, 2006; Heyes et al., 2006; Hollweg et al., 2009; Jonsson et al., 2012; Lehnherr et al., 2011; Monperrus et al., 2007a; Ortiz et al., 2015; Rodríguez Martín-Doimeadios et al., 2004; Schartup et al., 2015a; Sharif et al., 2014) was used to extrapolate the rates used in the simulations (Table 4). By setting k_m and k_{dm} in one or more redox layers at a time (OL, SOL, AOL, SED) and keeping photochemical transformations in surface water at a fixed rate (Table 3), we run several test simulations exploring most of the possible pathways of MeHg production, degradation and accumulation in the Black Sea. We selected one simulation for each set-up (7 simulations) based on comparison of the modeled and measured $MeHg_D$ profiles. The comparison was performed through the Taylor diagram (Taylor, 2001), using the R package plotrix (Lemon, 2006; R Core Team, 2013); the diagram synthetizes the agreement between model output and measurements taking into account the correlation coefficient (r), the standard deviation (s.d.) and the root mean squared error (RMS). The simulations selected (Table 4) and the rationale behind each are as follows:

1) **methylation in OL (*m1*):** biotic Hg_D methylation and $MeHg_D$ demethylation occur in the OL (σ_θ 10.5–15.64). The $MeHg_D$ produced is adsorbed by POM and Fe/Mn oxides ($MeHg_P$) and transported along with Hg_P to SOL-AOL, where they are both released as Hg^{II}_D and $MeHg_D$ during POM degradation and Fe/Mn oxides reduction;

2) **methylation in SOL (*m2*):** $MeHg_D$ is produced and degraded by bacteria in the SOL (σ_θ 15.64–16.2), scavenged by Fe/Mn oxides, transported downward as $MeHg_P$, and released as $MeHg_D$ in the UAOL (σ_θ>16.2) under more reductive conditions;

3) **methylation in SOL-UAOL (*m3*):** biotic Hg_D methylation and $MeHg_D$ demethylation occur in SOL and UAOL (σ_θ 15.64 – 17.04). $MeHg_D$ produced in the suboxic layer is scavenged by Fe/Mn oxides ($MeHg_P$) and released as $MeHg_D$ in the UAOL (σ_θ>16.2), where additional $MeHg_D$ is produced;

4) **methylation in AOL (*m4*):** biotic methylation and demethylation occur in the AOL excluding the BBL (σ_θ 16.2 – 17.2) after dissolution of Mn/Fe oxides that release Hg^{II}_D;

5) **methylation throughout the water column (*m5*):** biotic methylation and demethylation occur throughout the water column, with different rates according to the redox conditions;

6) **methylation in sediment (*m6*):** Hg_D is methylated and demethylated in the sediment, from which $MeHg_D$ is released *via* pore-water diffusion;

7) **absence of methylation *in situ* (*m7*):** input from rivers and Marmara Sea (Mediterranean Sea) inflow are the only source of $MeHg_T$ to the Black Sea.

	m1 - OL methylation			***m2 - SOL methylation***			***m3 - SOL-UAOL methylation***			
layer	**k_m**	**k_{dm}**	**model MeH_D**	**k_m**	**k_{dm}**	**model MeH_D**	**k_m**	**k_{dm}**	**model MeH_D**	
	d^{-1}	d^{-1}	pM	d^{-1}	d^{-1}	pM	d^{-1}	d^{-1}	pM	
PHOT1	0.004	0.042	0.14	-	-	0.12	-	-	0.12	
PHOT1	0.004	0.042	0.13	-	-	0.12	-	-	0.12	
CIL	0.004	0.042	0.13	-	-	0.14	-	-	0.14	
OXCL	0.004	0.042	0.13		-	0.15			0.15	
SOL	-	-	0.13	0.0045	0.032	0.17	0.0045	0.054	0.16	
UAOL1	-	-	0.19	-	-	0.25	0.0045	0.016	0.52	
UAOL2	-	-	0.20	-	-	0.25	0.0045	0.016	0.56	
DAOL	-	-	0.20	-	-	0.26	-	-	0.59	
BBL	-	-	0.20			0.26	-	-	0.59	
SED1	-	-		-	-		-	-		
SED2	-	-		-	-		-	-		
r			***0.97***			***0.96***			***0.97***	
RMS			***0.12***			***0.09***			***0.01***	
sd			***0.04***			***0.06***			***0.23***	

	m4 - AOL methylation			**m5 - Whole water column methylation**			**m6 - Sediment methylation**			**m7 - No met**
	k_m	**k_{dm}**	**model MeH_D**	**k_m**	**k_{dm}**	**model MeH_D**	**k_m**	**k_{dm}**	**model MeH_D**	**model MeH_D**
	d^{-1}	d^{-1}	pM	d^{-1}	d^{-1}	pM	d^{-1}	d^{-1}	pM	pM
PHOT1			0.16	0.004	0.045	0.13	-	-	0.10	0.10
PHOT1	-	-	0.16	0.004	0.045	0.12	-	-	0.09	0.09
CIL	-	-	0.18	0.004	0.045	0.13	-	-	0.10	0.10
OXCL	-	-	0.21	0.004	0.045	0.14	-	-	0.10	0.10
SOL	-	-	0.25	0.004	0.041	0.19	-	-	0.09	0.09
DAOL1	0.0014	0.006	0.46	0.0014	0.0039	0.56	-	-	0.14	0.14
UAOL2	0.0014	0.006	0.50	0.0014	0.0039	0.63	-	-	0.15	0.15
DAOL	0.0014	0.004	0.68	0.0014	0.0039	0.72	-	-	0.15	0.15
BBL	-	-	0.68	-	-	0.72	-	-	0.15	0.15
SED1	-	-		-	-		0.0135	0.042		
SED2	-	-		-	-		0.0135	0.042		
r			***0.94***			***0.97***			***0.97***	***0.97***
RMS			***0.01***			***0.01***			***0.14***	***0.14***
sd			***0.22***			***0.28***			***0.02***	***0.02***

Table 4. Synthesis of methylation and demethylation rates (k_m and k_{dm}) used in the selected simulations. Next to the rates applied, there are modeled MeHg concentrations of each simulation, with the statistics summarizing the **m**odel performances that are the correlation coefficient (r), the standard deviation (sd) and the root mean squared error (RMS).

4.3 Results

4.3.1 Observed vertical profiles of Hg and MeHg

Across the 10 deep stations sampled in the Black Sea, we observed similar vertical profiles for Hg_D and $MeHg_D$, with lower concentrations in the OL that slightly increase in the SOL and rise in the AOL, with a double peak of both Hg_D and $MeHg_D$ concentrations. Figure 2 shows the vertical distribution of Hg_D, $MeHg_D$ and other biogoechemical variables against σ_θ, while Figure 5 shows the distribution of $MeHg_D$ against depth along the cruise transect. Figure 6 shows the average concentration profiles focusing on the dynamic in the SOL-AOL.

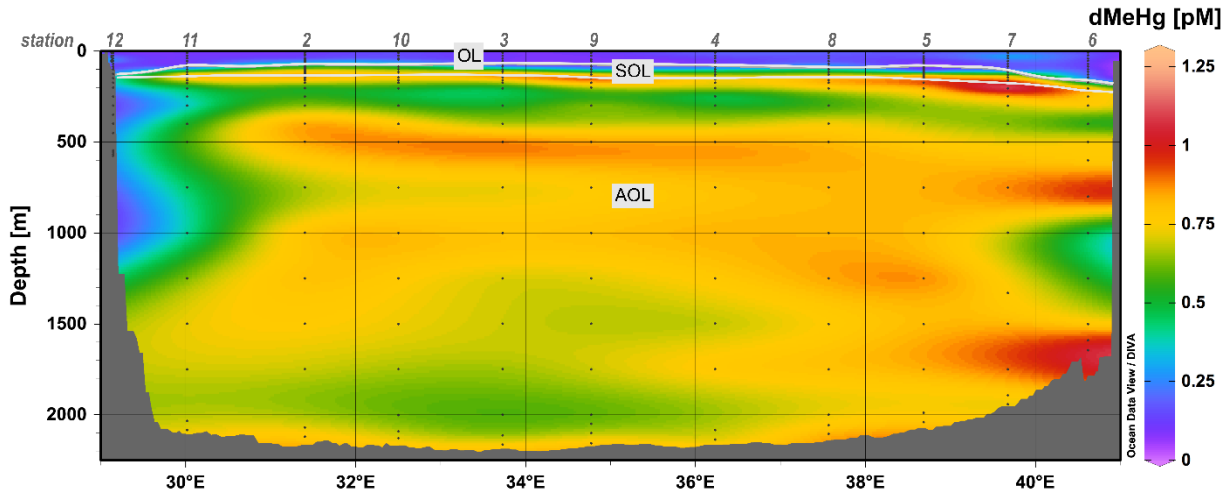

Figure 5. Distribution of $MeHg_D$ (pM) along the 2013 GEOTRACES MEDBlack cruise transect. The contours of oxic layer (OL), suboxic layer (SOL) and anoxic layer (AOL) are indicated by the grey lines.

The mean value of Hg_D is 1.9 pM in the OL (1.1 – 3.0 pM) and 2 pM in the SOL (1.4 – 3.2 pM), increasing up to 3.4 pM (2.0 – 5.0 pM) in the AOL. Likewise, $MeHg_D$ concentrations average 125 fM in the OL (74 – 198 fM) and 158 fM in the SOL (84 – 364 fM), rising up to 709 fM in the AOL (342 – 1200 fM). The same trend is observed for MeHg%, which is the 8% of Hg_T in the OL (3 – 16%), the 11% in the SOL (8 – 15%) and the 23% in the AOL (9 – 57%). The first maximum of Hg_D and $MeHg_D$ occurs at 100 – 200 m-depth, which is within the layer UAOL1 (σ_θ 16.3 – 16.5, see Figure 6); however the increase of Hg_D appears at a shallower depth (~110 m-depth) in the water column than the increase of $MeHg_D$ (~120 m-depth), and the Hg_D profile is smoother than that of MeHg. In fact, the slight increase of average $MeHg_D$ levels in the SOL compared to the OL (~ 26%) is driven by a few data points located close to the SOL-AOL interface (Figure 2).

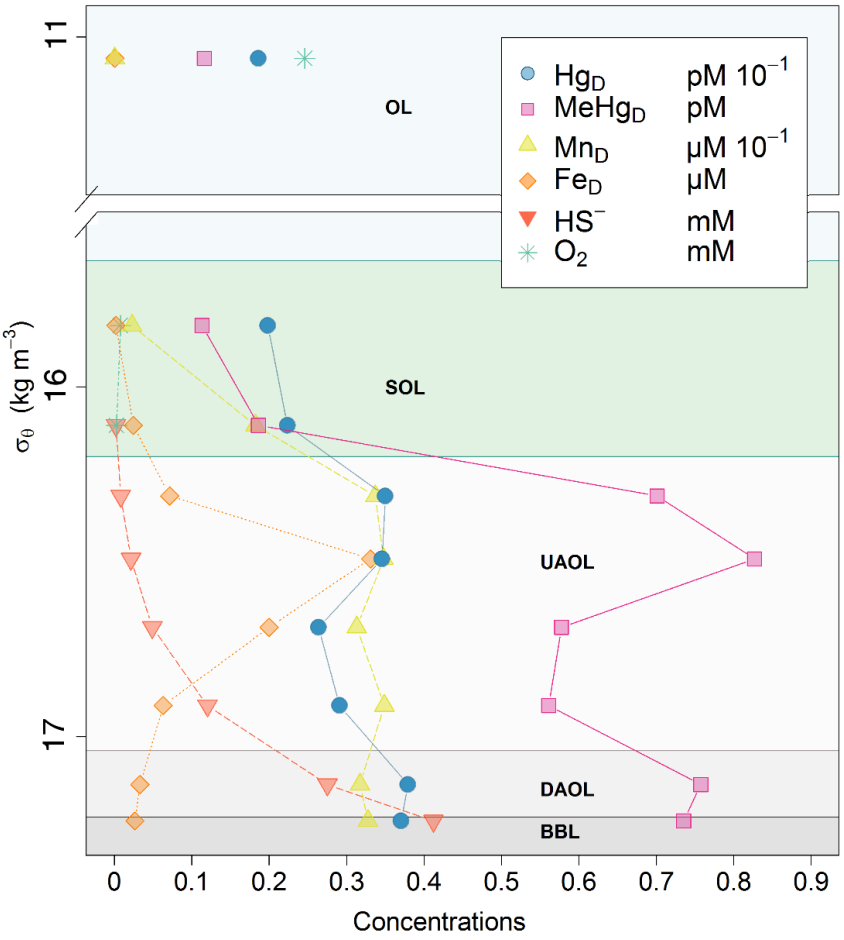

Figure 6. Averaged profiles (stations 1-10) of the concentrations of Hg and MeHg observed during the cruise in the oxic layer (OL, light cyan boxes), suboxic layer (SOL, green box) and anoxic layer (AOL, grey boxes) of the Black Sea. The profiles of O_2 and HS^- illustrate the transition from oxic to suboxic and anoxic conditions, and the increase of dissolved Mn and Fe concentrations in the AOL is shown. Potential density anomaly ($\sigma_\theta = \sigma(S,\theta,0)$-1000, kg m^{-3}) is used as vertical coordinate, omitting the range from σ_θ=11.5 to σ_θ=15.5 to emphasize the dynamics in the AOL.

Concentrations of dissolved Mn (Mn_D) rise in the SOL and peak below the SOL-AOL interface (σ_θ~16.3), whilst concentrations of dissolved Fe (Fe_D) increase at the SOL-AOL interface and reach a maximum slightly deeper (σ_θ~16.5). Then, Mn_D concentrations remain elevated and constant until the sea bed, while Fe_D decreases sharply below its maximum, as it precipitates as $FeS_{(s)}$. At the isopycnals between σ_θ 16.7 and 16.9 (UAOL2) is a local minimum of Hg_D and $MeHg_D$ concentrations, which then increase to a second Hg maximum at σ_θ 17.04 -17.24, in the DAOL (450 – 1880 m-depth). Concentrations of HS^- range 5 – 25 µM at the density level of the first Hg maximum, and 295 – 446 µM at the density level of the second Hg maximum. Considering only the data from SOL and AOL, there is

a weak correlation of Hg_D to Fe_D (r=0.69, *p<0.001*) and Mn_D (r=0.35, *p<0.01*); and a weak correlation of $MeHg_D$ concentrations to both Mn_D and Fe_D (r=0.55 *p<0.001*).

Lamborg et al., (2008) observed two deep maxima of Hg_D (σ_θ~16.5 and σ_θ >17) in the western gyre, but in contrast to our results they detected only a shallow $MeHg_D$ maximum at σ_θ~16.2 and decreasing concentrations toward the sea bed. We believe that this discrepancy is due to the different analytical methodologies. We applied an isotope dilution method which allows to access the recovery of the analytes. Following our standard protocol for seawater (Heimbürger et al., 2015) the isotopic spikes ^{199}iHg and ^{201}MMHg added prior to derivatization and extraction, were undetectable for the anoxic seawater samples. Oxygenation of the samples prior to derivatization and extraction allowed for full spike recovery (section 2.1). Lamborg et al., (2008) did not use isotope dilution and their method might not have been efficient for the analysis of the anoxic Black Sea waters.

Cossa and Coquery, (2005) measured only Hg_T with a maximum (~6 pM) at ~200 m-depth (σ_θ~16.5), coincident with the region of maximum of Fe_D. Below, Hg_T concentrations decreased sharply (~2 pM at 400 m-depth) and increased again to intermediate values (~4 pM) at 1400 m-depth, which was the maximum depth sampled.

The distribution of MeHg along the stratified water column of the Gotland Sea (Baltic Sea) is consistent with that of the Black Sea: concentrations are minimum above the halocline and maximum in anoxic water (Soerensen et al., 2016). Sulfide levels in the anoxic water of Gotland Sea (~150 μM) are lower but comparable to those of the Black Sea (Neretin et al., 2003).

4.3.2 Simulation performance

By testing a number of methylation and demethylation rates (k_m and k_{dm}) for each model set-up (section 2.6), we found that the rates applied to the simulations affect modeled MeHg concentrations but have little or no effect on the shape of modeled profiles (not shown). Therefore, for each set-up we selected the k_m and k_{dm} that yield the best agreement with observed $MeHg_D$ concentrations and then analyzed the performance of each set-up though the Taylor diagram (Figure 7), which compares observed and modeled $MeHg_D$ profiles.

Modeled $MeHg_D$ concentrations of each simulation are given in Table 4, along with the k_m and k_{dm} rates applied, and the statistics summarizing their performances. The simulations *m3* (k_m and k_{dm} in SOL-UAOL), *m4* (k_m and k_{dm} in AOL) and *m5* (k_m and k_{dm} in all the model layers) are closest to the reference point, being the ones that reproduce to some extent the increase of $MeHg_D$ in the AOL (RMS<0.01 pM, s.d.>0.2 pM). The simulations *m3* and *m5* correlate better with measurements (r=0.97) than the

simulation *m4*, which slightly overestimates MeHg concentrations in the SOL and underestimates the upper MeHg maximum in the UAOL1, and has a lower correlation coefficient (r=0.94). Overall, the simulation *m5* (RMS=0.006 pM, s.d.=0.28 pM) fits best with the observed $MeHg_D$ profile (Figure /, Table 4). In this simulation, k_m is slightly higher in the OL and SOL (~0.004 d^{-1}) compared to the AOL (~0.0014 d^{-1}), but demethylation is more efficient in the OL and SOL (k_{dm}~0.04 d^{-1} with a ratio k_{dm}/k_m ~10) compared to the AOL (k_{dm}~0.004 d^{-1} with a ratio k_{dm}/k_m ~3). All other simulations (*m1, m2, m6, m7*) differ more from the measurements and show higher errors (RMS>0.08 pM) and lower standard deviations (s.d.<0.1 pM). Despite the low k_{dm}/k_m ratio (~3) set in the simulation *m6* (k_m and k_{dm} only in the sediment), the modeled $MeHg_D$ profile overlaps with that of simulation *m7*, which included only external input of MeHg without any *in situ* production, showing that diffusive fluxes from sediment unlikely affect water column concentrations.

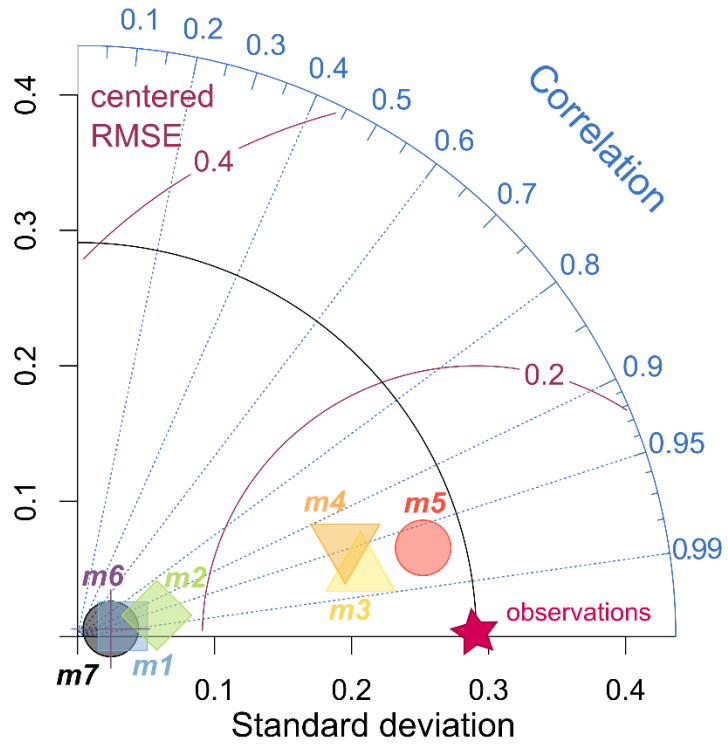

Figure 7. Taylor diagram of the variable $MeHg_D$, comparing the performance of simulations with methylation and demethylation of Hg. The angular coordinate of each point indicates the correlation of the simulation with the observed data (blue dashed lines). The distance from the reference point (purple star), indicates the centered root mean squared error (RMS, red archs). The distance from the origin is proportional to the standard deviation (x axis). *m1*=methylation and demethylation in OL (cyan square), *m2*= methylation and demethylation in SOL (green diamond), *m3*=methylation and demethylation in SOL-UAOL (yellow triangle), *m4*=methylation and demethylation in AOL (orange reverse triangle), *m5*=methylation and demethylation throughout the water column (red dot), *m6*=methylation and demethylation in sediment (violet cross), *m7*= no methylation (black dot).

4.3.3 Modeled Hg and MeHg concentrations

The output of the best fitting simulation (*m5*) is in good agreement with measured values (Figure 8): modeled Hg_T concentrations are ~2 pM in the OL and in the SOL (where Hg_D accounts respectively for 90% and 94% of Hg_T) and increase to 3.5 pM in the AOL (Hg_D ~97%). $MeHg_T$ concentrations average 140 fM in the OL ($MeHg_D$ ~90%) and increase to 196 fM in the SOL ($MeHg_D$ ~96%) and 657 fM in the AOL ($MeHg_D$ ~97%). The modeled reservoir of Hg_D in the water column is 1590 kmol (319 t) of which 346 kmol (22%; 69 t) are present as $MeHg_D$; the mismatch between modeled and measured concentrations amounts to 229 kmol for Hg_D and to 19 kmol for $MeHg_D$. The Hg_T modeled reservoir in the water amounts to 1683 kmol, including 357 kmol of $MeHg_T$. Concentrations in the surface sediment (first 3 cm) increase with time up to 730 and 120 pmol/g (146 and 24 ng/g) of Hg_T and $MeHg_T$. Estimated Hg_T is close to the average value measured in surface sediment (798 pmol/g). The Hg inventory of the sediment (10 cm-depth) is about 1140 and 200 kmol (229 and 40 t) of Hg_T and $MeHg_T$, slightly lower but comparable to the reservoir in the waters.

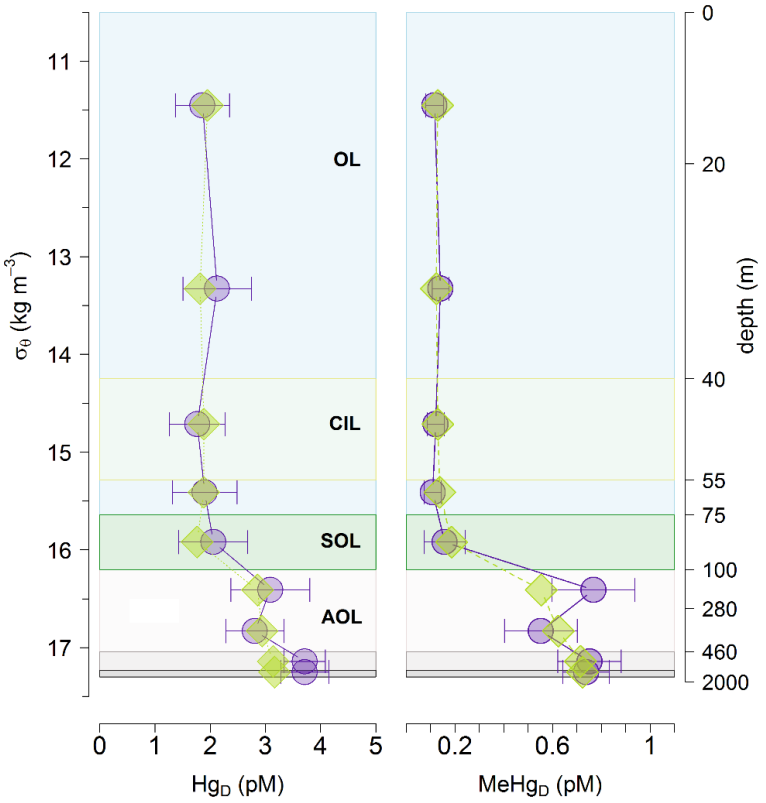

Figure 8. Comparison between observed (purple circles) and modeled (green diamonds, from simulation *m5*) concentration profiles of Hg_D (left panel) and $MeHg_D$ (right panel). Potential density anomaly ($\sigma_\theta = \sigma(S, \theta, 0)$-1000, kg/m^3) is used as vertical coordinate.

Temporal evolution of modeled Hg_T and $MeHg_T$ concentrations in of the water column for the years 1850-2050 is shown in Figure 9 along with the temporal evolution of Hg and MeHg input reconstructed after Amos et al., (2015) and Horowitz et al., (2014). Surface and subsurface Hg_T show a fast response to changes in atmospheric and riverine loadings, and follow seasonal variability. $MeHg_T$ differs from Hg_T, because it is much less affected by external loadings and is rather controlled by *in situ* production. In the AOL, Hg_T and $MeHg_T$ dynamics are more similar; concentrations increase almost linearly until the end of the simulation, when concentrations in the other layers are recovering due to reduced anthropogenic Hg emissions since the 1970's.

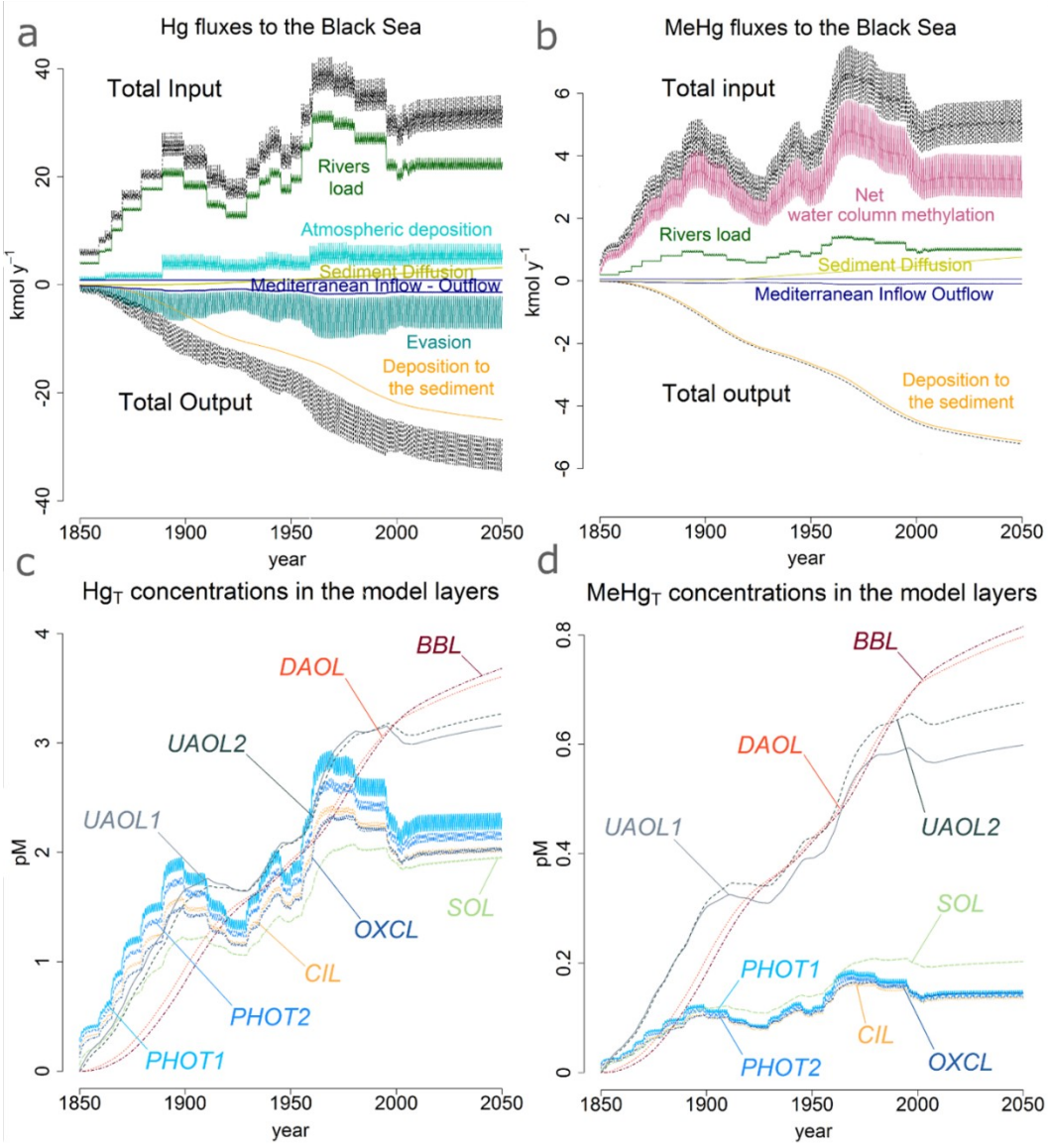

Figure 9. Modelled temporal evolution of a) Hg_T and b) MeHg fluxes to the Black Sea; and c) Hg_T d) $MeHg_T$ concentrations in the 9 water layers for the 1850-2050 time period

4.3.5 Budget of Hg species in the Black Sea

Starting from modeled concentrations of simulation *m5*, we computed the mass balance of Hg_T and $MeHg_T$ in the Black Sea (Figure 10), considering inputs from rivers and Azov Sea, and the exchanges with the atmosphere, the sediment and the Marmara Sea (Mediterranean Sea). In its present state, Hg_T inputs to the water column (31 kmol/y) are estimated to exceed the outputs (29 kmol/y). The most relevant input is riverine load (71%, 22 kmol/y), followed by atmospheric deposition (17%, 5.3 kmol/y). Little Hg comes from sediment *via* pore-water diffusion of Hg_D (7%, 2.3 kmol/y), from the Marmara Sea inflow (<3%, 0.9 kmol/y) and from the Azov Sea (~1%, 0.4 kmol/y). The main loss of Hg from the water (78%) is settling and deposition of 23 kmol/y of Hg_P. Evasion of Hg^0 accounts for 17% (5 kmol/y) of the output from the water and the outflow to the Marmara Sea for 5% (1.4 kmol/y). 6% of Hg that deposits to the sediment is buried below 10 cm-depth (1.5 kmol/y), while 10% moves back to the water through pore-water diffusion; the remainder constitutes the sediment reservoir.

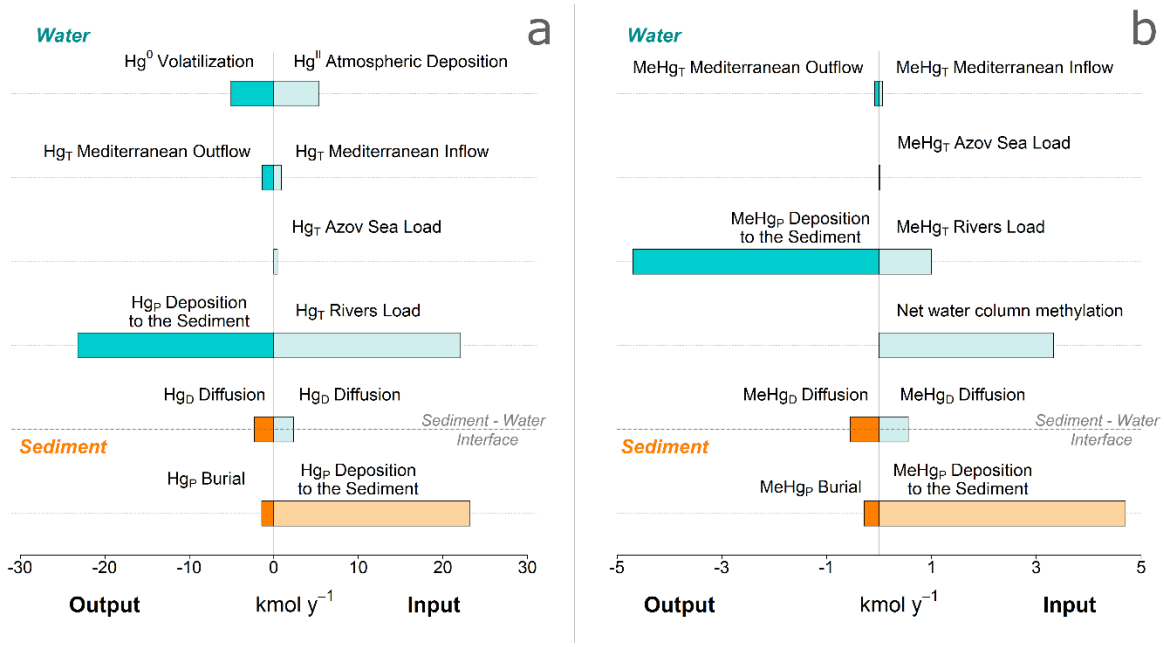

Figure 10. Budget of a) Hg_T and b) $MeHg_T$ in the Black Sea fot the year 2013, computed from results of simulation *m5*. Input to water (light cyan) and sediment (light orange) are plotted on the right side of each panel. Output from water (dark cyan) and sediment (dark orange) are plotted on the left side

For MeHg, the model estimated that inputs to the water (~1.6 kmol/y) are lower than the outputs (4.8 kmol/y), because the bulk of MeHg (~3.3 kmol/y) comes from in situ methylation in the AOL. Indeed, the amount of $MeHg_D$ that is demethylated in the OL and SOL (27.8 and 10 kmol/y) exceeds the amount of Hg_D^{II} that is methylated (27.3 and 7 kmol/y), while the opposite is true in the AOL (258 kmol/y

methylated and 251 kmol/y demethylated). The net production of MeHg occurs mostly in the UAOL1 (4 kmol/y) and UAOL2 (2 kmol/y), while it amounts to 0.9 and 0.2 kmol/y in the DAOL and BBL. Rivers account for 1 kmol/y of MeHg (20% of the sum of input and net production that is ~5 kmol/y) and pore-water diffusion for 0.6 kmol/y (11%). Minimal contributions come from the Marmara and Azov Seas which together account for 1.6% (0.06 and 0.02 kmol/y). Around 4.7 kmol/y of MeHg leave the water column after settling and deposition, while 0.09 kmol/y moves to the Marmara Sea transported by the Mediterranean outflow.

4.4 Discussion

4.4.1 Cycling of Hg species among the redox layers of the Black Sea

We observed an association between the upper maximum of Hg_D and $MeHg_D$ concentrations and the maximum of Mn_D in the Black Sea water column, (σ_θ 16.3-16.5) as previously observed for Hg_D and Mn_D or Fe_D (Lamborg et al., 2008) and for Hg_D and $MeHg_D$ in other stratified systems (Han et al., 2007a; Mason et al., 1993). These observations are usually explained as a consequence of the involvement of Hg species in a 'shuttle' transportation process based on Mn/Fe oxides (Neretin et al., 2003), invoked to explain the distribution of phosphates in the Black Sea (Dellwig et al., 2010; Pakhomova and Yakushev, 2013; Shaffer, 1986) and the distribution of Hg species in stratified water bodies with anoxic bottom water (Cossa and Coquery, 2005; Han et al., 2007a; Mason et al., 1993). The shuttle theory is as follows: Hg is scavenged from surface layers by POM and Mn/Fe oxides and settles toward the bottom of the SOL, where NOM remineralization driven by oxide reduction causes Hg_D release. Reduced Mn/Fe diffuse upward and are oxidized at the top of the SOL; likewise, Hg_D and $MeHg_D$ released (or produced) in the AOL diffuse upward and are scavenged by oxides. Therefore, Hg species are trapped in this cycle between suboxic and anoxic waters. The cycling of Mn between oxidized and reduced species plays a major role in the Black Sea and in the Baltic Sea, being more intensive than the Fe cycle (Konovalov et al., 2004; Neretin et al., 2003; Pakhomova and Yakushev, 2013), however mixed phases of Mn and Fe oxides have been observed (Dellwig et al., 2010).
In the seasonally anoxic waters of Offatts Bayou (USA), the maximum of Fe/Mn oxides was coincident with a particle enrichment in Hg and MeHg, and dissolved species concentrations were highest in the anoxic water (with sulfides ~200 μM). This was ascribed to Hg species release from oxide dissolution and to methylation in suboxic waters, and possibly to enhanced Hg species solubility through sulfide complexation (Han et al., 2007a). In the stratified waters of Pettaquamscutt Estuary (USA), $MeHg_D$ concentrations were lowest in oxic water, maximum in the lower pycnocline (coincident with a

maximum of bacteriochlorophyll *a* and *e*), and at intermediate levels in anoxic waters. Mason et al., (1993) argued that $MeHg_D$ is produced in the lower pycnocline and can diffuse downward but not upward due to scavenging by Mn/Fe oxides, and that complexation by sulfides and/or methylation in anoxic water might enhance $MeHg_D$ levels below.

Although these processes are represented in a simpified fashion in our model, by parametrizing production of POM within the SOL and its degradation in the UAOL1 (Figure 3b), they induce retention of Hg species in the deep water, as suggested by the temporal increase of modeled Hg concentrations in the 4 layers of the AOL (Figure 9).

4.4.2 Hg methylation along the redox gradient

The comparison among simulations of Hg methylation and demethylation in the Black Sea highlights that it is important to take into account the production of MeHg in the anoxic water to simulate the Hg cycle in the Black Sea (Figure 7). Moreover, mass balance calculations indicate that methylation in the AOL might be the most relevant source of MeHg to the basin and thus, a process that needs to be further investigated to gain more insight into MeHg dynamics. Based on the Fe peak in the upper anoxic layer (UAOL1) methylation might be driven by Fe reducing bacteria, which have been reported to prompt Hg desorption and methylation by using Fe oxides as electron acceptors (Hellal et al., 2015; Kerin et al., 2006; Schaefer et al., 2011; Si et al., 2015), whereas sulfate reducing bacteria (Benoit et al., 2001; King et al., 2000; Moreau et al., 2015; Schaefer et al., 2014) are likely to contribute significantly to Hg methylation in the lower layers of the AOL (UAOL2 and DAOL) where HS^- concentrations are higher than 40 µM and increase with depth. Based on the recent identification of new bacterial strains able to methylate Hg (Gilmour et al., 2013), there are other potential candidates for Hg methylation in the AOL of the Black Sea. These are methanogens and the species *Desulfitobacterium metallireducens* (genus Firmicutes), who can use either Mn or Fe oxides as electron acceptors (Villemur et al., 2006). Fuchsman et al., (2011) reported that both methane-oxidizing and manganese reducing bacteria are abundant in the waters of the lower SOL and in the UAOL.

The local minimum of Hg_D and $MeHg_D$ that we observed in the UAOL2 of the Black Sea (Figure 6) might be due to their partial pyritization (co-precipitation) in the formation of FeS_2 (Morse and Luther, 1999), as it occurs at the depth where Fe_D concentrations drop. Such a process has been proposed also for the cycling of Hg species in the Pettaquamscutt Estuary (Mason et al., 1993), while it has been suggested to affect the water profile of Hg^{II} but not that of MeHg in Offatts Bayou, probably because of

the higher POM concentrations in the shallow bay that outcompete FeS_2 for binding sites (Han et al., 2007a).

The increase of dissolved Hg species concentrations at depth, in the DAOL, might be due to enhanced solubility of Hg species in presence of sulfides and DOM (Han et al., 2007a; Mason et al., 1993; Ravichandran et al., 1999, 1998; Skyllberg, 2008; Slowey, 2010; Sunderland et al., 2006; Waples et al., 2005) and to net *in situ* methylation favored by DOM (Graham et al., 2012; Moreau et al., 2015; Schaefer et al., 2011; Schaefer and Morel, 2009). In sulfidic systems, some components of the DOM (thiols, humic acids, cysteine) delay or inhibit the precipitation of $HgS_{(s)}$, and favor its dissolution, promoting the formation of nanoparticles that have been measured within the dissolved fraction (Deonarine and Hsu-Kim, 2009; Gerbig et al., 2011; Slowey, 2010) and can be methylated (Jonsson et al., 2012; Kucharzyk et al., 2015; Zhang et al., 2014, 2012). These recent experimental findings might provide a mechanistic explanation for the lower maximum of $MeHg_D$ observed in the Black Sea. Low Hg/DOM ratios seem to favor these processes (Gerbig et al., 2011; Graham et al., 2012; Slowey, 2010), and the ratio throughout the AOL is low (~0.2 nmolHg/mgDOM), with a slight DOC increase in DAOL and BBL (Ducklow et al., 2007; Margolin et al., 2016). Other recent research has shown that the binding of MeHg to reduced sulfur groups on minerals (FeS_m, $HgS_{(s)}$ and CdS) and organic surfaces (thiols), leads to the microbial production of dimethylmercury (DMHg) under hypoxic conditions (Jonsson et al., 2016). Although DMHg was not isolated from the MeHg pool during the measurements, nor it is currently included in the model, it might constitute a significant fraction of $MeHg_D$ in the deep water of the Black Sea. The notion of methylation in anoxic sulfidic water (especially in the DAOL) is in contrast with previous studies, which suggested that methylation is hindered at sulfide levels >10 μM (Benoit et al., 2001, 1999a, 1999b; Lamborg et al., 2008). Such an inhibition would be due to a shift of inorganic Hg speciation from a neutral complex (HgS^0) to charged species (e.g. $HgHS_2^-$) that cannot diffuse through microbial cell membranes. However, the hypothesis of sulfide inhibition on Hg methylation has been questioned because:

1) binding and solubility constants used to model the interactions among Hg/sulfide and Hg/DOM are highly uncertain (Drott et al., 2007; Hsu-Kim et al., 2013; Merritt and Amirbahman, 2009; Skyllberg, 2008);

2) Hg speciation in the presence of sulfides is affected by DOM composition that can delay or inhibit the precipitation of $HgS_{(s)}$ and enhance its dissolution. HgS nanoparticles are reactive intermediates of these processes, and Hg methylation occurs at their surfaces (Deonarine and Hsu-Kim, 2009; Gerbig et al.,

2011; Hsu-Kim et al., 2013; Jonsson et al., 2012; Kucharzyk et al., 2015; Ravichandran et al., 1999, 1998; Skyllberg, 2008; Slowey, 2010; Waples et al., 2005; Zhang et al., 2014, 2012);
3) it has been shown that Hg uptake by bacteria can be an energy-dependent transport mediated by carrier proteins, and not only a passive diffusion process (Schaefer et al., 2014, 2011; Schaefer and Morel, 2009).

Beyond methylation of HgS nanoparticles observed in laboratory experiments, there is evidence that adds weight to the argument of methylation under sulfidic conditions. Coquery et al., (2003) observed maximum levels of $MeHg_D$ in anoxic water of a tropical reservoir, and attributed these to *in situ* methylation by sulfate reducing bacteria. Eckley and Hintelmann, (2006) detected methylation only under hypoxic-anoxic conditions in a group of seasonally stratified lakes, with maximum rates just below the oxycline that remained elevated down to the bottom of the lake (HS^- up to 30 μM). Hollweg et al., (2009) detected Hg methylation in the sediments of Chesapeake Bay at sulfides levels as high as 100 – 1000 μM, though rates were maximum where HS^- concentrations were about 1 μM. Merritt and Amirbahman, (2008) reported that in pore-water profiles of the Penobscot River Estuary maximum MeHg were coincident with HS^- ranging from 0.5 to 30 μM. In the sediment of Passamaquoddy Bay, Sunderland et al., (2006b) observed the highest MeHg/Hg ratio in the zone with sulfide levels between 1300 and 6000 μM. Moreover, Hg methylation has been detected in freshwater, marine and salt marsh sediments, as well as in pure cultures of bacteria, at mM levels of sulfides (Drott et al., 2007; King et al., 2000; Langer et al., 2001).

Some authors have pointed out that the decrease of Hg methylation with depth, frequently observed in the sediments, might be attributable to the limitation of available organic substrates (electron donors), rather than to increasing sulfide levels (Drott et al., 2007; Merritt and Amirbahman, 2009). That would also explain why profiles of MeHg in the Black Sea water column differ from profiles commonly observed in pore-water.

The UAOL-DAOL is a net DOC removal zone (Margolin et al., 2016), indicating that a fraction of DOM is bioavailable. Moreover, the SOL-AOL interface is a zone of important microbial biodiversity, where a number of microbial metabolisms coexist (Fuchsman et al., 2011) and chemosynthesis occurs (Yılmaz et al., 2006). Large aggregates of precipitates, organic and inorganic matter that form in the SOL and sink, operate as carriers of bacteria (Fuchsman et al., 2011). Mercury methylation and demethylation have been detected in particles and marine snow aggregates under laboratory conditions (Ortiz et al., 2015). It has been proposed that in the Black Sea the entire S cycling may be occurring within the micro-niches offered by marine snow aggregates (Fuchsman et al., 2011).

4.4.3 Budget of Hg and MeHg

The budget of Hg_T and $MeHg_T$ in the Black Sea presented here is built on a 1D biogeochemical model for Hg cycling in the water column and the sediments. The implementation is based on extensive measurements along 10 stations in the Black Sea water column and sediment, and supported by an off-line coupling with a model for Hg cycling in the atmosphere. Here, we discuss the modeled budget of Hg species and compare it to the budget of Hg_T estimated by Lamborg et al., (2008) based on water column measurements at two sites in the Black Sea.

According to our budget, riverine sources are the most relevant input of Hg_T to the basin, while Hg fluxes at the Bosporus are negligible. By contrast, the major source of MeHg is net methylation in the AOL and a net production of at least 3.3 kmol/y in the AOL is necessary to explain the observed MeHg profile in the Black Sea. We estimated a riverine Hg load of 21 kmol/y, higher than the 8 kmol/y estimated by Lamborg et al., (2008), who concluded that the flux is probably higher. The scarcity of observations from Black Sea tributaries calls for a more thorough investigation. Atmospheric deposition to the Black Sea is estimated to be 5.3 kmol/y (7.5 kmol/y when scaled to the whole surface area). This is close to the 8 kmol/y estimated by Lamborg et al., (2008) and corresponds to a deposition rate of 3.6 $\mu g/m^2y$, which is within the range estimated for the Mediterranean Sea (AMAP/UNEP, 2013; Gencarelli et al., 2015). Evasion of Hg^0 from the water roughly compensate deposition (5 kmol/y, 7.2 for the whole surface area), and is much lower than the 93 kmol/y estimated by Lamborg et al., (2008). The concentrations of Hg^0 measured by Lamborg et al., (2008) in surface water (300 fM) are slightly lower than the modeled 210 fM. It has been shown that estimates of evasion fluxes are affected by the parametrization of gas exchange (that can induce a variation ~30%) and by the concentrations of Hg^0 and wind speed used in computations (that can induce a variation ~300%, see Soerensen et al., 2013 and reference therein). The evasion rate computed by Lamborg et al., (2008) and that computed by our model (respectively 600 $pmol/m^2d$ and 47 $pmol/m^2d$) lie on the upper and lower range of the rates observed in coastal, shelf and ocean stations (Andersson et al., 2007; Gårdfeldt et al., 2003b; Soerensen et al., 2013). Thus, both estimates are unlikely to be representative of average conditions throughout the year. Hg_D from sediment due to pore-water diffusion has a small overall impact on our budget (2.3 kmol/y) and is lower than but consistent with the 4 kmol/y predicted by Lamborg et al., (2008), who included also the contribution of the shelf sediments. Our estimate of inflow (0.9 kmol/y of Hg_T and 0.06 of $MeHg_T$) and outflow (1.4 kmol/y of HgT and 0.09 of $MeHg_T$) at the Mediterranean boundary, based on water column measurements on both sides, implies a small net export of Hg species (0.5

kmol/y of Hg_T). These fluxes are much lower than those estimated by Lamborg et al., (2008) who assumed high concentrations in the Marmara inflow (24 pM).

4.5. Conclusions

This paper has investigated Hg and MeHg dynamics along the redox layers of the Black Sea water column integrating new measurements and numerical modeling. $MeHg_D$ concentrations observed during the 2013 GOETRACES MEDBlack cruise were considerably higher in the AOL than in the rest of water column, and modeling and mass balance computations indicate that Hg methylation in the anoxic water is likely to be the primary MeHg source to the basin. Our outcomes add to an increasing amount of evidence that Hg can be methylated under sulfidic conditions, when the NOM pool of the system is bioavailable to bacteria and it contains functional groups which inhibit the precipitation of HgS. During the timespan of the simulation (1850 – 2050) modeled concentrations of Hg species increase with time in the deepest layers of the Black Sea (AOL), owing to recycling between suboxic and anoxic water that prevent upward diffusion. Overall, concentrations of Hg species in the AOL appear to depend on the balance between: 1) the amount of Hg_T (mostly inorganic) that enters surface layers and is transported to the SOL; 2) the cycling of Hg and MeHg between the SOL and AOL, driven by the redox cycle of Mn; 3) the net production of MeHg in the AOL; 4) the transport toward the sediment of the particulate fraction, which is the only removal pathway from deep waters and concerns only a small fraction of the total pool (modeled Hg_P and $MeHg_P$ are about 3% of Hg_T and $MeHg_T$ in the AOL). The cycling of Hg in the Black Sea promotes accumulation of Hg species in the deepest water rather than in surface or intermediate water, which might provide a good explanation for the lower observed bioaccumulation rates, as compared to those in the Mediterranean Sea (Harmelin-Vivien et al., 2009). However, the thickness of the oxic layer in the Black Sea has shallowed in the past 60 years, which might be a worrisome trend (Capet et al., 2015). Moreover, in other water bodies, the hypoxic-anoxic conditions induced at the bottom of the water column by summer stratification, could promote methylation over areas much larger than previously thought, generating a significant amount of MeHg that would then be advected to the rest of the water column during the subsequent mixing period.

Acknowledgments, Samples, and Data

The original dataset from the 2013 GEOTRACES MEDBlack can be accessed at the BCO-DMO database http://www.bco-dmo.org/resources. We acknowledge the Dutch funding agency (project number: 822.01.015) of the national science foundation NWO for funding of this work as part of GEOTRACES. This work was supported by research grant ERC-2010-StG_20091028 from the

European Research Council to JES. We thank Andrew Margolin for helpful discussion on the cruise dataset and the redox layers of the Black Sea. We thank Léa Cabrol for valuable advices on microbiological aspects. We thank Thomas Pichler for accepting GR as visiting student at the University Bremen.

References

Agirbas, E., A. M. Feyzioglu, and U. Kopuz (2014), Seasonal Changes of Phytoplankton Chlorophyl a, Primary Production and threir Relation in the Continental Shelf Area of the South Eastern Black Sea, *Turkish J. Fish. Aquat. Sci.*, *14*, 713–726, doi:10.4194/1303-2712-v14.

AMAP/UNEP (2013), *Technical Background Report for the Global Mercury Assessment 2013.*, Oslo, Norway / UNEP ChemicalsBranch, Geneva, Switzerland.

Amos, H. M., D. J. Jacob, D. Kocman, H. M. Horowitz, Y. Zhang, S. Dutkiewicz, M. Horvat, E. S. Corbitt, D. P. Krabbenhoft, and E. M. Sunderland (2014), Global biogeochemical implications of mercury discharges from rivers and sediment burial, *Environ. Sci. Technol.*, *48*(16), 9514–9522, doi:10.1021/es502134t.

Amos, H. M. et al. (2015), Observational and modeling constraints on global anthropogenic enrichment of mercury, *Environ. Sci. Technol.*, *49*(7), 4036–4047, doi:10.1021/es5058665.

Andersson, M. E., K. Gårdfeldt, I. Wängberg, F. Sprovieri, N. Pirrone, and O. Lindqvist (2007), Reprint of "Seasonal and daily variation of mercury evasion at coastal and off shore sites from the Mediterranean Sea," *Mar. Chem.*, *107*(1), 104–116, doi:10.1016/j.marchem.2007.06.020.

De Baar, H. J. W. et al. (2008), Titan: A new facility for ultraclean sampling of trace elements and isotopes in the deep oceans in the international Geotraces program, *Mar. Chem.*, doi:10.1016/j.marchem.2007.07.009.

Benoit, J. M., R. P. Mason, and C. C. Gilmour (1999a), Estimation of mercury-sulfide speciation in sediment pore waters using octanol-water partitioning and implications for availability to methylating bacteria, *Environ. Toxicol. Chem.*, *18*(10), 2138–2141, doi:10.1002/etc.5620181004.

Benoit, J. M., C. C. Gilmour, R. P. Mason, and A. Heyes (1999b), Sufide Controls on Bioavailability to Methylating Bacteria in Sediment Pore Waters, *Environ. Sci. Technol.*, *33*(6), 951–957.

Benoit, J. M., C. C. Gilmour, and R. P. Mason (2001), Aspects of bioavailability of mercury for methylation in pure cultures of Desulfobulbus propionicus (1pr3), *Appl. Environ. Microbiol.*, *67*(1), 51–58, doi:10.1128/AEM.67.1.51-58.2001.

Black, F. J., B. A. Poulin, and A. R. Flegal (2012), Factors controlling the abiotic photo-degradation of monomethylmercury in surface waters, *Geochim. Cosmochim. Acta*, *84*, 492–507, doi:10.1016/j.gca.2012.01.019.

Bouchet, S. et al. (2013), MMHg production and export from intertidal sediments to the water column of a tidal lagoon (Arcachon Bay, France), *Biogeochemistry*, *114*(1–3), 341–358, doi:10.1007/s10533-012-9815-z.

Canu, D., and G. Rosati (2017), Long-term scenarios of mercury budgeting and exports for a Mediterranean hot spot (Marano-Grado Lagoon, Adriatic Sea)., *Estuar. Coast. Shelf Sci.*, 1–11, doi:10.1016/j.ecss.2016.12.005.

Capet, A., E. V. Stanev, J.-M. Beckers, J. W. Murray, and M. Grégoire (2015), Recent decline of the Black Sea oxygen inventory, *Biogeosciences Discuss.*, *12*(19), 16233–16253, doi:10.5194/bgd-12-16233-2015.

Clarkson, T. W., and L. Magos (2006), The toxicology of mercury and its chemical compounds., *Crit. Rev. Toxicol.*, *36*(8), 609–662, doi:10.1080/10408440600845619.

Coquery, M., D. Cossa, T. Peretyazhko, S. Azemard, and L. Charlet (2003), Methylmercury formation in the anoxic waters of the Petit-Saut reservoir (French Guiana) and its spreading in the adjacent Sinnamary river, *Jounal Phys. IV Fr.*, *107*(1999), 327–331, doi:10.1051/jp4:20030308.

Cossa, D., and M. Coquery (2005), The Mediterranean Mercury Anomaly, a Geochemical or a Biologocal Issue, in *The Mediterranean Sea*, edited by A. Saliot, pp. 177–208, Springer Berlin Heidelberg, Berlin, Heidelberg.

Cossa, D., B. Averty, and N. Pirrone (2009), The origin of methylmercury in open Mediterranean waters, *Limnol. Oceanogr.*, *54*(3), 837–844, doi:10.4319/lo.2009.54.3.0837.

Cossa, D., M. Harmelin-Vivien, C. Mellon-Duval, V. Loizeau, B. Averty, S. Crochet, L. Chou, and J.-F. Cadiou (2012), Influences of bioavailability, trophic position, and growth on methylmercury in hakes (Merluccius merluccius) from Northwestern Mediterranean and Northeastern Atlantic., *Environ. Sci. Technol.*, *46*(9), 4885–93, doi:10.1021/es204269w.

Cossa, D., C. Garnier, R. Buscail, N. Elbaz-Poulichet, Francoise Mikac, E. Patel-Sorrentino, Nathalie Tessier, S. Rigaud, V. Lenoble, and C. Gobeil (2014), A Michaelis–Menten type equation for describing methylmercury dependence on inorganic mercury in aquatic sediments, *Biogeochemistry*, *119*(1), 35–43.

Dellwig, O., T. Leipe, C. März, M. Glockzin, F. Pollehne, B. Schnetger, E. V. Yakushev, M. E. Böttcher, and H.-J. Brumsack (2010), A new particulate Mn–Fe–P-shuttle at the redoxcline of anoxic basins, *Geochim. Cosmochim. Acta*, *74*(24), 7100–7115, doi:10.1016/j.gca.2010.09.017.

Deonarine, A., and H. Hsu-Kim (2009), Precipitation of Mercuric Sulfide Nanoparticles in NOM-Containing Water: Implications for the Natural Environment, *Environ. Sci. Technol.*, *43*(7), 2368–2373, doi:10.1021/es803130h.

Drott, A., L. Lambertsson, E. Björn, and U. Skyllberg (2007), Imortance of Dissolved Neutral Mercury Sulfides for Methyl Mercury Producton in Contaminated Sediments, *Environ. Sci. Technol.*, *41*(7), 2270–2276.

Ducklow, H. W., D. a. Hansell, and J. a. Morgan (2007), Dissolved organic carbon and nitrogen in the Western Black Sea, *Mar. Chem.*, *105*(1–2), 140–150, doi:10.1016/j.marchem.2007.01.015.

Eckley, C. S., and H. Hintelmann (2006), Determination of mercury methylation potentials in the water column of lakes across Canada, *Sci. Total Environ.*, *368*(1), 111–125, doi:10.1016/j.scitotenv.2005.09.042.

Fitzgerald, W. F., C. H. Lamborg, and C. R. Hammerschmidt (2007), Marine Biogeochemical Cycling of Mercury Marine Biogeochemical Cycling of Mercury, *Public Health*, *107*(February), 641–662, doi:10.1021/cr050353m.

Froelich, P. N., G. P. Klinkhammer, M. L. Bender, N. A. Luedtke, G. R. Heath, D. Cullen, P. Dauphin, D. Hammond, B. Hartman, and V. Maynard (1979), Early oxidation of organic matter in pelagic sediments of the eastern equatorial Atlantic: suboxic diagenesis, *Geochim. Cosmochim. Acta*, *43*(7), 1075–1090, doi:10.1016/0016-7037(79)90095-4.

Fuchsman, C. a., J. B. Kirkpatrick, W. J. Brazelton, J. W. Murray, and J. T. Staley (2011), Metabolic strategies of free-living and aggregate-associated bacterial communities inferred from biologic and chemical profiles in the Black Sea suboxic zone, *FEMS Microbiol. Ecol.*, *78*(3), 586–603, doi:10.1111/j.1574-6941.2011.01189.x.

Gårdfeldt, K. et al. (2003), Evasion of mercury from coastal and open waters of the Atlantic Ocean and the Mediterranean Sea, *Atmos. Environ.*, *37*, 73–84, doi:10.1016/S1352-2310(03)00238-3.

Gencarelli, C. N., F. De Simone, I. M. Hedgecock, F. Sprovieri, and N. Pirrone (2014), Development and application of a regional-scale atmospheric mercury model based on WRF/Chem: A Mediterranean area investigation, *Environ. Sci. Pollut. Res.*, *21*(6), 4095–4109, doi:10.1007/s11356-013-2162-3.

Gencarelli, C. N., F. De Simone, I. M. Hedgecock, F. Sprovieri, X. Yang, and N. Pirrone (2015), European and Mediterranean mercury modelling: Local and long-range contributions to the deposition flux, *Atmos. Environ.*, *117*(August), 162–168, doi:10.1016/j.atmosenv.2015.07.015.

Gencarelli, C. N., J. Bieser, F. Carbone, F. De Simone, I. M. Hedgecock, V. Matthias, O. Travnikov, X. Yang, and N. Pirrone (2017), Sensitivity model study of regional mercury dispersion in the atmosphere, *Atmos. Chem. Phys. Discuss.*, *17*, 627–643, doi:10.5194/acp-2016-663.

Gerbig, C. A., C. S. Kim, J. P. Stegemeier, J. N. Ryan, and G. R. Aiken (2011), Formation of nanocolloidal metacinnabar in mercury-DOM-sulfide systems, *Environ. Sci. Technol.*, *45*(21), 9180–9187, doi:10.1021/es201837h.

Gerringa, L. J. A., M. J. A. Rijkenberg, J. Bown, A. R. Margolin, P. Laan, and H. J. W. de Baar (2016), Fe-Binding Dissolved Organic Ligands in the Oxic and Suboxic Waters of the Black Sea , *Front. Mar. Sci.* , *3*, 84.

Gilmour, C. C., M. Podar, A. L. Bullock, A. M. Graham, S. D. Brown, A. C. Somenahally, A. Johs, R. A. Hurt, K. L. Bailey, and D. A. Elias (2013), Mercury Methylation by Novel Microorganisms from New Environments, *Environ. Sci. Technol.*, *47*(20), 11810–11820, doi:10.1021/es403075t.

Graham, A. M., G. R. Aiken, and C. C. Gilmour (2012), Dissolved organic matter enhances microbial mercury methylation under sulfidic conditions, *Environ. Sci. Technol.*, *46*(5), 2715–2723, doi:10.1021/es203658f.

Gregg, M. C., and E. Yakushev (2005), Surface ventilation of the Black Sea's cold intermediate layer in the middle of the western gyre, *Geophys. Res. Lett.*, *32*(3), 1–4, doi:10.1029/2004GL021580.

Grégoire, M., and K. Soetaert (2010), Carbon, nitrogen, oxygen and sulfide budgets in the Black Sea: A biogeochemical model of the whole water column coupling the oxic and anoxic parts, *Ecol. Modell.*, *221*(19), 2287–2301, doi:http://dx.doi.org/10.1016/j.ecolmodel.2010.06.007.

Grell, G. A., S. E. Peckham, R. Schmitz, S. A. McKeen, G. Frost, W. C. Skamarock, and B. Eder (2005), Fully coupled "online" chemistry within the WRF model, *Atmos. Environ.*, *39*(37), 6957–6975, doi:10.1016/j.atmosenv.2005.04.027.

Hammerschmidt, C. R., and W. F. Fitzgerald (2006), Bioaccumulation and Trophic Transfer of Methylmercury in Long Island Sound, *Arch. Environ. Contam. Toxicol.*, *51*(3), 416–424, doi:10.1007/s00244-005-0265-7.

Hammerschmidt, C. R., W. F. Fitzgerald, C. H. Lamborg, P. H. Balcom, and P. T. Visscher (2004), Biogeochemistry of methylmercury in sediments of Long Island Sound, *Mar. Chem.*, *90*(1), 31–52, doi:10.1016/j.marchem.2004.02.024.

Han, S., A. Obraztsova, P. Pretto, K.-Y. Choe, J. Gieskes, D. D. Deheyn, and B. M. Tebot (2007a), Biogeochemical factors affecting mercury methylation in sediments of the Venice Lagoon, Italy., *Environ. Toxicol. Chem.*, *26*(4), 655–63, doi:10.1897/06-392R.1.

Han, S., R. D. Lehman, K.-Y. Choe, and G. a. Gill (2007b), Chemical and physical speciation of mercury in Offatts Bayou: A seasonally anoxic bayou in Galveston Bay, *Limnol. Oceanogr.*, *52*(4), 1380–1392, doi:10.4319/lo.2007.52.4.1380.

Harmelin-Vivien, M., D. Cossa, S. Crochet, D. Bănaru, Y. Letourneur, and C. Mellon-Duval (2009), Difference of mercury bioaccumulation in red mullets from the north-western Mediterranean and Black seas, *Mar. Pollut. Bull.*, *58*(5), 679–685, doi:10.1016/j.marpolbul.2009.01.004.

Heimbürger, L.-E., D. Cossa, J.-C. Marty, C. Migon, B. Averty, A. Dufour, and J. Ras (2010), Methyl mercury distributions in relation to the presence of nano- and picophytoplankton in an oceanic water column (Ligurian Sea, North-western Mediterranean), *Geochim. Cosmochim. Acta*, *74*(19), 5549–5559, doi:10.1016/j.gca.2010.06.036.

Heimbürger, L.-E., J. E. Sonke, D. Cossa, D. Point, C. Lagane, L. Laffont, B. T. Galfond, M. Nicolaus, B. Rabe, and M. R. van der Loeff (2015), Shallow methylmercury production in the marginal sea ice zone of the central Arctic Ocean, *Sci. Rep.*, *5*, 10318.

Hellal, J. et al. (2015), Mercury mobilization and speciation linked to bacterial iron oxide and sulfate reduction: A column study to mimic reactive transfer in an anoxic aquifer, *J. Contam.*

Hydrol., *180*, 56–68, doi:10.1016/j.jconhyd.2015.08.001.

Heyes, A., R. P. Mason, E. H. Kim, and E. Sunderland (2006), Mercury methylation in estuaries: Insights from using measuring rates using stable mercury isotopes, *Mar. Chem.*, *102*(1–2), 134–147, doi:10.1016/j.marchem.2005.09.018.

Hollweg, T. A., C. C. Gilmour, and R. P. Mason (2009), Methylmercury production in sediments of Chesapeake Bay and the mid-Atlantic continental margin, *Mar. Chem.*, *114*(3–4), 86–101, doi:10.1016/j.marchem.2009.04.004.

Hollweg, T. A., C. C. Gilmour, and R. P. Mason (2010), Mercury and methylmercury cycling in sediments of the mid-Atlantic continental shelf and slope, *Limnol. Oceanogr.*, *55*(6), 2703–2722, doi:10.4319/lo.2010.55.6.2703.

Horowitz, H. M., D. J. Jacob, H. M. Amos, D. G. Streets, and E. M. Sunderland (2014), Historical Mercury Releases from Commercial Products : Global Environmental Implications, *Environ. Sci. Technol.*, *48*, 10242–10250, doi:dx.doi.org/10.1021/es501337j.

Hsu-Kim, H., K. H. Kucharzyk, T. Zhang, and M. A. Deshusses (2013), Mechanisms regulating mercury bioavailability for methylating microorganisms in the aquatic environment: A critical review, *Environ. Sci. Technol.*, *47*(6), 2441–2456, doi:10.1021/es304370g.

Jonsson, S., U. Skyllberg, M. B. Nilsson, P. Westlund, A. Shchukarev, E. Lundberg, and E. Björn (2012), Mercury Methylation Rates for Geochemically Relevant HgII Species in Sediments, *Environ. Sci. Technol.*, *46*, 11653−11659.

Jonsson, S., N. M. Mazrui, and R. P. Mason (2016), Dimethylmercury Formation Mediated by Inorganic and Organic Reduced Sulfur Surfaces, *Sci. Rep.*, *6*(August), 27958, doi:10.1038/srep27958.

Jung, G., I. M. Hedgecock, and N. Pirrone (2009), Model Development ECHMERIT V1 . 0 – a new global fully coupled mercury-chemistry and transport model, *Geosci. Model Dev.*, *2*, 175–195.

Kerin, E. J., C. C. Gilmour, E. Roden, M. T. Suzuki, J. D. Coates, and R. P. Mason (2006), Mercury methylation by dissimilatory iron-reducing bacteria., *Appl. Environ. Microbiol.*, *72*(12), 7919–21, doi:10.1128/AEM.01602-06.

King, J. K., J. E. Kostka, M. E. Frischer, and M. Saunders (2000), Sulfate-Reducing Bacteria Methylate Mercury at Variable Rates in Pure Culture and in Marine Sediments, *Appl. Environ. Microbiol.*, *66*(6), 2430, doi:10.1128/AEM.66.6.2430-2437.2000.Updated.

Konovalov, S., S. Tuğrul, Ö. Baştürk, and İ. Salihoğlu (1997), Spatial Isopycnal Analysis of the Main Pycnocline Chemistry of the Black Sea: seasonal and interannual variations, in *Sensitivity to Change: Black Sea, Baltic Sea and North Sea*, edited by E. Özsoy and A. Mikaelyan, pp. 197–210, Springer Netherlands, Dordrecht.

Konovalov, S., A. Samodurov, T. Oguz, and L. Ivanov (2004), Parameterization of iron and manganese cycling in the Black Sea suboxic and anoxic environment, *Deep Sea Res. Part I*

Oceanogr. Res. Pap., *51*(12), 2027–2045, doi:http://dx.doi.org/10.1016/j.dsr.2004.08.005.

Konovalov, S. K., and J. W. Murray (2001), Variations in the chemistry of the Black Sea on a time scale of decades (1960-1995), *J. Mar. Syst.*, *31*(1–3), 217–243, doi:10.1016/S0924-7963(01)00054-9.

Kucharzyk, K. H., M. A. Deshusses, K. A. Porter, and H. Hsu-Kim (2015), Relative contributions of mercury bioavailability and microbial growth rate on net methylmercury production by anaerobic mixed cultures, *Environ. Sci. Process. Impacts*, *17*(9), 1568–1577, doi:10.1039/C5EM00174A.

Lamborg, C. H., O. Yiğiterhan, W. F. Fitzgerald, P. H. Balcom, C. R. Hammerschmidt, and J. Murray (2008), Vertical distribution of mercury species at two sites in the Western Black Sea, *Mar. Chem.*, *111*, 77–89, doi:10.1016/j.marchem.2007.01.011.

Lamborg, C. H., C. R. Hammerschmidt, and K. L. Bowman (2016), An examination of the role of particles in oceanic mercury cycling, *Philos. Trans. R. Soc. A Math. Phys. Eng. Sci.*, *374*(2081), 20150297, doi:10.1098/rsta.2015.0297.

Langer, C. S., W. F. Fitzgerald, P. T. Visscher, and G. M. Vandal (2001), Biogeochemical cycling of methylmercury at, *Barn Isl. Salt Marsh, Stonington, CT, USA. Wetl. Ecol. Manag.*, *9295e310*(Ii), 295–310.

Lehnherr, I., V. L. St. Louis, H. Hintelmann, and J. L. Kirk (2011), Methylation of inorganic mercury in polar marine waters, *Nat. Geosci.*, *4*(April), 298–302, doi:10.1038/ngeo1134.

Lemon, J. (2006), Plotrix: a package in the red light district of R, *R-News*, *6*(4), 8–12.

Liu, B., L. a. Schaider, R. P. Mason, J. P. Shine, N. N. Rabalais, and D. B. Senn (2015), Controls on methylmercury accumulation in northern Gulf of Mexico sediments, *Estuar. Coast. Shelf Sci.*, *159*, 50–59, doi:10.1016/j.ecss.2015.03.030.

Margolin, A. R., L. J. A. Gerringa, D. A. Hansell, and M. J. A. Rijkenberg (2016), Net removal of dissolved organic carbon in the anoxic waters of the Black Sea, *Mar. Chem.*, *183*, 13–24, doi:10.1016/j.marchem.2016.05.003.

Mason, R. P., and W. F. Fitzgerald (1990), Alkylmercury species in the equatorial Pacific, *Nature*, *347*(6292), 457–459.

Mason, R. P., W. F. Fitzgerald, J. Hurley, a. K. Hanson, P. L. Donaghay, and J. M. Sieburth (1993), Mercury biogeochemical cycling in a stratified estuary, *Limnol. Oceanogr.*, *38*(6), 1227–1241, doi:10.4319/lo.1993.38.6.1227.

Melaku Canu, D., G. Rosati, C. Solidoro, L.-E. Heimbürger, and A. Acquavita (2015), A comprehensive assessment of the mercury budget in the Marano–Grado Lagoon (Adriatic Sea) using a combined observational modeling approach, *Mar. Chem.*, *177*, 742–752, doi:10.1016/j.marchem.2015.10.013.

Merritt, K. A., and A. Amirbahman (2008), Methylmercury cycling in estuarine sediment pore waters (Penobscot River estuary, Maine, USA), *Limnol. Oceanogr.*, *53*(3), 1064–1075, doi:10.4319/lo.2008.53.3.1064.

Merritt, K. A., and A. Amirbahman (2009), Mercury methylation dynamics in estuarine and coastal marine environments - A critical review, *Earth-Science Rev.*, *96*(1–2), 54–66, doi:10.1016/j.earscirev.2009.06.002.

Monperrus, M., E. Tessier, D. Amouroux, A. Leynaert, P. Huonnic, and O. F. X. Donard (2007a), Mercury methylation, demethylation and reduction rates in coastal and marine surface waters of the Mediterranean Sea, *Mar. Chem.*, *107*(1), 49–63, doi:10.1016/j.marchem.2007.01.018.

Monperrus, M. et al. (2007b), The biogeochemistry of mercury at the sediment-water interface in the Thau Lagoon. 2. Evaluation of mercury methylation potential in both surface sediment and the water column, *Estuar. Coast. Shelf Sci.*, *72*(3), 485–496, doi:10.1016/j.ecss.2006.11.014.

Moreau, J. W., C. M. Gionfriddo, D. P. Krabbenhoft, J. M. Ogorek, J. F. DeWild, G. R. Aiken, and E. E. Roden (2015), The Effect of Natural Organic Matter on Mercury Methylation by Desulfobulbus propionicus 1pr3, *Front. Microbiol.*, *6*, 1389, doi:10.3389/fmicb.2015.01389.

Morel, F. M. M., A. M. L. Kraepiel, and M. Amyot (1998), The chemical cycle and bioaccumulation of mercury, *Annu. Rev. Ecol. Syst.*, *29*, 543–566, doi:10.1146/annurev.ecolsys.29.1.543.

Morse, J. W., and G. W. Luther (1999), Chemical influences on trace metal-sulfide interactions in anoxic sediments, *Geochim. Cosmochim. Acta*, *63*(19), 3373–3378, doi:10.1016/S0016-7037(99)00258-6.

Muresan, B., D. Cossa, J. D., F. Prévot, and S. Kerbellec (2007), The biogeochemistry of mercury at the sediment-water interface in the Thau lagoon. 1. Partition and speciation, *Estuar. Coast. Shelf Sci.*, *72*, 472–484, doi:10.1016/j.ecss.2006.11.015.

Murray, J. W., K. Stewart, S. Kassakian, M. Krynytzky, and D. Dijulio (2007), Oxic, suboxic, and anoxic conditions in the Black Sea, in *The Black Sea Flood Question: Changes in Coastline, Climate, and Human Settlement*, pp. 1–21.

Neretin, L. N., C. Pohl, G. Jost, T. Leipe, and F. Pollehne (2003), Manganese cycling in the Gotland Deep, Baltic Sea, *Mar. Chem.*, *82*(3–4), 125–143, doi:10.1016/S0304-4203(03)00048-3.

Oguz, T., H. W. Ducklow, and P. Malanotte-Rizzoli (2000), Modeling distinct vertical biogeochemical structure of the black sea: Dynamical coupling of the oxic, suboxic, and anoxic layers, *Global Biogeochem. Cycles*, *14*(4), 1331–1352, doi:10.1029/1999GB001253.

Oken, E., A. L. Choi, M. R. Karagas, K. Mariën, C. M. Rheinberger, R. Schoeny, E. Sunderland, and S. Korrick (2012), Which fish should i eat? Perspectives influencing fish consumption choices, *Environ. Health Perspect.*, *120*(6), 790–798, doi:10.1289/ehp.1104500.

Ortiz, V. L., R. P. Mason, and J. Evan Ward (2015), An examination of the factors influencing

mercury and methylmercury particulate distributions, methylation and demethylation rates in laboratory-generated marine snow, *Mar. Chem.*, *177*, 753–762, doi:10.1016/j.marchem.2015.07.006.

Ozsoy, E., and B. Ünlüata (1997), Oceanography of the Black Sea: a review of some recent results, *Earth-Science Rev.*, *42*, 231–272.

Özsoy, E., and Ü. Ünlüata (1997), Oceanography of the Black Sea: A review of some recent results, *Earth-Science Rev.*, *42*(4), 231–272, doi:http://dx.doi.org/10.1016/S0012-8252(97)81859-4.

Pakhomova, S., and E. V Yakushev (2013), Manganese and Iron at the Redox Interfaces in the Black Sea, the Baltic Sea, and the Oslo Fjord, in *Chemical Structure of Pelagic Redox Interfaces SE - 98*, vol. 22, edited by E. V Yakushev, pp. 67–93, Springer Berlin Heidelberg.

Panin, N., and D. Jipa (2002), Danube River Sediment Input and its Interaction with the North-western Black Sea, *Estuar. Coast. Shelf Sci.*, *54*(3), 551–562, doi:10.1006/ecss.2000.0664.

R Core Team (2013), R: A language and environment for statistical computing,

Ravichandran, M., G. R. Aiken, M. M. Reddy, and J. N. Ryan (1998), Enhanced dissolution of cinnabar (mercuric sulfide) by dissolved organic matter isolated from the Florida Everglades, *Environ. Sci. Technol.*, *32*(21), 3305–3311, doi:10.1021/es9804058.

Ravichandran, M., G. R. Aiken, J. N. Ryan, and M. M. Reddy (1999), Inhibition of precipitation and aggregation of metacinnabar (HgS) by humic substances isolated from the Florida Everglades, *Abstr. Pap. Am. Chem. Soc.*, *217*(9), 105–ENVR, doi:10.1021/es9811187.

Rodríguez Martín-Doimeadios, R. C., E. Tessier, D. Amouroux, R. Guyoneaud, R. Duran, P. Caumette, and O. F. X. Donard (2004), Mercury methylation/demethylation and volatilization pathways in estuarine sediment slurries using species-specific enriched stable isotopes, *Mar. Chem.*, *90*(1–4 SPEC. ISS.), 107–123, doi:10.1016/j.marchem.2004.02.022.

Schaefer, J. K., and F. M. M. Morel (2009), High methylation rates of mercury bound to cysteine by Geobacter sulfurreducens, *Nat. Geosci*, *2*(2), 123–126.

Schaefer, J. K., S. S. Rocks, W. Zheng, L. Liang, B. Gu, F. M. M. M. Morel, W. Zhang, L. Liang, B. Gu, and F. M. M. M. Morel (2011), Active transport, substrate specificity, and methylation of Hg(II) in anaerobic bacteria, *Proc. Natl. Acad. Sci. U. S. A.*, *108*(21), 8714–8719, doi:10.1073/pnas.1105781108.

Schaefer, J. K., A. Szczuka, and F. M. M. Morel (2014), Effect of divalent metals on Hg(II) uptake and methylation by bacteria, *Environ. Sci. Technol.*, *48*(5), 3007–3013, doi:10.1021/es405215v.

Schartup, A. T., R. P. Mason, P. H. Balcom, T. a. Hollweg, and C. Y. Chen (2013), Methylmercury production in estuarine sediments: Role of organic matter, *Environ. Sci. Technol.*, *47*, 695–700, doi:10.1021/es302566w.

Schartup, A. T., U. Ndu, P. H. Balcom, R. P. Mason, and E. M. Sunderland (2015a), Contrasting

effects of marine and terrestrially derived dissolved organic matter on mercury speciation and bioavailability in seawater, *Environ. Sci. Technol.*, *49*(10), 5965–5972, doi:10.1021/es506274x.

Schartup, A. T., P. H. Balcom, A. L. Soerensen, K. J. Gosnell, R. S. D. Calder, R. P. Mason, and E. M. Sunderland (2015b), Freshwater discharges drive high levels of methylmercury in Arctic marine biota, *Proc. Natl. Acad. Sci.*, *112*(38), 11789–11794, doi:10.1073/pnas.1505541112.

Schijf, J., H. J. W. de Baar, J. R. Wijbrans, and W. M. Landing (1991), Dissolved rare earth elements in the Black Sea, *Deep Sea Res. Part A. Oceanogr. Res. Pap.*, *38*, S805–S823, doi:10.1016/S0198-0149(10)80010-X.

Shaffer, G. (1986), Phosphate pumps and shuttles in the Black Sea, *Nature*, *321*(6069), 515–517.

Sharif, A., M. Monperrus, E. Tessier, S. Bouchet, H. Pinaly, P. Rodriguez-Gonzalez, P. Maron, and D. Amouroux (2014), Fate of mercury species in the coastal plume of the Adour River estuary (Bay of Biscay, SW France), *Sci. Total Environ.*, *496*, 701–713, doi:10.1016/j.scitotenv.2014.06.116.

Si, Y., Y. Zou, X. Liu, X. Si, and J. Mao (2015), Mercury methylation coupled to iron reduction by dissimilatory iron-reducing bacteria, *Chemosphere*, *122*, 206–212, doi:10.1016/j.chemosphere.2014.11.054.

De Simone, F., C. N. Gencarelli, I. M. Hedgecock, and N. Pirrone (2014), Global atmospheric cycle of mercury: a model study on the impact of oxidation mechanisms, *Environ. Sci. Pollut. Res.*, *21*(6), 4110–4123, doi:10.1007/s11356-013-2451-x.

De Simone, F., C. N. Gencarelli, I. M. Hedgecock, and N. Pirrone (2016), A Modeling Comparison of Mercury Deposition from Current Anthropogenic Mercury Emission Inventories, *Environ. Sci. Technol.*, *50*(10), 5154–5162, doi:10.1021/acs.est.6b00691.

Skyllberg, U. (2008), Competition among thiols and inorganic sulfides and polysulfides for Hg and MeHg in wetland soils and sediments under suboxic conditions: Illumination of controversies and implications for MeHg net production, *J. Geophys. Res.*, *113*, 1–14, doi:10.1029/2008JG000745.

Slowey, A. J. (2010), Rate of formation and dissolution of mercury sulfide nanoparticles: The dual role of natural organic matter, *Geochim. Cosmochim. Acta*, *74*(16), 4693–4708, doi:http://dx.doi.org/10.1016/j.gca.2010.05.012.

Soerensen, A. L., R. P. Mason, P. H. Balcom, and E. M. Sunderland (2013), Drivers of Surface Ocean Mercury Concentrations and Air–Sea Exchange in the West Atlantic Ocean, *Environ. Sci. Technol.*, *47*(14), 7757–7765, doi:10.1021/es401354q.

Soerensen, A. L., A. T. Schartup, E. Gustafsson, B. G. Gustafsson, E. Undeman, and E. Björn (2016), Eutrophication Increases Phytoplankton Methylmercury Concentrations in a Coastal Sea—A Baltic Sea Case Study, *Environ. Sci. Technol.*, (October), acs.est.6b02717, doi:10.1021/acs.est.6b02717.

Sunderland, E. M., F. A. P. C. Gobas, B. A. Branfireun, and A. Heyes (2006), Environmental controls on the speciation and distribution of mercury in coastal sediments, *Mar. Chem.*, *102*(1–2),

111–123, doi:10.1016/j.marchem.2005.09.019.

Sunderland, E. M., D. P. Krabbenhoft, J. W. Moreau, S. A. Strode, and W. M. Landing (2009), Mercury sources, distribution, and bioavailability in the North Pacific Ocean: Insights from data and models, *Global Biogeochem. Cycles*, *23*(2), 1–14, doi:10.1029/2008GB003425.

Talley, L. D., G. L. Pickard, W. J. Emery, and J. H. Swift (2011), Physical Properties of Seawater, in *Descriptive Physical Oceanography*, pp. 29–65, Elsevier.

Taylor, K. E. (2001), Summarizing multiple aspects of model performance in a single diagram, *J. Geophys. Res.*, *106*(D7), 7183–7192, doi:10.1029/2000JD900719.

Tuğrul, S., J. W. Murray, G. E. Friederich, and I. Salihoğlu (2014), Spatial and temporal variability in the chemical properties of the oxic and suboxic layers of the black sea, *J. Mar. Syst.*, *135*, 29–43, doi:10.1016/j.jmarsys.2013.09.008.

Villemur, R., M. Lanthier, R. Beaudet, and F. Lépine (2006), The Desulfitobacterium genus, *FEMS Microbiol. Rev.*, *30*(5), 706–733, doi:10.1111/j.1574-6976.2006.00029.x.

Walsh, J. P., and C. A. Nittrouer (2009), Understanding fine-grained river-sediment dispersal on continental margins, *Mar. Geol.*, *263*(1–4), 34–45, doi:10.1016/j.margeo.2009.03.016.

Waples, J. S., K. L. Nagy, G. R. Aiken, and J. N. Ryan (2005), Dissolution of cinnabar (HgS) in the presence of natural organic matter, *Geochim. Cosmochim. Acta*, *69*(6), 1575–1588, doi:10.1016/j.gca.2004.09.029.

Whalin, L., E.-H. Kim, and R. Mason (2007), Factors influencing the oxidation, reduction, methylation and demethylation of mercury species in coastal waters, *Mar. Chem.*, *107*(3), 278–294, doi:10.1016/j.marchem.2007.04.002.

Woitke, P., J. Wellmitz, D. Helm, P. Kube, P. Lepom, and P. Litheraty (2003), Analysis and assessment of heavy metal pollution in suspended solids and sediments of the river Danube., *Chemosphere*, *51*(8), 633–42, doi:10.1016/S0045-6535(03)00217-0.

Wool, T. A., R. B. Ambrose, J. L. Martin, and E. A. Comer (2001), Water Quality Analysis Simulation Program (WASP) Version 6.0: User's Manual.,

Yakushev, E. V, and A. Newton (2013), Redox Interfaces in Marine Waters, in *Chemical Structure of Pelagic Redox Interfaces: Observation and Modeling*, edited by V. E. Yakushev, pp. 1–12, Springer Berlin Heidelberg, Berlin, Heidelberg.

Yakushev, E. V, F. Pollehne, G. Jost, I. Kuznetsov, B. Schneider, and L. Umlauf (2007), Analysis of the water column oxic/anoxic interface in the Black and Baltic seas with a numerical model, *9th Int. Estuar. Biogeochem. Symp. Estuaries Enclosed Seas under Chang. Environ. Cond.*, *107*(3), 388–410, doi:http://dx.doi.org/10.1016/j.marchem.2007.06.003.

Yılmaz, A., Y. Çoban-Yıldız, F. Telli-Karakoç, and A. Bologa (2006), Surface and mid-water sources of organic carbon by photoautotrophic and chemoautotrophic production in the Black Sea,

Deep Sea Res. Part II Top. Stud. Oceanogr., *53*(17–19), 1988–2004, doi:http://dx.doi.org/10.1016/j.dsr2.2006.03.015.

Yücel, M., W. S. Moore, I. B. Butler, A. Boyce, and G. W. Luther (2012), Recent sedimentation in the Black Sea: New insights from radionuclide distributions and sulfur isotopes, *Deep Sea Res. Part I Oceanogr. Res. Pap.*, *66*, 103–113, doi:10.1016/j.dsr.2012.04.007.

Zhang, T., B. Kim, C. Levard, B. C. Reinsch, G. V. Lowry, M. A. Deshusses, and H. Hsu-Kim (2012), Methylation of mercury by bacteria exposed to dissolved, nanoparticulate, and microparticulate mercuric sulfides, *Environ. Sci. Technol.*, *46*(13), 6950–6958, doi:10.1021/es203181m.

Zhang, T., K. H. Kucharzyk, B. Kim, M. A. Deshusses, and H. Hsu-Kim (2014), Net Methylation of Mercury in Estuarine Sediment Microcosms Amended with Dissolved, Nanoparticulate, and Microparticulate Mercuric Sulfides, *Environ. Sci. Technol.*, *48*(16), 9133–9141, doi:10.1021/es500336j.

Zhang, Y., D. J. Jacob, S. Dutkiewicz, H. M. Amos, M. S. Long, and E. M. Sunderland (2015), Biogeochemical drivers of the fate of riverine mercury discharged to the global and Arctic oceans, *Global Biogeochem. Cycles*, *29*, 854–864, doi:10.1002/2015GB005124.

Chapter 5: An analysis of MeHg biomagnification in the food web of Augusta Harbor

5.1. Introduction

The Augusta Harbor (Figure 1) is located on the eastern Sicilian coast (Italy) and occupies a surface area of about 23.5 km^2. During the 1960s, the area underwent a rapid industrialization and artificial dams were built to separate part of the Augusta Bay from the Ionian Sea. The activities of several chemical and petrochemical plants as well as oil refineries have caused widespread pollution of the harbor. Among these, a chlor-alkali plant operated from 1958 to 2005 with emissions estimated to be ~260 kg/y of Hg in the decade from '60s to '70s and ~765 kg in the year 2001 (Salvagio Manta et al., 2016; Sprovieri et al., 2011 and reference therein). As a consequence, worrisome levels of Hg have been detected in the sediment, pore-water, water and biota, especially in the southernmost part, and fishing ban has been established in the whole area within the harbor (Bagnato et al., 2013; Bonsignore et al., 2013; Salvagio Manta et al., 2016; Sprovieri et al., 2011). These recent studies have looked into the distribution and transport of total Hg (Hg_T) in the environmental compartments of the bay, providing a thorough dataset of the overall Hg_T dynamics that includes bioaccumulation and exchanges at both the interfaces between sediment-water and water-atmosphere.

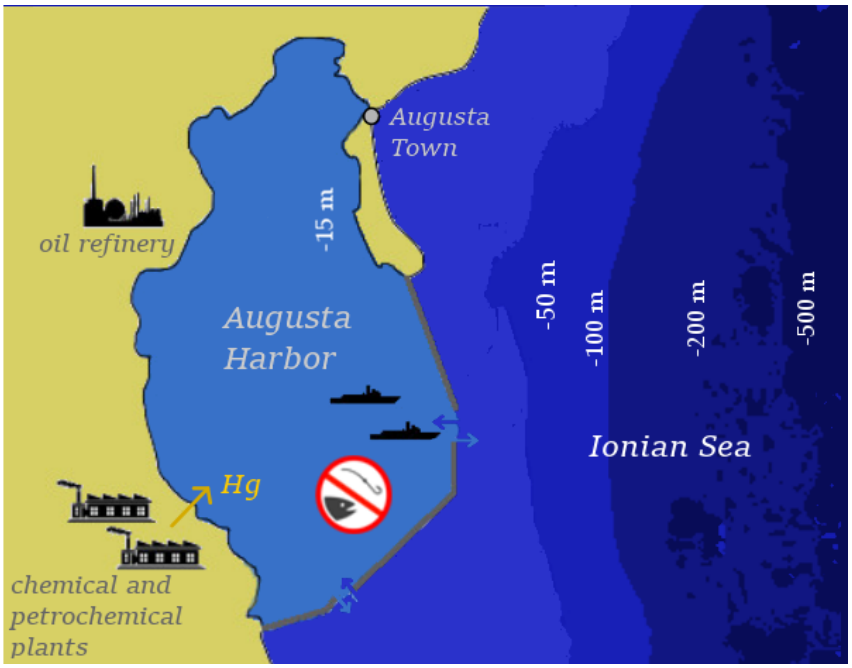

Figure 1. The Augusta Harbor (Sicily, Italy) and major nearby industrial activities. Close to the eastern inlet of harbor is shown the slope of the Ionian Sea with increasing depths.

MeHg levels and dynamics in the Augusta Harbor were not assessed so far, and here we developed a 1D model of Hg cycling to provide an initial estimate of MeHg concentrations in water and sediment. We used scenario analysis to provide a range of Hg and MeHg concentrations in water, which were used along with measured Hg_T concentrations in fish muscles (Bonsignore et al., 2013) to compute bioaccumulation factors (BAF) and investigate the biomagnification process in the ecosystem of the Augusta Harbor.

Bioaccumulation factors (BAF) are useful tools in evaluating the bioaccumulation and biomagnification of Hg and MeHg within and across ecosystems. The BAF is defined as the ratio between Hg in biota (wet weight, w.w.) and dissolved Hg in water and, depending on available data, it can be computed both on Hg basis $\left(\mathrm{BAF}_{Hg} = \frac{[Hg_T]_{biota\ w.w.}}{[Hg_D]_{water}}, L/kg\right)$ or on MeHg basis $\left(\mathrm{BAF}_{MeHg} = \frac{[MeHg_T]_{biota\ w.w.}}{[MeHg_D]_{water}}, L/kg\right)$.

The information synthetized by the BAF make it easier to perform inter-comparison exercises. Indeed, comparing BAF among species within an ecosystem allow the assessment of biomagnification; whilst the comparison of BAF among organisms of the same species/trophic levels belonging to different ecosystems offers an idea of the differential bioavailability and transfer efficiency of MeHg along trophic webs.

The computation of BAF has been proposed as a tool for setting water quality criteria for Hg, however it has been acknowledged that such a scope can be achieved only using site-specific BAF (U.S.EPA, 2010). In other words, due to the many confounding factors that affect bioaccumulation, it is not possible to extrapolate BAF values from one ecosystem to another. Moreover, the use of BAF implies a simple linear relationship between aquatic and biological fraction of MeHg, but MeHg concentrations are known to be very heterogeneous and dynamic, thus the use of a restricted dataset of water MeHg values might bias results being not representative of the true temporal signal to which organisms were exposed (Pollman and Axelrad, 2014).

Nonetheless, it is important to establish and model relationships and between contaminant exposure and bioaccumulation for management purposes, also to unravelling the potential impacts of climate change on the fate of Hg in ecosystems. As reviewed by Marques et al., (2010), climate change will effect both the biotic and abiotic processes governing the fate of Hg species. On the one hand, it may lead to increase of methylation and/or increase of resuspension processes of sediment-bound Hg (see also Chapter 3 of this work); on the other hand, temperature will increase the uptake, bioaccumulation and toxicity of metals in many organisms, while reducing their ability to deal with physiological stressors such as contaminants.

5.2. Methods

5.2.1 Model implementation

The WASP model is a dynamic box model for Hg (Wool et al., 2001) whose structure and processes are described in Chapters 2, 3 and 4. Here we implemented the model (Table 1) as a 1 dimensional (1D) water column of 15 m depth underneath by two sediment layers with Hg_T concentrations of 58 nmol/g. In the Augusta harbor, sediment concentrations decrease from South (average 120 nmol/g, range 0.5 – 2800) to East and North (respectively averaging 24 and 5 nmol/g) and thus a finer spatial resolution would be appropriate. However, due to current lack of data on hydrodynamic exchanges suitable to our model, we chose to explore the system in 1D in the first place.

Physical features	*Surface Area*	23.5	km^2	
	Average Depth	15	m	
	Modeled Volume	$3.5\ 10^8$	m^3	
	Tidal exchange	±200	m^3/s	*De Marchis et al., (2014)*
	Sea Surface Temperature	16 - 12	ºC	Bosc et al., (2004)
	Light irrandiance	245- 1000	W/m^2	*Bosc et al., (2004)*
Ionian Sea Boundary	*SPM*	0.12	mgL	Boldrin et al., (2002)
	POM	0.02	mgL	*Boldrin et al., (2002)*
	Hg	6.00	ngL	Salvagio Manta et al., (2016)
	MeHg	0.1	1.7%	
Hg loads	*Atmospheric Deposition*	6	ug/m^2y	*Gencarelli et al., (2015)*
	Point-sources Hg	11.4	kg/y	*European pollutant emission register*
	Point-sources MeHg	0.57	kg/y	*%5 of Hg*
Water	Hg_T	45 – 650	ng/L	Salvagio Manta et al., (2016)
Sediment	*Hg*	58	nmol/g	
	bulk density	1.4	kg/m^3	Sprovieri et al., (2011)
	Methylation/ demethlation	See table 1		
	Molecular diffusion coefficient	$Hg_{(25^\circ)}$= 9.5E-6 $MeHg_{(25^\circ)}$= 1.08E-5	cm^2/s	*Rothenberg et al. (2008)*
Photochemical Transformations	*Photo-reduction*	$6.5\ 10^{-4}$	1/s	*Whalin et al., (2007)*
	Photo-oxidation	$4\ 10^{-4}$	1/s	*Whalin et al., (2007)*
	Photo-demetylation	$6\ 10^{-7}$	1/s	*Whalin et al., (2007)*

Table 1. Data, parameters and coefficients applied to the model

Tidal exchanges with the Ionian Sea were extrapolated from the work of De Marchis et al., (2014), who simulated the hydrodynamic circulation of the bay with a 3D model. Their study investigated the period from 11th October 2006 to 15th October 2006, during which the wind conditions were representative of the whole year. We simulated only the tidal fluxes at the Eastern mouth that is where most of the exchange occurs.

Atmospheric deposition of Hg and Hg^0 atmospheric concentrations were set in agreement to Gencarelli et al., (2015). Point-source loads were set to 11.4 kg/y (0.06 kmol/y), according to the report for the year 2005 (European Pollutant Emission Register, http://www.eea.europa.eu/data-and-maps/data/eper-the-european-pollutant-emission-register-4). We assumed that 5% of Hg point source loads are made of MeHg.

Model processes were forced with monthly values of light irradiance and sea surface water temperature according to Bosc et al., (2004). All the data and coefficient used in the model implementation are given in Tables 2 and 3.

To explore the impact of methylation and boundary concentrations on the modeled MeHg concentrations, we performed 4 alternative simulations, as summarized in Table 2: the baseline scenario with sediment methylation only (***Bas***), two scenarios of water methylation (***WM1*** and ***WM2***), and a scenario with lowered boundary value (***LB***).

In the ***Bas*** simulation, Hg concentrations at the sea boundary were set at a fixed value of 30 pM, because the values that have been measured outside the bay are much higher than in the rest of Ionian Sea. Salvagio Manta et al., (2016) reported Hg_T concentrations of 30 pM (range 13 – 60 pM) in February 2012, and Fantozzi et al., (2013) detected 93 pM of Hg_T in August 2010. However, to be sure that the model was not biased by excessive boundary values, we implemented the simulation (***LB***), lowering the boundary concentrations to 20 pM.

Methylation and demethylation rates (k_m and k_{dm}) in sediment were set in all of the simulations (Table 2), in agreement with Hines et al., (2012). Two additional simulations were performed that include methylation and demethylation in the water column, according to the rates observed in the Mediterranean Sea (Monperrus et al., 2007; Sharif et al., 2014). Lower rates were set in the simulation ***WM1***, and higher rates in the ***WM2,*** to assess how these processes affect MeHg levels in water.

Simulation	***Bas***	***LB***	***WM1***	***WM2***
Sea boundary condition (Hg_T, pM)	30	20 (-33%)	30	30
Site of methylation and demethylation	sediment	sediment	water and sediment	water and sediment
Water k_m	-	-	0.001	0.03
Water k_{dm}	-	-	0.038	0.55
Sediment k_m	0.004	0.004	0.004	0.02
Sediment k_{dm}	0.01	0.01	0.01	0.31
	Sediment k_m and k_{dm} (Hines et al., 2012) Water k_m and k_{dm} (Monperrus et al., 2007; Sharif et al., 2014)			

Table 2. Synthesis of the variations applied to the model simulations baseline (***Bas),*** lower boundaries ***(LB),*** water methylation 1 (***WM1***) and water methylation 2 (***WM2***).

5.2.2 Computation of trophic levels (TL) of the organisms and bioaccumulation factors (BAF)

Bonsignore et al., (2013) measured Hg_T concentration in a number of fishes and cephalopods species of the Augusta bay, both inside and outside the harbor, and we use this dataset to investigate biomagnification.

To understand the structure of the trophic web, we assigned a trophic level (TL) to each species analyzed in Bonsignore et al., (2013) according to the information available on FishBase (www.fishbase.org, last visited 02/21/2016); for TL of cephalopods we referred to Froese et al., (2005).

The 4 simulations that we ran provided a range of Hg and MeHg concentrations that we used to compute estimates of BAF_{Hg} and BAF_{MeHg} along the trophic web of the Augusta Bay. BAF_{Hg} values were computed by dividing the average Hg_T concentration (w.w.) in fish muscles by the highest, lowest and average modeled Hg_D concentrations.

BAF_{MeHg} values were estimated in the same way, however to infer MeHg concentrations in muscles from measured Hg_T, we assumed that %MeHg increases along with the TL as observed in the field by many authors (Dominik et al., 2014; Faganeli et al., 2014; Hammerschmidt and Fitzgerald, 2006). We set %MeHg as following: species of TL > 2.8 and < 3.5 have 70% of MeHg in muscles; species of TL = 3.5 have 80% of MeHg in muscles; species of TL > 3.5 and TL < 4 have 90% of MeHg in muscles; and species of TL ≥ 4 have 95% MeHg in muscles.

5.3. Results and discussion

5.3.1 Comparison among simulations

Table 3 summarizes modeled output of Hg_T and $MeHg_T$ in the water for the 4 simulations (***Bas, LB, WM1***, ***WM2***) and the variation induced on Hg_T and $MeHg_T$ water concentrations with respect to the output of the ***Bas*** simulation. The reduction applied to the sea boundary conditions (-33%) in the simulation ***LB*** leads to a 28% decrease of Hg_T concentrations in the water, whereas it does not

affect MeHg levels. Modeled MeHg water concentrations are elevated mostly because of the estimated point-source loads of MeHg (5% of Hg_T that is 0.5 k/y or 2.65 mol/y, over a quite small volume of $3.5 \cdot 10^8$ m^3).

The inclusion of low k_m and k_{dm} (Table 2) in the simulation ***WM1*** induces a decrease of MeHg concentrations (-48%) in the water compared to the ***Bas*** simulation, indicating net demethylation. Conversely, the higher k_m and lower ratio of k_{dm}/k_m parametrized in the simulation ***WM2*** (Table 2) cause a shift toward net methylation in the water, thus provoking higher MeHg concentrations (+57%).

The remarkable difference in modeled MeHg concentrations between the simulations ***WM1*** and ***WM2*** (1.2 and 3.5 pM) highlights the importance of addressing site-specific occurrence of water methylation that can be crucial to bioaccumulation in the trophic web.

	Hg_T water	***Variation***	***$MeHg_T$ water***	***$MeHg_T$ Variation***
	average		average	
	pM		pM	
Bas	58		2.2	
LB	42	-28%	2.2	0%
WM1	58	0%	1.2	-48%
WM2	63	+9%	3.5	+57%

Table 3. Summary of modeled output of Hg_T and $MeHg_T$ in the water of the simulations implemented. The % variation of the output Hg_T and $MeHg_T$ of simulations ***LB, WM1 and WM2*** with respect to the ***Bas*** simulation is given.

5.3.2 Estimated bioaccumulation factors

The estimated BAF_{Hg} and BAF_{MeHg} for each species from inside and outside the Augusta Harbor are shown in Figure 2 against the estimated TL. The trophic structure of the ecosystem explains about 58% of the inter-species variance of both BAF_{Hg} (R^2=0.59, $p<0.05$) and BAF_{MeHg} (R^2=0.57, $p<0.05$) inside the harbor. Outside the harbor there are less data available, and the relation is significant only when BAF_{MeHg} is considered (R^2=0.77, $p<0.05$).

As no data on MeHg concentrations outside the harbor are available, BAF values computed for fishes from outside the harbor are biased by the use of MeHg water concentrations computed for the water inside the harbor. In fact BAF, are one order of magnitude lower than those for fishes from inside the harbor, however they are still useful for comparison.

Computed log BAF_{MeHg} values for organisms inside the harbor range 5.8 – 7 and are within observed range in other works; they are lower than those estimated for the ecosystem of the Venice Lagoon, and higher than those estimated for the Adriatic Sea.

In the Venice Lagoon, the organism of highest TL analyzed was *Atherina boyeri* (TL = 3.3) for which the authors (Dominik et al., 2014) computed a BAF_{MeHg} ~7.15, based on water MeHg measurements of Guédron et al., (2012). The Venice Lagoon is a shallow environment, thus the highest BAF_{MeHg} may be due to the tight connection between waters and sediments that enhances the influence of the sediment contamination on Hg levels in the water and the interconnection of benthic and pelagic food webs.

Conversely, a retrospective analysis of bioaccumulation in the Adriatic Sea collating data from the year 1999, 2003 and 2004, including fishes up to TL= 4.5 (*Sarda sarda*) estimated a maximum BAF_{MeHg} at ~5 (Cinnirella et al., 2013).

The work on the Adriatic Sea rely on a small and fragmented dataset (Cinnirella et al., 2013), however we can speculate that the BAF_{MeHg} are lower than in the Venice Lagoon and Augusta Harbor because the latter are much more confined environments where the high residence time of water can promote methylation and bioaccumulation.

In the dataset of Augusta, the highest TL organisms inside the bay are *Scorpaena scrofa* (TL=4.3), *Murena helena* (TL=4.2), and *Sphyraena sphyraena* (TL=4) which have the highest BAF_{Hg} and BAF_{MeHg} (6.4 - 6.8 L/kg). The variance (σ^2) of the specie-specific BAF_{MeHg} values, induced by the range of water MeHg concentrations used to compute them, is always 0.12 L/kg.

The efficiency of biomagnification (biomagnification power) differs among ecosystems owing to multiple factors such as the fraction of MeHg that is bioavailable; the coincidence between the habitat of organisms and the site(s) of highest MeHg production; the structure of the trophic web, and the variability among location of growth rates of a given species (Cossa et al., 2012). However, the use of non-synoptic dataset and the limited data on MeHg concentrations could have also affect the computations of BAF for Augusta Harbor, Venice Lagoon and Adriatic Sea.

Organisms from outside the harbor are mostly small pelagic planktivorous fishes, such as *Engraulis encrasicolus* and *Sardina pilchardus*, and have lower TL than those inside. *Pagello bogaraevo* and *Trachurus trachurus* are the fishes of highest TL (4.2 and 3.7) and consistently exhibit the highest $logBAF_{MeHg}$ (5.8 and 5.5), comparable with those estimated for the Adriatic Sea (Cinnirella et al., 2013b).

In analyzing the bioaccumulation of the Augusta Bay ecosystem, Bonsignore et al., (2013) concluded that the depth of the habitat is a key factor in determining the level of Hg in the organisms of the Augusta ecosystem; however we argue that the trophic levels might be a more important driver. For instance, *Sphyraena sphyraena* (TL=4) and *Scorpaena scrofa* (TL=4.3) are both predators, but *Sphyraena sphyraena* that is pelagic has higher BAF_{Hg} and BAF_{MeHg} than *Scorpaena scrofa* (benthic), and similar BAFs to *Murena helena* (benthic, TL=4.2). The other

pelagic species caught inside the harbor, *Caranx rhoncus*, also have higher BAF than benthic and demersal organisms of comparable trophic levels (see Figure 2).

Outside the harbor the highest BAF is that of the demersal fish *Pagellus bogaraevo*, which is that of highest trophic level (4.2) while all the other small pelagic fishes are of TL≤3.7.

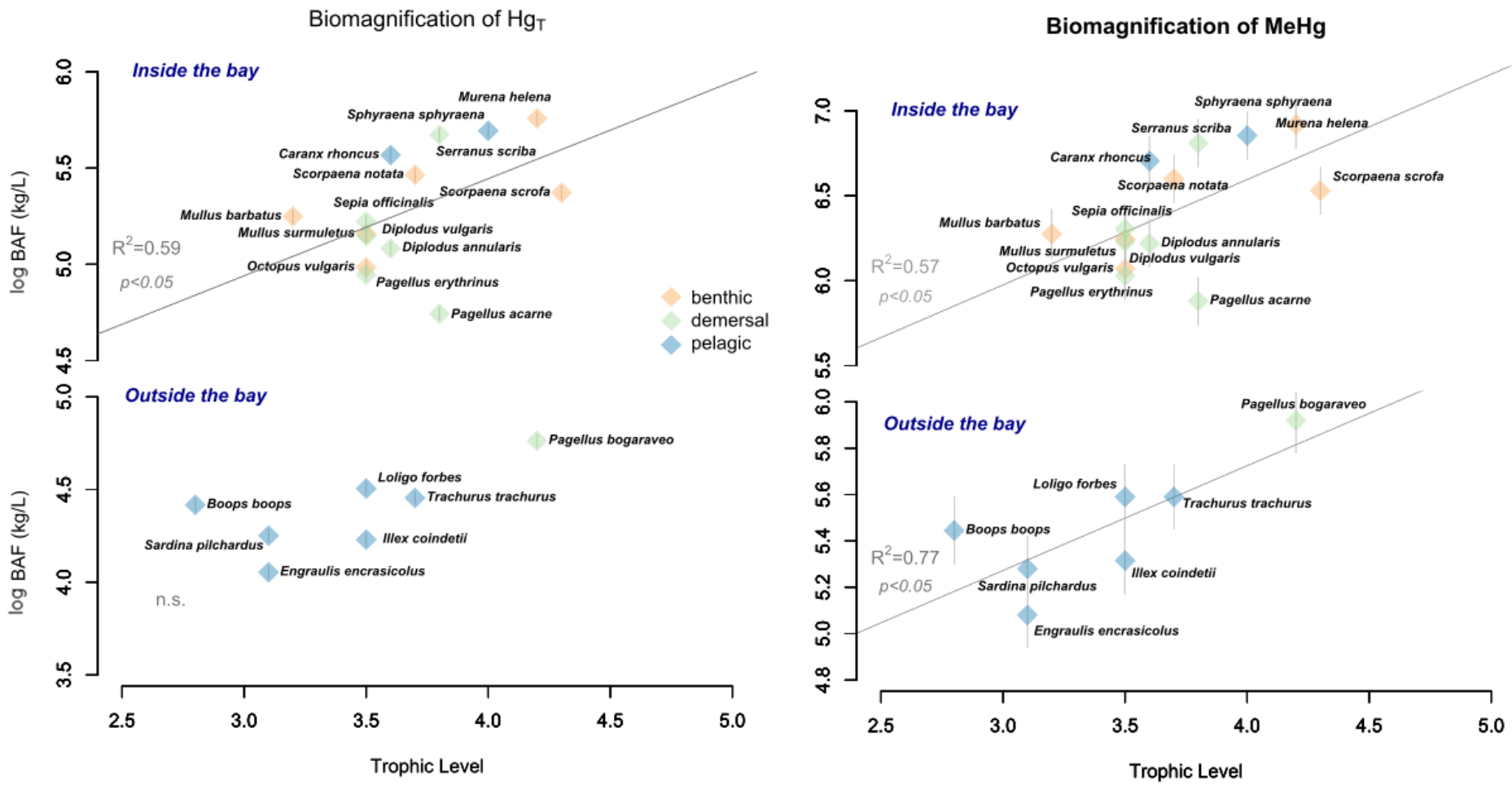

Figure 2. Scatterplots of the logarithm of BAF_{Hg} and BAF_{MeHg} computed in this work against the trophic level estimated from fishbase.

References

Bagnato, E., Sproveri, M., Barra, M., Bitetto, M., Bonsignore, M., Calabrese, S., Di Stefano, V., Oliveri, E., Parello, F., Mazzola, S., 2013. The sea–air exchange of mercury (Hg) in the marine boundary layer of the Augusta basin (southern Italy): Concentrations and evasion flux. Chemosphere 93, 2024–2032. doi:10.1016/j.chemosphere.2013.07.025

Boldrin, a., Miserocchi, S., Rabitti, S., Turchetto, M.M., Balboni, V., Socal, G., 2002. Particulate matter in the southern Adriatic and Ionian Sea: Characterisation and downward fluxes. J. Mar. Syst. 33–34, 389–410. doi:10.1016/S0924-7963(02)00068-4

Bonsignore, M., Salvagio Manta, D., Oliveri, E., Sprovieri, M., Basilone, G., Bonanno, A., Falco, F., Traina, A., Mazzola, S., 2013. Mercury in fishes from Augusta Bay (southern Italy): Risk assessment and health implication. Food Chem. Toxicol. 56, 184–194. doi:10.1016/j.fct.2013.02.025

Bosc, E., Bricaud, A., Antoine, D., 2004. Seasonal and interannual variability in algal biomass and primary production in the Mediterranean Sea, as derived from 4 years of SeaWiFS observations. Global Biogeochem. Cycles 18, n/a-n/a. doi:10.1029/2003GB002034

Cinnirella, S., Pirrone, N., Horvat, M., Kocman, D., Kotnik, J., 2013a. Mercury bioaccumulation in the Mediterranean. E3S Web Conf. 1, 11005. doi:10.1051/e3sconf/20130111005

Cinnirella, S., Pirrone, N., Horvat, M., Kocman, D., Kotnik, J., 2013b. Mercury bioaccumulation in the Mediterranean. E3S Web Conf. 1, 11005. doi:10.1051/e3sconf/20130111005

Cossa, D., Harmelin-Vivien, M., Mellon-Duval, C., Loizeau, V., Averty, B., Crochet, S., Chou, L., Cadiou, J.-F., 2012. Influences of bioavailability, trophic position, and growth on methylmercury in hakes (Merluccius merluccius) from Northwestern Mediterranean and Northeastern Atlantic. Environ. Sci. Technol. 46, 4885–93. doi:10.1021/es204269w

De Marchis, M., Freni, G., Napoli, E., 2014. Three-dimensional numerical simulations on wind- and tide-induced currents: The case of Augusta Harbour (Italy). Comput. Geosci. 72, 65–75. doi:10.1016/j.cageo.2014.07.003

Dominik, J., Tagliapietra, D., Bravo, A.G., Sigovini, M., Spangenberg, J.E., Amouroux, D., Zonta, R., 2014. Mercury in the food chain of the Lagoon of Venice, Italy. Mar. Pollut. Bull. 88, 194–206. doi:10.1016/j.marpolbul.2014.09.005

Faganeli, J., Hines, M.E., Horvat, M., Falnoga, I., Covelli, S., 2014. Methylmercury in the gulf of trieste (Northern Adriatic sea): From microbial sources to seafood consumers. Food Technol. Biotechnol. 52, 188–197.

Fantozzi, L., Manca, G., Ammoscato, I., Pirrone, N., Sprovieri, F., 2013. The cycling and sea-air exchange of mercury in the waters of the Eastern Mediterranean during the 2010 MED-OCEANOR cruise campaign. Sci. Total Environ. 448, 151–162. doi:10.1016/j.scitotenv.2012.09.062

Froese, R., Garthe, S., Piatkowski, U., Pauly, D., 2005. Trophic signatures of marine organisms in the Mediterranean as compared with other ecosystems. Belgian J. Zool. 135, 139–143.

Gencarelli, C.N., De Simone, F., Hedgecock, I.M., Sprovieri, F., Yang, X., Pirrone, N., 2015. European and Mediterranean mercury modelling: Local and long-range contributions to the deposition flux. Atmos. Environ. 117, 162–168. doi:10.1016/j.atmosenv.2015.07.015

Guédron, S., Huguet, L., Vignati, D.A.L., Liu, B., Gimbert, F., Ferrari, B.J.D., Zonta, R., Dominik, J., 2012. Tidal cycling of mercury and methylmercury between sediments and water column in the Venice Lagoon (Italy). Mar. Chem. 130–131, 1–11. doi:10.1016/j.marchem.2011.12.003

Hammerschmidt, C.R., Fitzgerald, W.F., 2006. Bioaccumulation and Trophic Transfer of Methylmercury in Long Island Sound. Arch. Environ. Contam. Toxicol. 51, 416–424. doi:10.1007/s00244-005-0265-7

Hines, M.E., Poitras, E.N., Covelli, S., Faganeli, J., Emili, A., Žižek, S., Horvat, M., 2012. Mercury methylation and demethylation in Hg-contaminated lagoon sediments (Marano and Grado Lagoon, Italy). Estuar. Coast. Shelf Sci. 113, 85–95. doi:10.1016/j.ecss.2011.12.021

Marques, A., Nunes, M.L., Moore, S.K., Strom, M.S., 2010. Climate change and seafood safety: Human health implications. Food Res. Int. 43, 1766–1779. doi:10.1016/j.foodres.2010.02.010

Monperrus, M., Tessier, E., Amouroux, D., Leynaert, A., Huonnic, P., Donard, O.F.X., 2007. Mercury methylation, demethylation and reduction rates in coastal and marine surface waters of the Mediterranean Sea. Mar. Chem. 107, 49–63. doi:10.1016/j.marchem.2007.01.018

Pollman, C.D., Axelrad, D.M., 2014. Mercury bioaccumulation factors and spurious correlations. Sci. Total Environ. 496, vi–xii. doi:10.1016/j.scitotenv.2014.07.050

Salvagio Manta, D., Bonsignore, M., Oliveri, E., Barra, M., Tranchida, G., Giaramita, L., Mazzola, S., Sprovieri, M., 2016. Fluxes and the mass balance of mercury in Augusta Bay (Sicily, southern Italy). Estuar. Coast. Shelf Sci. 181, 134–143. doi:10.1016/j.ecss.2016.08.013

Sharif, A., Monperrus, M., Tessier, E., Bouchet, S., Pinaly, H., Rodriguez-Gonzalez, P., Maron, P., Amouroux, D., 2014. Fate of mercury species in the coastal plume of the Adour River estuary (Bay of Biscay, SW France). Sci. Total Environ. 496, 701–713. doi:10.1016/j.scitotenv.2014.06.116

Sprovieri, M., Oliveri, E., Di Leonardo, R., Romano, E., Ausili, A., Gabellini, M., Barra, M., Tranchida, G., Bellanca, A., Neri, R., Budillon, F., Saggiomo, R., Mazzola, S., Saggiomo, V., 2011. The key role played by the Augusta basin (southern Italy) in the mercury contamination of the Mediterranean Sea. J. Environ. Monit. 13, 1753. doi:10.1039/c0em00793e

U.S.EPA, 2010. Guidance for implementing the January 2001 methylmercurywater quality criterion. Washington DC.

Wool, T.A., Ambrose, R.B., Martin, J.L., Comer, E.A., 2001. Water Quality Analysis Simulation Program (WASP) Version 6.0: User's Manual.

Conclusions

This work has provided a modeling analysis of Hg cycle in coastal and marine ecosystems, highlighting how different processes drive Hg species dynamics depending on local physical and biogeochemical settings. In coastal environments that are polluted owing to past anthropogenic activities, such as the Marano-Grado Lagoon, Hg and MeHg in the sediment can be one of the major drivers for water concentrations. In contrast, sedimentary processes seems to be negligible in deep environments such as the Black Sea, where the major transport pathway is from surface to deep water, linked to the biological pump of carbon.

The modeled budget of Hg species in the Marano-Grado Lagoon have shown how a small coastal lagoon can significantly impact the overall cycle of the Mediterranean Sea, suggesting that a thorough re-assessment of Hg species export from polluted coastal sites might improve our understanding of Hg dynamics in the Mediterranean. The scenario analysis of long-term evolution of the Marano-Grado Lagoon has indicated that this system is vulnerable to climate changes, owing to both a predicted increase of MeHg production, and to the alteration of hydrodynamic features that control sediment settling and resuspension. The investigation in the Black Sea has sparked a light on the production of MeHg in sulfidic environments, demonstrating that the notion of inhibition of methylation by sulfides needs to be revised, as already concluded by other authors. While the permanent stratified structure of the Black Sea is quite peculiar, it is an ideal environment to understand the fate of Hg in presence of sulfide, a process that is relevant both in sediment (at a much smaller scale) and in water bodies characterized by seasonal stratification. The analysis of Hg accumulation in the biota of the Augusta Harbor has confirmed that biomagnification occurs in the trophic web of the Augusta bay and has provided site-specific bioaccumulation factors (BAF) that can be employed to estimate the response of the organisms to future changes of Hg loadings and concentrations.

The implementation of models calibrated with available site-specific data has been useful to constrain quantitatively the fluxes of Hg species in the systems investigated. The combined use of observations and models helps to point out and overcome the uncertainties related to both the spatial-temporal resolution of experimental samplings, and to the approximations of some modeled processes that are not fully understood. In recent years, biogeochemical models of Hg have benefited from increasing global efforts to improve the amount and quality of measurements, but they have been also essential in indicating inconsistency among conclusions drawn by different studies. Therefore, a continuous interaction between the experimental and modeling scientific communities is more than desirable.